THE UNIVERSITY
of EDINBURGH

The role of Trichoplein in endothelial cell function and autophagy

Andrea Martello

Submitted for the degree of Doctor of Philosophy

University of Edinburgh 2018

Declaration

I declare that this thesis is an original report of my research, has been written by me and has not been submitted for any previous degree. The experimental work is almost entirely my own work; the collaborative contributions have been indicated clearly and acknowledged. Due references have been provided on all supporting literatures and resources.

Acknowledgments

I am immensely grateful to all those who have accompanied me on this journey through my PhD, they have made me grow as a person and as a scientist. I owe a big thank to Andrea Caporali, because his commitment to me as a supervisor and on a personal level has exceeded my expectations. Andrea taught me the scientific rigor and logical thinking applied to biology but, above all, he was of great inspiration because of his enthusiasm and ability to see beyond the obstacles the “bigger picture”.

Patrick has always been thoughtful to my needs and ready to help me. I took advantage of his great experience and listeners ability and I received from him great advices and sensible guidance.

I have numerous collaborators who helped my work to take shape, in particular Lisa Imrie, Roderick Carter, Shonna Johnston, Lorraine Rose. Noor Gammoh from IGMM deserves a special thank for all the numerous constructive discussion and tools she shared with me.

I was lucky enough to encounter Vlad Miscianinov, a friend and colleague who shared with me all the joys and sorrows coming from a PhD life and Marco Melfi a very gifted master student who contributed with his work to this thesis and nevertheless he was always in a good mood.

Finally, I have a debt with my family for all the support and encouragement they provide me every day and my girlfriend Lucia who always stand by me and without which I would not have arrived where I am now.

Abstract

Autophagy is an essential quality control function of the cell. It selectively degrades harmful protein aggregates and/or damaged organelles, enabling maintenance of cellular homeostasis. Basal autophagy also mediates proper cardiovascular function. A variety of cardiovascular risk factors cause defective autophagy, consequently, pharmacotherapy with compounds to re-establish physiological levels of autophagy and stimulate pro-survival effects in the vasculature is an emerging strategy for cardiovascular disease. Therefore, it is crucial for the design of new pharmacological therapy the identification of novel key genes involved in the regulation of autophagy in vascular cells.

In two recent studies Caporali et al showed how miR-503 might be considered a suppressor of postishemic neovascularization in type I diabetes and suggested some critical genes targeted by miR-503 whom downregulation may be crucial for the detrimental effect on endothelial cells and pericyte. Among the putative targets of miR-503 not prioritized in the previous studies but of potential interest for endothelial cell functions there was TCHP.

Trichoplein (TCHP) was first identified as a keratin binding protein in 2005 and was described having a role in cancer progression, cellular apoptosis, cell cycle, primary cilium formation, mitochondria fragmentation and mitochondria-endoplasmic reticulum tethering. Using biochemical and bioinformatics approaches, I have demonstrated that TCHP is a novel target of miR-503. The data presented in this thesis will address the hypothesis that TCHP regulates endothelial function through the control of autophagy.

TCHP expression in ECs was reduced when cultivated in high glucose in combination with low growth factors condition. Notably, ECs sorted from mice with Type-1 diabetes showed low levels of Tchp compared to non-diabetic mice. Knockdown of TCHP in ECs *in vitro* was characterized by marked changes in the tubulin cytoskeleton organization, resulting in an impaired

microtubule network, reduced EC migration, reduced barrier function and impaired EC sprouting. Loss of TCHP function in ECs *in vitro* led to a defective autophagy, resulting in accumulation of SQSTM1/p62 and unfolded protein aggregates. Therefore, blocking autophagic flux in ECs resulted in premature cellular senescence as demonstrated by the appearance of β-galactosidase staining, the senescence-associated secretory phenotype (SASP) and increased expression of p16INK4A. This phenotype was associated with activation of the mTOR pathway and could be rescued using mTOR inhibitors. Thus, Torin-1 improved the migratory capacity of TCHP knockdown cells and rescued their senescent phenotype. In addition, ultrastructure analysis, immunofluorescence and epidermal growth factor pulse chase experiments revealed substantial abnormalities in the endosome and lysosome compartments in TCHP knock down cells.

Remarkably, Tchp knockout mice exhibited a decreased cardiac vascularization and a significant accumulation of SQSTM1/p62 in cardiac vessels and cardiomyocytes, as a demonstration of defective autophagic flux. Finally, I observed loss of TCHP and an increase of SQSTM1/p62 and aggregates in the vessel wall derived-ECs, from patients with vascular dysfunction and premature coronary artery disease. Remarkably ECs from patients exhibited impaired migration and increased expression of SASP, resembling the phenotype of TCHP knockdown cells. In line with this, function in EC from patients was rescued by Torin-1 treatment.

Taken together, these results reveal for the first time the pivotal role played by TCHP in the vascular endothelium and identify a new mechanism by which pathological conditions, through the silencing of TCHP, lead to the endothelial dysfunction. Importantly, this study highlights a fundamental link between EC function and cellular proteostasis, through the control of autophagy, and suggests a new therapeutic direction in cardiovascular disease.

Lay Summary

The blood vessels in the human body are lined with a thin layer of endothelial cells. In healthy people, endothelial cells help to form new vessels by migrating and dividing. In diabetic patients and in patients with dysfunctional endothelium, these endothelial cells are faulty and weak, which can lead to vessel-related problems like ischemia (lack of blood flow to parts of the body), atherosclerosis (hardening of the arteries) and delayed healing of wounds. Therefore, it is important to identify proteins that regulate the function of endothelial cells because they can be new therapeutic targets.

I have discovered that a protein called trichoplein (TCHP) helps endothelial cells to migrate and to survive, and cells without TCHP are more easily damaged by cellular insults. I believe that diabetes and related stresses, such as decreased levels of oxygen and growth factor as well as high levels of glucose, may cause vessel-related problems by diminishing the levels of TCHP in endothelial cells.

Furthermore, I have observed that low levels of TCHP, reduced a biological process called “autophagy”. Often diabetic patients have a defective autophagy and malfunctioning of this process has been linked to several cardiovascular complications. Autophagy is a cellular process helping the cells of our bodies to stay healthy, destroying damaged organelles and recycling them into their basic building blocks; or helping them to survive to low nutrient conditions, digesting unnecessary portions of the cell to obtain energy for essential cellular functions. In fact, I described that endothelial cells defective for TCHP expression are engulfed in protein aggregate, secrete pro-inflammatory signals and acquire features typical of aged cells. I demonstrate a positive correlation between the reactivation of autophagy and the improvement of this phenotype. Finally, I found that EC from patients with premature coronary artery disease have low levels of TCHP, accumulation of protein aggregates, and migratory defects that can be ameliorated by stimulating autophagy.

Table of Contents

Declaration **2**
Acknowledgments **3**
Abstract **4**
Lay Summary **6**
CHAPTER 1: **11**
Introduction **11**
1.1 Trichoplein 12
1.1.1 Identification and function 12
1.1.4 TCHP and mitochondria 14
1.2 Endothelial cell function 15
1.2.1 Angiogenesis: definition 15
1.2.2 Mechanisms of angiogenesis 17
1.2.3 Mechanisms of endothelial cell migration 20
1.2.4 Endothelial dysfunction and vascular disease 21
1.2.5 Mitochondrial function in vascular disease 23
1.2.6 Vascular senescence 25
1.3 Autophagy 29
1.3.1 Definition of autophagy 29
1.3.2 Regulation of autophagy 30
1.3.3 Autophagy in ECs 32
1.3.4 Autophagy as therapeutic target in vascular diseases 33
1.4 Hypothesis 35
1.5 Aims 35
CHAPTER 2: **36**
Materials and Methods **36**
Cell lines and cell culture 37
Lentiviral vectors 37
Total protein extraction and quantification 39
Western blot 39
Native-PAGE of mitochondrial electron chain complexes 42
Mitochondrial isolation protocol 42
Solubilisation of mitochondria 43
Running Native-PAGE gels 43

Seahorse: Mitochondrial respiration stress test 43
Cell preparation for Seahorse 43
Seahorse Bio-analyzer XF Cell Mito Stress Test protocol 44
Flow cytometry 44
PROTEOSTAT® Aggresome 45
Immunofluorescence 45
Immunohistochemistry 47
ImageJ and CellProfiler analysis 47
Quantification of mitochondrial localization – CellProfiler 47
RNA extraction and quantitative real-time analysis 48
Cells transfection, transduction and functional assays 49
ATP Colorimetric/Fluorometric Assay 49
NAD/NADH Quantitation 50
Luciferase assays 51
Animal experiments 51
Isolation of endothelial cells from mouse limb muscles 51
Statistical analysis 52
CHAPTER 3: 53
Does TCHP regulate EC function and senescence? 53
3.1 Introduction 54
3.1.2 Hypothesis 58
3.1.3 Aims 58
3.2 Materials and Methods 59
3.3 Results 63
3.3.1 TCHP localization in endothelia cells and vessels 63
3.3.2 TCHP is target of miR-503 65
3.3.3 TCHP regulation *in vitro* 66
3.3.4 TCHP regulation *in vivo* 68
3.3.5 TCHP knockdown affects EC morphology 70
3.3.6 Lack of TCHP impairs EC angiogenesis, migration and barrier function in vitro 72
3.3.7 TCHP KD affects microtubule density and actin localization 74
3.3.8 TCHP is required for cell cycle progression 76
3.3.9 TCHP knockdown sensitizes ECs to cell death in response to different cell death inducing stimuli 77

3.3.10 Gene expression regulation by knockdown of TCHP 79
3.3.11 Analysis of the senescence associated phenotype after TCHP downregulation 81
3.4 Discussion 83
3.4.1 TCHP localization and regulation 83
3.4.2 TCHP knockdown impairs EC functions 84
3.4.3 TCHP knockdown sensitizes ECs to apoptotic death 86
3.4.4 TCHP knockdown induces premature senescence phenotype 87
3.5 Conclusion 88
CHAPTER 4: 89
Does TCHP regulate the autophagy process? 89
4.1 Introduction 90
4.1.2 Hypothesis 92
4.1.3 Aims 92
4.2 Materials and Methods 93
4.3 Results 96
4.3.1 TCHP KD affects autophagy homeostasis 96
4.3.2 Regulation of autophagic flux in TCHP KD cells 100
4.3.3 TCHP knockdown regulates lysosomal function 102
4.3.4 TCHP knockdown affects endo-lysosomal pathway 104
4.3.5 Accumulation of aggregates in TCHP KD cells 107
4.3.6 Activation of autophagic flux in TCHP KD cells restores migration and decrease inflammation 109
4.3.7 ECs from patients with premature coronary artery disease have low level of TCHP and express SAPS gene 110
4.3.8 Torin-1 restores EC functionality in ECs from patients with premature coronary artery disease 111
4.3.9 Characterization of TCHP knockout mice 114
4.4 Discussion 115
4.4.1 Regulation of autophagic flux by TCHP 115
4.4.2 Regulation of endolysosomal pathway 116
4.4.3 Regulation of TCHP-related phenotype by mTOR inhibitor 117
4.4.5 Conclusion 119
CHAPTER 5: 121
Does TCHP regulate mitochondrial function in ECs? 121
5.1 Introduction 122

5.1.2 Hypothesis 125
5.1.3 Aims 125
5.2 Materials and Methods 126
5.3 Results 130
5.3.1 Lack of TCHP does not affect mitochondria localization 130
5.3.2 Quantification of total mitochondrial mass and ROS in TCHP KD cells 132
5.3.3 Analysis of mitochondrial function with respect to mitochondrial respiration in cell lacking TCHP 134
5.3.4 Analysis of relative abundance of electron transport chain complexes in TCHP KD cells 137
5.3.5 TCHP KD affects energy balance in ECs 139
5.4 Discussion 142
5.4.1 Mitochondria localization and size 142
5.4.2 Effect of TCHP KD on ROS production 142
5.4.3 Mitochondria bioenergetics 143
5.4.4. Effect of TCHP KD on EC energy balance 144
5.4.5 Conclusion 145
CHAPTER 6: 146
Discussion and Conclusions 146
6.1 TCHP in endothelial cell function 147
6.2 TCHP as novel regulator of autophagy 150
6.3 Role of TCHP in mitochondrial function and bioenergetics 152
6.4 Future work 154
6.4.1 Identification of TCHP partner proteins and their functions 154
6.4.2 Role of TCHP in post-ischaemic angiogenesis 155
6.5 Conclusion 156
References 157

CHAPTER 1:

Introduction

1.1 **Trichoplein**

1.1.1 **Identification and function**

Trichoplein (TCHP,alias MITOSTATIN) is a cytosolic ubiquitously expressed 62 kDa protein identified like keratin-binding protein in 2005 using yeast two hybrid technique (Nishizawa, Izawa et al. 2005). This protein showed a low degree of sequence similarity to trichohyalin, plectin and myosin heavy chain, and is a K8/18-binding protein.

In 2009, the cloning of TCHP was confirmed as a novel protein endowed with tumour suppressor activity, located on chromosome 12q24, frequently deleted in a variety of malignant neoplasms (Vecchione, Fassan et al. 2009). TCHP gene mutation and downregulation have been observed in multiple cancers (reduced in 22% of advanced bladder cancer, in 23% of breast carcinomas and in 35% of prostate cancer analysed) and its potential as a tumour suppressor has been reported recently. In various cancer cell lines, the ectopically expressed TCHP inhibited cell growth, migration, invasion, adhesion and tumour formation in vivo (Vecchione, Fassan et al. 2009, Fassan, D'Arca et al. 2011).

TCHP mRNA consist of 3151 base pair (bp) transcript of which 1497 bp are the protein coding Open Reading Frame (ORF). The highest RNA expression was detected in the heart, skeletal muscle, kidney, liver, and testis. Northern Blot analysis performed with TCHP coding sequence (CDS) brought to the identification of two additional RNA products a larger 5.5 Kb transcript, observed in the heart and skeletal muscle and a smaller 1.24 Kb RNA transcript detected only in the heart (Vecchione, Fassan et al. 2009). The sequence and regulation of this two additional RNAs as well as their coding capacity was not further investigated.

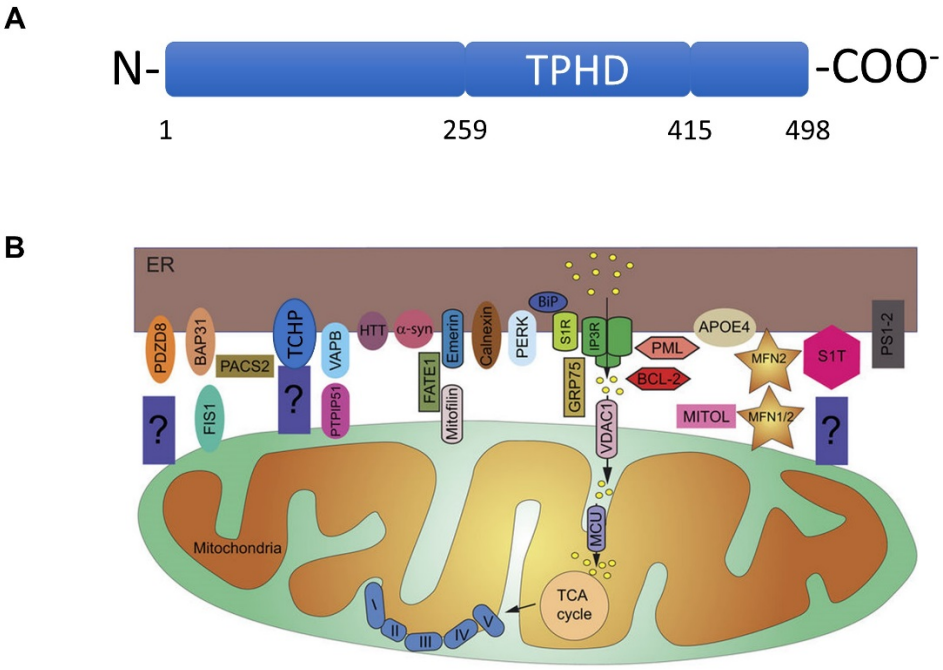

Figure 1.1 Structure and localization of TCHP
A, TCHP was identified as a 498aa protein able to bind cytokeratin in epithelial cell (Nischizawa M. et al. J Cell Sci. 2005 Mar); **B**, Localization of TCHP in mitochondrial-associated membranes. Modified from Benjamin Delprat, Tangui Maurice & Cécile Delettre Cell Death & Disease volume 9, Article number: 364 (2018)

1.1.2 **TCHP and cilium**

TCHP is concentrated at the subdistal/medial region of both mother and daughter centrioles and activates centriolar Aurora A kinase in growing cells (Inoko, Matsuyama et al. 2012). During ciliogenesis, trichoplein disappears from the mother centrioles, and depletion of this protein in cycling epithelial cells induces unscheduled primary cilia formation, whereas overexpression blocks ciliogenesis, indicating that TCHP negatively controls ciliogenesis at the mother centrioles (Inoko, Matsuyama et al. 2012). In proliferating cells, TCHP knockdown induced primary cilia formation, resulting in cell cycle arrest at the G0/G1 phase (Inaba, Goto et al. 2016)

Recently it has been shown that ubiquitin–proteasome system removes TCHP from the mother centrioles and thereby causes Aurora A inactivation, leading to ciliogenesis (Kasahara, Kawakami et al. 2014).

1.1.3 **TCHP and cytoskeleton**

TCHP binds the centrosomal proteins Odf2 and Ninein, regulating Ninein recruitment to the centrosome, resulting therefore indispensable to microtubules-anchoring activity of Ninein at the centrosome (Ibi, Zou et al. 2011). Noteworthy, Ninein appears to have a cytoplasmic distribution in pericyte and endothelial cells (ECs) with a markedly increased expression in tip versus stalk cells (Matsumoto, Schiller et al. 2008). Migrating ECs have a highly polarized structure, with the appearance of membrane ruffles at the leading edge and asymmetrical localization of signalling molecules and the cytoskeleton (Lamalice, Le Boeuf et al. 2007). There is a growing body of evidence that coordinated action of microtubules and actin filaments is necessary for the cell polarization and migration (Li and Gundersen 2008). Thus, the above evidence could support an important role for TCHP in regulating EC migration and angiogenesis.

1.1.4 **TCHP and mitochondria**

Recent studies indicate that TCHP plays an important role in the physiology of mitochondria. It was reported that TCHP reside on outer mitochondrial membrane (OMM) where take contact with Mitofusin2 (Mfn2) promoting a fission-like phenotype and a redistribution of mitochondria near the nuclear membranes(Vecchione, Fassan et al. 2009, Cerqua, Anesti et al. 2010). Moreover, TCHP regulates ER–mitochondria tethering via Mfn2 acting as a negative modulator of ER–mitochondria juxtaposition and conferring H2O2 induced cell death resistance (Cerqua, Anesti et al. 2010). Furthermore, in a breast cancer cell model was recently described that increased level of TCHP enables decorin evoked mitophagy through a peroxisome proliferator-activated receptor γ coactivator-1α (PGC-1α) dependent mechanism.

Interestingly, the authors reported that depletion of TCHP causes an increased production and release of VEGFA (Neill, Torres et al. 2014).
Recently, it has been reported that keratins, likely through TCHP-mtf2 interactions, regulate both structural and dynamic functions of β-cell mitochondria, which could have implications for downstream insulin secretion (Silvander, Kvarnstrom et al. 2017). Therefore, the mitochondrial network in primary cultured K8 knockout β cells is more fragmented compared with wild-type mitochondria, correlating with decreased levels of mtf2 and TCHP. K8 knockout β-cell mitochondria have decreased levels of total and mitochondrial cytochrome c, which correlates with a reduction in electron transport complexes I and IV. This provokes loss of mitochondrial membrane potential and reduction of ATP and insulin amount (Silvander, Kvarnstrom et al. 2017).

1.2 **Endothelial cell function**

1.2.1 **Angiogenesis: definition**

Angiogenesis is creation of new vessels from pre-existing ones (Risau 1997). A number of recent studies have provided great insight into the molecular mechanisms underlying this process, and led to an established mechanistic framework of vessel branching (Carmeliet and Jain 2011) (Potente, Gerhardt et al. 2011). Hypoxia is one of the key drivers of the process, and together with an array of pro-angiogenic signals, ECs respond to hypoxia by becoming motile and protrude filopodia. These aptly named tip cells, advance into the microenvironment, leading trailing stalk cells that establish a lumen and proliferate to support sprout elongation. Vessel loops are created by the anastomosis of neighbouring tip cells, and the initiation local blood flow alongside the recruitment of pericytes, and establishment of the basement membrane, stabilise these new connections. Remodelling and pruning of the newly established vascular network allow fine tuning to suit the needs of the local microenvironment and once the pro-angiogenic signals cease, the ECs assume a quiescent state.

A crucial step in the liberation of ECs during branching is the detachment of the pericyte (Carmeliet 2005). The quiescent vessel detects an angiogenic signal, such as VEGF, which stimulates ECs to release ANG-2, and in turn prompts pericytes to unshackle themselves from the basement membrane by proteolytic degradation (Augustin, Koh et al. 2009). This process is primarily mediated by matrix metalloproteinases (MMPs) (Arroyo and Iruela-Arispe 2010). ECs then loosen their junctions, and the vessels dilate. VEGF signals the endothelial cell layer to increase its vascular permeability, leading to the extravasation of plasma proteins, and consequently the initial extracellular matrix (ECM) scaffolds are constructed. Further angiogenic factors are released from the ECM via proteases to create a pro-angiogenic milieu, and in order to prevent ECs moving *en masse*, one endothelial cell, known as the tip cell, is selected to lead the advance (Adams and Alitalo 2007). Neighbouring cells assume an ancillary role as stalk cells, which divide to elongate the new vessel and establish a lumen. The precise specification of tip and stalk cells is governed by the NOTCH signalling pathway (Phng and Gerhardt 2009, Eilken and Adams 2010). Stalk cells appear to have high levels of NOTCH signalling, unlike tip cells that possess relatively low levels. Conversely, tip cells express high levels of the NOTCH ligand DLL4. An integrated, intracellular, negative feedback network has been proposed to develop between VEGF and NOTCH (Bentley, Mariggi et al. 2009, Potente, Gerhardt et al. 2011). VEGF stimulates tip cell induction and filapodia formation via VEGF receptor-2 (VEGFR2), and enhances DLL4 expression in the same cells. However, DLL4-mediated activation of NOTCH in neighbouring ECs inhibits tip cell behaviour by down-regulating VEGFR2 and VEGF receptor-3 (VEGFR3), while up regulating VEGF receptor-1 (VEGFR1) (Phng and Gerhardt 2009) (Bentley, Mariggi et al. 2009).

1.2.2 **Mechanisms of angiogenesis**

1.2.2.1 **Hypoxia:**

The principal signalling pathway induced by hypoxia involves the activation of a transcription factor, hypoxia-induced factor (HIF), which induces the expression of a set of genes appropriate to respond to this situation. The classical paradigm is that of a change in cellular metabolism induced by HIF1 in conditions of hypoxia, from aerobic metabolism to anaerobic pathways (Semenza 2012). HIF is not functional in oxygenated cells, but becomes active in the presence of hypoxic stress and in various other conditions, such as autocrine stimulation by growth factors or hormones. The target genes of HIF are involved in metabolism, erythropoiesis, pH homeostasis, and autophagy (Semenza 2012). Indeed, HIFα controls the expression of numerous major players involved in angiogenesis and vascular remodelling, including vascular endothelial growth factor (VEGF-A) and its receptor VEGFR1, CXCL12 (stroma-derived factor 1 or SDF-1), angiopoietin 2, platelet-derived growth factor (PDGF-BB), and SCF (stem cell factor) or c-Kit ligand.

Mice constitutively expressing HIF1-α in cardiomyocytes display improved cardiac function after MI, associated with increased VEGF expression and angiogenesis in the myocardium (Kido, Du et al. 2005). The prominent role of the HIF pathway in post-ischemic angiogenesis has further been shown through its indirect activation by Prolyl Hydroxylase Domain proteins (PHDs). Oral administration of a PHD inhibitor in rats improved microvascular density in the peri-infarct area, preventing deterioration of cardiac function and left ventricle (Silvander, Kvarnstrom et al.) dilation after MI (Bao, Qin et al. 2010). In a model of hind-limb ischemia, knockdown of PHD enhanced neovascularization through upregulation of VEGF and endothelial Nitric Oxide Synthase (eNOS) as well as recruitment of proangiogenic myeloid cells (Loinard, Ginouves et al. 2009).

1.2.2.2 ***Inflammation:***

The first evidence linking inflammation and angiogenesis was the expression of the proangiogenic Insulin Growth Factor-1 (IGF-1) by infiltrating monocytes in the ischemic porcine myocardium associated to capillary sprouting after microembolization (Kluge, Zimmermann et al. 1995). During ischemia, inflammatory cells release angiogenic factors, such as VEGF and TNF-α, that enhance vascular permeability and promote the recruitment of further inflammatory cells (Costa, Incio et al. 2007, Grivennikov, Greten et al. 2010, Eltzschig and Carmeliet 2011, Konisti, Kiriakidis et al. 2012). Leukocytes and macrophages release matrix, among others, metalloproteinases (MMPs), plasminogen and cathepsins, that promote extracellular matrix (ECM) remodelling, favouring the formation of new vessels (Rüegg 2006, Kundu and Surh 2012). Neutrophils also release chemokines that enhance both, angiogenesis and inflammation (Kundu and Surh 2008, Noonan, De Lerma Barbaro et al. 2008). Finally, inflammatory cells produce Reactive Oxygen species (Masotti, Miller et al.) that act as a proangiogenic stimulus (Guzik, Korbut et al. 2003, Reuter, Gupta et al. 2010).

Consistently with this relationship between angiogenesis and inflammation, different molecules that are relevant in inflammation have been involved in new vessel formation. For instance, monocyte chemoattractant protein-1 (MCP-1) induces collateral growth after femoral artery occlusion in the rabbit (Ito, Arras et al. 1997). This effect is mediated by the attraction of monocytes and depends on the presence of Intercellular Adhesion Molecule-1 (ICAM-1)(Hoefer, van Royen et al. 2004). Similarly, P-selectin is involved in angiogenesis, as P-selectin knockout mice show reduced reperfusion and less leukocytes expressing VEGF after hind limb ischemia (Egami, Murohara et al. 2006). Also, TNF-α enhances progenitor cell homing, VEGF and bFGF expression, and angiogenesis in mice hind limb ischemia (Kwon, Heo et al. 2013) (Goukassian, Qin et al. 2007). Toll-like receptors (TLRs), that play a key role in innate immunity (Takeda and Akira 2004, Kawai and Akira 2006, Grote, Schütt et al. 2011), represent a clear example of the intersection between angiogenesis and inflammation, as they are expressed in ECs

(West, Malinin et al. 2010, Grote, Schütt et al. 2011) and have been implicated in angiogenesis, and in VEGF expression (Leibovich, Chen et al. 2002, Pollet, Opina et al. 2003, Grote, Schuett et al. 2010, Paone, Galli et al. 2010).

There is also a synergy between the hypoxia pathway, controlled by HIF, and the induction and intensity of the inflammatory reaction, which is modulated principally by the transcription factor NF-κB. HIF-dependent hypoxic responses and the NF-κB-dependent inflammatory response are thus interdependent, and they amplify each other. Some inflammatory cytokines, including transforming growth factor (TGF)-β (McMahon, Charbonneau et al. 2006) and interleukin (IL)-1β (Hellwig-Burgel, Rutkowski et al. 1999), may favour HIF-1 activity. Alternatively, the HIF pathway controls expression of the chemokine CXCL12, which plays a major role in the post-ischemic inflammatory reaction (Loinard, Ginouves et al. 2009).

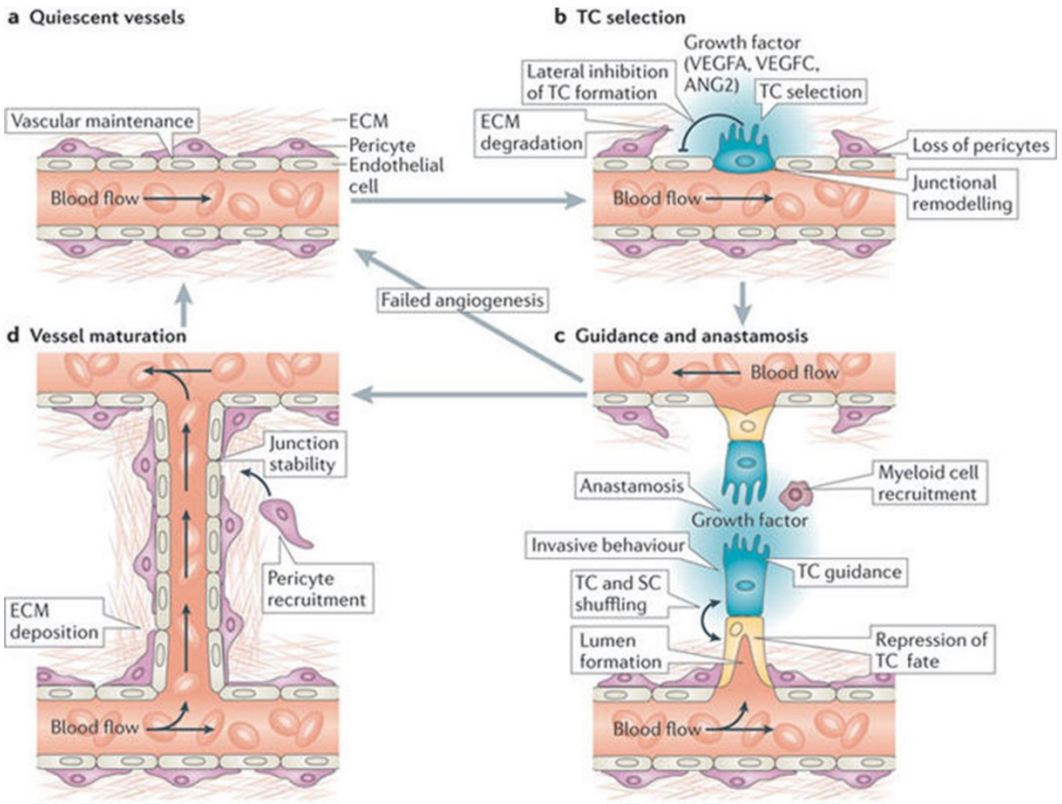

Figure 1.2*:* **Mechanism of angiogenesis**
Shane P. Herbert & Didier Y. R. Stainier Nature Reviews Molecular Cell Biology **volume 12**, pages 551–564 (2011)

1.2.3 **Mechanisms of endothelial cell migration**

Endothelial cell migration in an angiogenic sprout is a guided and, therefore, directed process and guidance cues are provided by the local environment (Michaelis 2014).

During sprouting angiogenesis, the previously described concept of tip and stalk cells is operative. The first step is, therefore, the selection of the cell that initiates sprout formation and becomes the tip cell. This is necessary because if all cells reacted in the same way to the stimulus, they would migrate in a similar manner and the vessel would disintegrate. Thus, only one tip cell has to become privileged to migrate by a fine-tuned feedback loop

entertained by VEGF and the Notch/Dll4 system (Hellstrom, Phng et al. 2007, Suchting, Freitas et al. 2007, Phng and Gerhardt 2009). Endothelial cell polarization and hence the directionality of filopodia extension during migration is dependent on Cdc42 activation (Gerhardt 2008).

Recently, the role for Hippo effectors YAP and TAZ in the regulation of vascular network remodelling through controlling ECs proliferation, filopodia formation, and cell migration has been characterized (Sakabe, Fan et al. 2017). The study demonstrated that a novel cytoplasmic function of YAP in the regulation of ECs migration through controlling the Rho family GTPase CDC42 activity. Moreover, these findings demonstrated a previously unrecognized YAP/TAZ function involved in the vascular network remodeling during angiogenesis (Sakabe, Fan et al. 2017).

The formation of branch-like filopodia by tip ECs is mediated by remodelling of the actomyosin and microtubule cytoskeleton, similar to the way in which neurite extensions protrude from neuronal cell bodies (Gerhardt, Golding et al. 2003). The formation of endothelial branches from lamellipodia has been described to be dependent on the local attenuation of myosin II-mediated contraction. The process is a consequence of a local loss of RhoA and RhoA kinase (ROCK) activity leading to reduced myosin light-chain phosphorylation. As a consequence, the cell branches by ‘‘escaping’’ retraction through cortical tension (Fischer, Gardel et al. 2009).

1.2.4 **Endothelial dysfunction and vascular disease**

Under basal conditions, the endothelium functions to maintain the vessel in a relatively neutral state favouring dilatation over constriction. The endothelial-dependent response to vasodilate is principally regulated in response to shear stress by a release of nitric oxide (NO) synthesized from the amino acid L-arginine by endothelial nitric oxide synthase (eNOS) (Vanhoutte, Shimokawa et al. 2017). Dysfunctional endothelium is seen when there is an imbalance between NO production and consumption. Such a pathologic state creates favourable conditions for platelet plus leukocyte activation and adhesion, as well as the activation of cytokines that increase the permeability

of the vessel wall to oxidized lipoproteins and inflammation mediators, finally resulting in structural damage of the arterial wall with smooth muscle (SMC) cell proliferation and atherosclerotic plaque formation (Vanhoutte, Shimokawa et al. 2017).

Abnormal endothelial function is attributed to high oxidative stress and inflammation – both processes lead to abnormal NO metabolism. Increased oxidative stress is characterized by a measurable increase in reactive oxygen species (Masotti, Miller et al.) which can result from impaired NO synthase, decreased L-arg uptake, increased oxidized LDL cholesterol (Ox-LDL), (Vergnani, Hatrik et al. 2000) or reduced superoxide dismutase (SOD) an enzyme pivotal in the clearing of ROS (Landmesser, Spiekermann et al. 2002). Another potential contributor to impaired NO bioavailability is the decrease in tetrahydrobiopterin (THB)(Li, Chen et al. 2011) or the presence of elevated levels in plasma of asymmetric dimethylarginine (ADMA), which is an endogenous competitive inhibitor of NO (Boger, Lentz et al. 2001).37,38 Finally, low-flow vascular states such as reduced cardiac output which reduces endothelial shear stress in conditions such as heart failure – possibly from reduced L-arginine (Hingorani, Cross et al. 2000).

Endothelial dysfunction is seen in patients with a family history of early cardiovascular disease and other risk factors such as hypertriglyceridemia (Lundman, Eriksson et al. 2001), elevated LDL and reduced HDL cholesterol (Ford, McConnell et al. 2009), nicotine use (Lavi, Prasad et al. 2007),10 obese patients with minimal coronary artery disease (CAD) (Al Suwaidi, Higano et al. 2001), patients with insulin resistant (Arcaro, Cretti et al. 2002) and elderly patients (Egashira, Inou et al. 1993).

The true prevalence of peripheral endothelial function worldwide is not fully known as I only have samples of larger studies which assess peripheral endothelial function in different methods and without specific guidelines regarding cut-off values for which a patient's endothelium is considered dysfunctional. Observations demonstrated that roughly 50% of those undergoing clinically indicated coronary angiography, but without obstructive

disease were found to have coronary endothelial dysfunction (Sharaf, Pepine et al. 2001).

The quantification of endothelial health has commonly been divided into peripheral endothelial function – a systemic measure of endothelial function – versus coronary endothelial function, which must be assessed with invasive angiography. Testing involves pharmacological and/or physiological stimulation of the endothelial release of NO and other vasoactive substances. All the techniques have in common that they measure the response of the vessels to endothelial-dependent stimuli, mainly reactive hyperemia or vasoactive substances. Indeed, both macrovascular endothelial dysfunction, as measured by flow-mediated dilation (Yeboah, Folsom et al. 2009) and microvascular endothelial dysfunction (Anderson, Charbonneau et al. 2011), have been found to be independent predictors of future cardiovascular events in large cohort studies in healthy individuals over and above traditional risk factor assessment.

1.2.5 **Mitochondrial function in vascular disease**

In comparison with other cell types with higher energy requirements, mitochondria content in ECs is modest and it composes 2–6% of the cell volume as opposed to 28% in hepatocytes and 32% in cardiac myocytes (Dromparis and Michelakis 2013). The low content of mitochondria in ECs may indicate that mitochondria-dependent oxidative phosphorylation is not that important for energy supplement in those cells. In fact, ECs obtain a large proportion of their energy from the anaerobic glycolytic metabolism of glucose. Mitochondria are more likely to serve primarily as essential signaling organelles in the vascular endothelium (Quintero, Colombo et al. 2006).

The cellular distribution of mitochondria is important for its function and its communication with another cellular organelle (especially endoplasmic reticulum, ER) and nucleus. For example, in ECs of arterioles isolated from human myocardium, mitochondria are anchored to the cytoskeleton. Those mitochondria release ROS in response to cell deformation by shear stress. (Liu, Li et al. 2008). In addition, exposure of pulmonary artery ECs to hypoxia

triggers a retrograde mitochondrial movement that requires microtubules and the microtubule motor protein dynein, resulting in the perinuclear clustering of mitochondria. This subcellular redistribution of mitochondria is accompanied by the accumulation of ROS in the nucleus, which can be attenuated by suppressing perinuclear clustering of mitochondria with nocodazole to destabilize microtubules (Al-Mehdi, Pastukh et al. 2012). Mitochondria are important component of the intracellular Ca^{2+} signaling and buffering system, played in tight functional and physical association with ER. For example mithocondria and ER distance seems to be critical for Ca^{2+} driven mitochondrial dependent apoptosis in EC during Peripheral Artery Hypertension (PAH)(Sutendra, Dromparis et al. 2011).

Endothelial mitochondria serve as a pivotal sensor of the local environment and transduce damage signals, which leads to mitochondria damage, endothelial dysfunction, vascular remodelling and vascular diseases (Tang, Luo et al. 2014).

Over the last decade, accumulating evidence has suggested a causative link between mitochondrial dysfunction and major phenotypes associated with endothelial senescence (Ziegler, Wiley et al. 2015). EC senescence is associated with impaired mitochondrial biogenesis, reduced mitochondrial mass and altered expression of components of the ETC and other mitochondrial components (Dai, Rabinovitch et al. 2012). Mitochondrial superoxide production increases with replicative senescence. Damaged mitochondria produce excessive superoxide and H2O2, which are major determinants of telomere-dependent senescence at the single-cell level that is responsible for cell-to-cell variation in replicative lifespan (Passos, Saretzki et al. 2007).

Dysfunction of the ETC critically participates in endothelial senescence. Deficiency of mitochondrial ETC complex IV plays an essential role in senescence-induced mitochondrial dysfunction. Mitochondria of senescent HUVECs show a significant and equal decrease in both fusion and fission activity, indicating that these processes are sensitive to aging and could

contribute to the accumulation of damaged mitochondria during aging (Jendrach, Pohl et al. 2005)

Decreased expression of Drp1 and Fis1, two proteins regulating mitochondrial fission, mediates mitochondrial elongation in senescent cells (Mai, Klinkenberg et al. 2010). Loss of mitochondria dynamics and mitochondrial potential are associated with increased ROS production and mtDNA damage and decrease mitochondria biogenesis and NO production in cultured ECs (Mai, Klinkenberg et al. 2010). High glucose and continuous oxidation of high density lipoprotein (HDL) under hyperglycemic condition induce mitochondrial dysfunction and EC apoptosis through mitochondrial fission and mitochondrial and cytosolic ROS generation (Matsunaga, Iguchi et al. 2001). Dysfunctional mitochondria are isolated from the mitochondrial network and are eliminated by selective type of autophagy called mitophagy. PINK and PARKIN are part of a well known mitochondrial quality control mechanism able to sense loss in mitochondrial potential, lipid and protein peroxidation and protein ubiquitination on the surface of damage mitochondria. Mitophagy is an important response to restrain excessive mROS production and its role in the surveillance and maintenance of functional mitochondria is highlight by the fact that many cardiovascular pathologies including diabetes mellitus, atherosclerosis and hypertensive heart shown impaired mitophagy. (Mai et al.,2012; Higdon et al.,2012). Moreover mitochondrial ROS in particular H2O2 are positive inducers of autophagy during environmental stress condition like hypoxia or starvation (Scherz-Shouval, Shvets et al. 2007).

1.2.6 **Vascular senescence**

Aging is a known major risk factor for cardiovascular disease (Niccoli and Partridge 2012). The aging process is also associated with adverse hemodynamic and metabolic changes that accelerate the development of cardiovascular disease. It is now accepted that changes in cardiovascular structure and function occur in healthy individuals as they age. These

alterations precede the onset of clinical disease and predict the future risk of developing atherosclerosis, hypertension and heart failure (North and Sinclair 2012). The age-associated changes in blood vessels that occur in healthy individuals include increased arterial wall thickness, luminal dilatation and reduced compliance (Minamino and Komuro 2008). In addition to these structural changes, endothelial function becomes impaired with increasing age, thereby increasing arterial stiffness. Aged ECs develop a dysfunctional phenotype that is characterized by reduced proliferation and migration, less expression of angiogenic molecules, and low production of nitric oxide (NO). Moreover, dysfunctional/senescent ECs develop pro-oxidant, pro-inflammatory, vasoconstrictor, and prothrombotic properties. Moreover, evidence indicates that cardiovascular repair systems become progressively impaired with aging (Lakatta 2003, Lakatta and Levy 2003, Lakatta and Levy 2003).

These impairments are attributed to the reduced production of proangiogenic factors (Fontana, Vinciguerra et al. 2012), impaired cell replication (de Almeida, Ribeiro et al. 2017), and a decrease in the number and function of stem and/or progenitor cells (Zhuo, Li et al. 2010, Cesselli, Aleksova et al. 2017). Even if these age-associated changes do not result in overt cardiovascular disease per se, they impair the capacity of the cardiovascular system and influence the severity and prognosis of subsequent disease. A senescent endothelial cell presents senescence-associated morphological alterations and functional adaptations, like senescent fibroblast (Unterluggauer, Hutter et al. 2007) . Most commonly, senescence-associated beta-galactosidase (SA-β-gal) activity is used to identify senescent cells. Lysosomal beta-galactosidase activity is normally detected at a low pH (usually pH 4), but becomes detectable at a higher pH (pH 6) in senescent cells due to marked expansion of the lysosomal compartment (Dimri, Lee et al. 1995). Cellular senescence is associated with the acquisition of the Senescence-Associated Secretory Phenotype (SASP), which is characterized by the activation of a pro-inflammatory transcriptional program (Acosta, Banito et al. 2013, Childs, Durik et al. 2015). According to a

recent hypothesis, the build-up of cells expressing the SASP may promote the development of both diabetes and its vascular complications (Childs, Durik et al. 2015, Palmer, Tchkonia et al. 2015).

Cellular and molecular mechanisms underlying age-associated changes of the cardiovascular system have been studied, but it remains unclear exactly how these alterations occur with advancing age. Interestingly, the main pathways involved in cellular senescence regulation, such as the NF-κB, the mechanistic target of rapamycin (mTOR), and the interleukin-1/NLR family pyrin domain containing 3 (IL-1/NLRP3) inflammasome pathways, are master modulators of the aging rate (Johnson, Rabinovitch et al. 2013, Youm, Grant et al. 2013, Zhang, Li et al. 2013). A number of adaptor proteins have been shown to control SASP factor secretion. The SASP is mostly induced by NF-κB, the main immunological transcription factor (Chien, Scuoppo et al. 2011). Upstream, p38 (Freund, Patil et al. 2011), JAK (Xu, Tchkonia et al. 2015), and other MAP kinases (Ferrand, Kirsh et al. 2015), are all involved in SASP induction and control. Interestingly, Jak2/Stat3 pathway inhibition redesigns the SASP, suppressing the secretion of certain factors indicating that selective SASP modulation could be feasible (Toso, Revandkar et al. 2014). Finally, highly interesting results in terms of SASP suppression have been obtained with the mTOR inhibitor rapamycin (Laberge, Sun et al. 2015), which has long been known to extend lifespan and health span in mice (Laberge, Sun et al. 2015). mTOR controls SASP protein secretion by enhancing IL-1α and MAP kinase activated protein kinase 2 (MAPKAP2) translation (Herranz, Gallage et al. 2015).

Interventions directed at preventing the adverse effects associated with the SASP are being explored. The most promising strategies involve delaying cellular senescence (Jurk, Wilson et al. 2014); SASP switch-off (Herranz, Gallage et al. 2015); SASP factor modulation (Toso, Revandkar et al. 2014); and selective removal or killing of existing senescent cells (Chang, Wang et al. 2016). Selective targeting and killing of senescent cells without damaging neighbouring, healthy cells requires identifying senescence-associated markers. High-throughput “omics” technologies (i.e., genomics,

metabolomics, metagenomics, and transcriptomics) are being applied to discover such markers (Valdes, Glass et al. 2013). Highly promising results are coming from work on SASP suppressor and senolytic agents (Childs, Gluscevic et al. 2017).

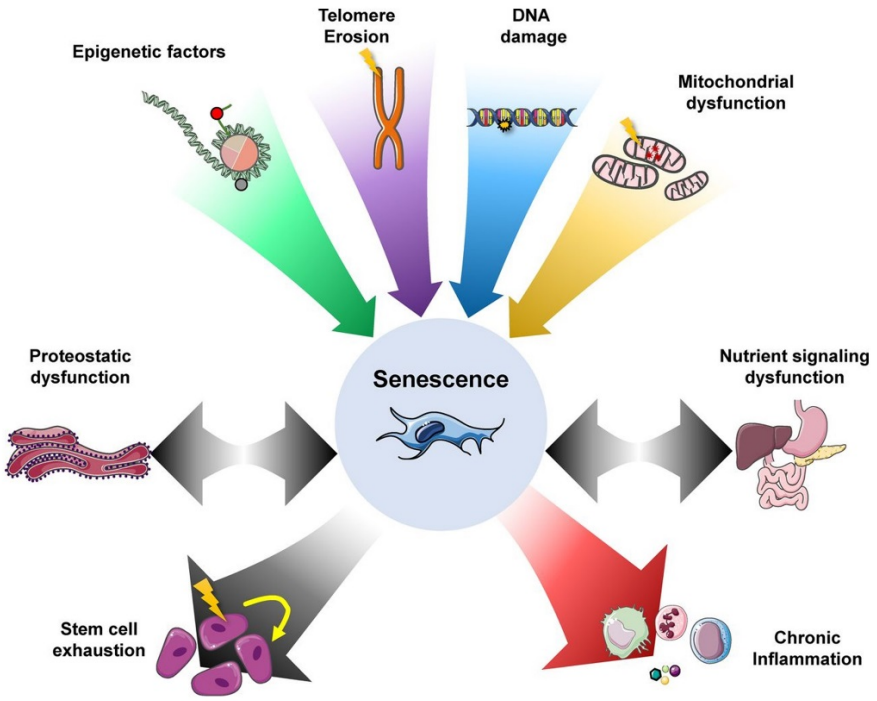

Figure 1.4: Senescence as a central hallmark of aging.
Graphical summary of the main causes leading to senescence and effects senescent cells produce in the surrounding tissue.
From Domhnall McHugh, and Jesús Gil *J Cell Biol* 2018;217:65-77

1.3 **Autophagy**

1.3.1 **Definition of autophagy**

Autophagy is a complex intracellular process that delivers cytoplasmic constituents for degradation into lysosomes. Three main types of autophagy have been described: microautophagy (Mizushima and Komatsu 2011), comprising direct engulfment of cytoplasmic material by lysosomes via inward invaginations of the lysosomal membrane, macroautophagy (Feng, He et al. 2014), characterized by formation of double-membrane sequestering compartments termed autophagosomes that fuse with lysosomes for delivery of cytoplasmic cargo, and chaperone-mediated autophagy (Klionsky, Abdalla et al. 2012), mediated by a chaperone complex and lysosomal-associated membrane protein type 2A to degrade cytosolic proteins with a specific targeting motif. Autophagy occurs at basal levels in most tissues to allow constitutive turnover of cytosolic components but is stimulated by environmental stress-related signals (eg, nutrient deprivation and oxidative injury) to recycle nutrients and to generate energy for maintenance of cell viability in adverse conditions (Klionsky, Abdalla et al. 2012). In addition to cellular stress, basal autophagy can be intensified by specific drugs, indicating that the autophagic machinery is a potential therapeutic target for diverse diseases. Indeed, given that autophagy is involved in the prevention of different human pathological conditions, including heart and liver disease, cancer, neurodegeneration, as well as infectious and metabolic disorders, the development of highly specific autophagy modulators has become a major clinical priority.

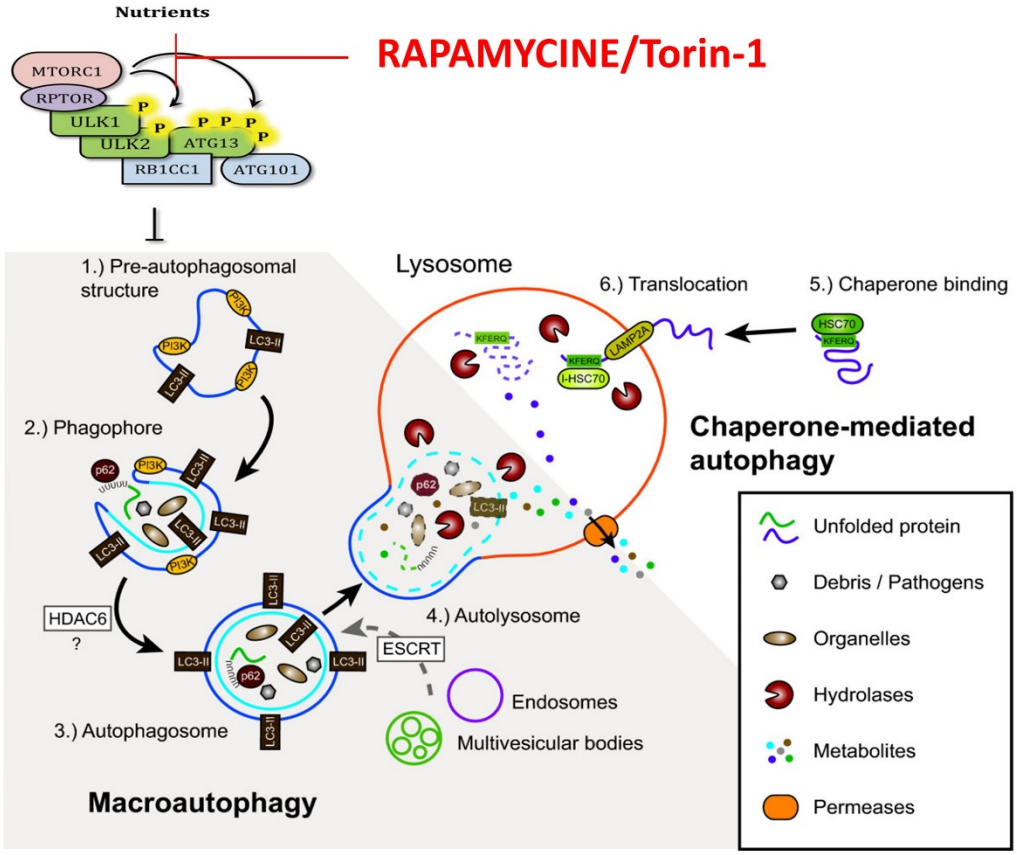

Figure 1.3: **Mechanisms of autophagy**
A simplified and schematic view of the main steps occurring during Macroautophagy.
Modified from Jaeger and Wyss-Coray *Molecular Neurodegeneration* 2009 **4**:16

1.3.2 **Regulation of autophagy**

One of the major regulators mTOR, an evolutionarily conserved serine/threonine kinase, which integrates metabolic signals including amino acids and growth factors as well as oxygen and energy level to coordinate cell growth, proliferation, and metabolic processes to maintain cellular homeostasis. mTOR forms two complexes with distinct functions, but only mTOR complex 1 (mTORC1) has been described in the regulation of autophagy: active mTORC1 performs an inhibitory effect on autophagy

induction by phosphorylating the initiation complex members (Meijer, Lorin et al. 2015)

TORC1 activity is regulated by multiple signalling pathways and molecules. Upon receptor tyrosine kinase activation in the presence of insulin-like and other growth factors, the serine/threonine kinase AKT phosphorylates and thus inhibits tuberous sclerosis complex (TSC1/TSC2), a GTPase-activating protein (GAP) for the small GTPase Rheb (Zhang, Gao et al. 2003). Consequently, Rheb is stabilized in an active, GTP-bound form and activates mTORC1, thereby repressing autophagy (Long, Ortiz-Vega et al. 2005). Subcellular localization of mTORC1 has an essential role in its regulation, as well. Amino acid sufficiency promotes the activation of RAG GTPases in a Ragulator complex-dependent manner (Sancak, Bar-Peled et al. 2010).

5′-AMP-activated protein kinase (AMPK), activated upon low cellular energy levels, regulates autophagy positively both by direct phosphorylation of ULK1 and indirectly by repressing mTORC1 activity (Bach, Larance et al. 2011). Autophagy regulation is not confined to the modulation of the induction. Upon hypoxia, HIF1α transcription factor activates expression of several genes necessary for metabolic adaptation to low oxygen levels. Among these hypoxia responsive genes, there are BNIP3 and BNIP3L, which were found to increase mitochondrial autophagy (Ney 2015). Among others, the ER-associated IP(3) receptor functions as an autophagy inhibitor by forming a complex with BECN1 and probably Bcl-2 (Vicencio, Ortiz et al. 2009). In addition, upon nutrient starvation, c-Jun N-terminal protein kinase 1 (JNK1) contributes to the induction of autophagy by phosphorylating Bcl-2 and thereby disrupting its interaction with BECN1 (Wei, Pattingre et al. 2008)

Oxidative stress promotes autophagy in another VPS34-dependent manner as well. Under these conditions, death-associated protein serine/threonine kinase (DAPK), a well-known regulator of cell death activates protein kinase D (PKD), which subsequently phosphorylates VPS34 leading to increased autophagosome formation (Eisenberg-Lerner and Kimchi 2012).

1.3.3 **Autophagy in ECs**

There is a growing body of literature that suggests that loss of autophagy may be a central mechanism through which risk factors elicit endothelial dysfunction, and that autophagy may be involved in the regulation of nitric oxide (NO) bioavailability.

For example, in ECs, shear stress–induced increases in endothelial nitric oxide synthase (NOS3) phosphorylation and NO production are markedly blunted in autophagy-deficient cells. Coincident with a reduction in NO, loss of autophagy promotes an increase in endothelial reactive oxygen species (Masotti, Miller et al.) and inflammatory cytokine production, suggesting that autophagy may regulate shear stress–induced vascular homeostasis, in part, through an NOS3-dependent pathway (Bharath, Mueller et al. 2014). These data have recently been confirmed using an ex vivo model of steady laminar shear stress, wherein autophagy inhibition (with 3-methyladenine) inhibits NOS3 expression, whereas autophagy stimulation (with rapamycin) increases endothelial NOS3 expression (Guo, Li et al. 2014). Emerging evidence also suggests that endothelial autophagy might modulate the uncoupling of NOS3 (with an increase in superoxide versus NO production). Similarly, recent data also suggest an important role of intracellular NO in the regulation of mitophagy, the selective process involving autophagic degradation of mitochondria.

A link between endothelial autophagy and angiogenesis comes from the analysis of mice deficient in AKT3. These animals have an impaired angiogenic response using a standard subcutaneous Matrigel plug assay. This same study also demonstrated that knockdown of AKT3 induces autophagy in ECs. Interestingly, this induction seemed to be independent of MTOR (a known AKT substrate and target) and instead dependent on XPO1/CRM1 (exportin 1/CRM1 homolog yeast), the major nuclear export receptor (Corum, Tsichlis et al. 2014). These data and the observations

discussed above suggest a negative correlation between autophagic flux and angiogenesis.

1.3.4 **Autophagy as therapeutic target in vascular diseases**

Considerable enthusiasm has emerged for the development of autophagy-inducing agents for the prevention or treatment of diseases in which the upregulation of autophagy is thought to be clinically beneficial (Levine, Packer et al. 2015). Several drugs currently approved by the FDA induce autophagy but generally have pleiotropic actions, making it difficult to parse out the role of autophagy induction in their therapeutic actions in patients. Nonetheless, preclinical studies demonstrate that certain autophagy-inducing agents fail to induce their beneficial effects in host organisms that are deficient in autophagy genes (Rubinsztein, Codogno et al. 2012).

FDA-approved compounds have been “repurposed” for use in preclinical models of diseases that are believed to respond favourably to autophagy enhancement, e.g., mTOR inhibitors in neurodegenerative diseases, EGFR and other tyrosine kinase inhibitors in diabetic nephropathy (Sarkar 2013).

Several drugs that have the potential to inhibit or stimulate autophagy have already been identified, and now ongoing clinical trials are testing their association with cytotoxic drugs in a variety of cancers (Towers and Thorburn 2016).

Activators of autophagy, for instance, rapamycin and its derivatives (everolimus) that trigger autophagy through the inhibition of mTOR have been evaluated as potential plaque stabilizing drugs. Local stent-based delivery of everolimus in atherosclerotic plaques from cholesterol-fed rabbits led to a striking reduction in macrophage content without altering SMCs (Vicencio, Ortiz et al. 2009).

Carbamazepine, valproic acid increases the intracellular clearance of misfolded protein accumulation through induction of autophagy by reducing the intracellular levels of IP3 (Williams, Cheng et al. 2002)

Interestingly, stimulation of autophagy by valproic acid decreases calcification by reducing matrix vesicle release in vascular SMCs (Dai, Zhao et al. 2013). Additionally, using a cell-based screening method, several calcium channel blockers and antiarrhythmic drugs, such as verapamil, loperamide, amiodarone, nimodipine, nitrendipine, niguldipine and pimozide, have been identified as autophagy inducers by inhibiting intracellular levels of calcium (Fleming, Noda et al. 2011)

The pan-caspase inhibitor benzyloxycarbonyl-Val-Ala-DL-Asp(O-methyl)-fluoromethylketone (z-VAD-fmk) can induce autophagy and necrotic cell death in macrophages and, indirectly, necrosis of vascular SMCs based mainly on the differential expression of receptor-interacting protein 1 (Martinet, Schrijvers et al. 2006). Trehalose, a disaccharide, enhances the clearance of autophagy substrates (Sarkar, Davies et al. 2007) . Trehalose supplementation restores the expression of autophagy markers and rescues vascular endothelial function by increasing NO bioavailability, reducing oxidative stress and normalizing inflammatory cytokines in arteries of ageing mice (Sarkar, Davies et al. 2007).

1.4 **Hypothesis**

The hypothesis addressed in this Thesis is:

“TCHP plays an important role in regulating the functionality of ECs acting through autophagy”

1.5 **Aims**

To address this hypothesis, experiments have been designed to determine whether:

1. TCHP regulates EC function.
2. TCHP regulates autophagic flux and senescence in ECs
4. Deficiency of TCHP in ECs alters mitochondrial function

CHAPTER 2:

Materials and Methods

Cell lines and cell culture

Human cell lines were the experimental model used in this study. HEK293T were grown in Dulbecco's modified eagle's medium (DMEM), BE12-741F, with 4.5g/L glucose, 2mM L-Glutamine, without Na Pyruvate manufactured by Lonza. 10% v/v Fetal bovine serum (FBS) and 1% v/v Penicillin/Streptomycin (Pen/Strep) were added to make complete media. HUVECs were the predominant in vitro model used in this study. HUVEC, catalogue number (cat#) C2519A, lot number (lot#) 0000466716 purchased from Lonza were cultured in endothelial basal media-2 (EBM™-2) purchased in the form of SingleQuots™ Kit, CC-4176, containing all supplementary growth factors required.

Endothelial cells from patients

The study was performed with the approval of the South-East Scotland Research Ethics Committee, in accordance with the Declaration of Helsinki and with the written informed consent of all participants. Patients with premature coronary artery disease and a family history of premature coronary artery disease (n = 8) were identified from the outpatient department, Royal Infirmary of Edinburgh, Scotland, UK. A control group of healthy age- and sex-matched subjects (n = 8) with no evidence of significant coronary artery disease following computed tomography coronary angiography (CTCA) was recruited from the Clinical Research Imaging Centre, Royal Infirmary of Edinburgh. Subjects attended the Clinical Research Facility at the Royal Infirmary of Edinburgh for vascular assessment and tissue sampling. Vessel wall endothelial cells were isolated by wire biopsy for in vitro expansion(Brittan, Hunter et al. 2015).

Lentiviral vectors

Two pLKO based, self-inactivating lentiviruses, able to infect mammalian cells lines, were produced for this study. One lentivirus vector was produced to knock-down the expression of TCHP using a short hairpin RNA (shRNA)

specifically targeting TCHP mRNA transcripts. A control lentivirus encoding a scrambled shRNA sequence was also produced. The pLKO DNA plasmid containing the shRNA sequence against human TCHP, was purchased from Sigma Aldrich Mission®RNAi team, product code TRCN0000127662. The scramble sequence shRNA plasmid was purchased from Addgene, plasmid #1864. Lentiviral vectors were produced by the Biomolecular Core of the Shared University Research Facilities at Edinburgh University. The packing plasmids used were pCMV-dR8.2 dvpr, plasmid #8455 from Addgene, and pCMV-VSVG, plasmid #8454 from Addgene respectively. HUVECs were infected with an MOI of 20 for 12-16 hours.

Impedance based scratch assays and barrier functions experiments

Electric Cell-substrate Impedance Sensing (ECIS) is an in vitro impedance measuring system to quantify the behavior of cells within adherent cell layers. Migration assay and endothelial barrier function were performed using ECIS machine using 8W1LE and 8W10E array, respectively. 60,000 cells are grown on the arrays on top of opposing, circular gold electrodes. A constant small alternating current is applied between the electrodes and the potential across is measured. The insulating properties of the cell membrane create a resistance towards the electrical current flow resulting in an increased electrical potential between the electrodes. The basis for the measurement of the electrical impedance of cells is Ohm's law, a basic electro-technical principle, which describes the relation between resistance (R), current (I) and voltage (U) in an electrical circuit at a given time (t). For the barrier function, the cell monolayer are stimulated with 20 ng/ml of VEGF and impedance is record for 24 hrs. For the migration, the gap in the monolayer is performed increasing the voltage on the electrodes. Speed is determined as the time the cells re-establish the monolayer.

Total protein extraction and quantification

Cells were rinsed once with ice-cold PBS when still in the plate, lysed with RIPA lysis buffer (20 mM Tris-HCl (pH 7.5),150 mM NaCl, 1 mM Na2EDTA, 1 mM EGTA, 1% NP-40, 1% sodium deoxycholate, 2.5 mM sodium pyrophosphate, 1 mM β-glycerophosphat, 1 mM Na3VO4, 1 µg/ml leupeptin and one tablet of EDTA-free protease inhibitor [Roche] per 10 ml) and collected in a tube using scrapers. The tubes contening the cells suspension were left 20 minute on ice to let the lysis complete and centrifuged at 13.000 r.p.m. in order to separate the cell lysate to the insoluble membranes. The Pierce™ BCA protein determination method was used to quantify the total amount of protein in order to load both SDS-PAGE and Native-PAGE gels. All protein determination assays were performed using the Pierce™ BCA protein assay kit cat# 3225 from Thermo Fisher Scientific. Protein determinations were performed according to the manufacturer's instructions. Briefly, 3 or 5 µl of the unknown samples are placed in the wells of a Microplate and then mixed with 200µl of working reagent made of 50:1 ratio of BCA Reagent A (sodium carbonate, sodium bicarbonate, bicinchoninic acid and sodium tartrate in 0.1M sodium hydroxide) and BCA Reagent B (4% cupric sulphate). After an incubation at 37 degrees for a variable period of time (usually between 30min to 2 hours) depending on the amount of proteins present in the samples, the absorbance for each samples and the standard curve was read at 562 nm with a standard platereader. The protein concentration was derived interpolating the 562nm absorbance value of each unknown samples with the absorbance values of known concentrations of a BSA standard curve. Usually 10 or 20 µg of proteins for samples were used for subsequent Western Blot application.

Western blot

Western blot was performed to assess protein expression levels. Sodium dodecyl sulfate - polyacrylamide gel electrophoresis (SDS-PAGE) analysis

using variable acrylamide percentage gels were prepared using Bio-Rad Mini-Protean® Tetra hand cast system. Standard compounds used; ProtoGel 30% (w/v) Acrylamide:0.8% (w/v) Bis-acrylamide stock (37.5:1), National diagnostics. TEMED, Cat# 161-0800, Bio-Rad. SDS, L4390-500g, Sigma Aldrich. Samples were treated by addition of Laemmli buffer 2x (65.8 mM Tris-HCl pH 6.8, 26.3% (w/v) glycerol, 2.1% SDS,0.01% bromophenol blue) in a 1:1 ratio to sample. The treated samples were incubated for 5 min at 100°C and cooled to 4 C^0 before loading. The electrophoresis was performed submerging the gel in a standard migration buffer (also called running buffer) for PAGE is 1X Tris-glycine Buffer pH 8.3 (25 mM Tris base,190 mM glycine,0.1% SDS). Equal amounts of proteins were loaded onto SDS-Polyacrilamide gels and transferred to Amersham™ Hybond™ 0.2µm polyvinylidene difluoride (PVDF) blotting membrane which was pre-activated with methanol. Mini Trans-Blot® cells were used to transfer proteins from gels to PVDF. The membranes were then blocked with 5% non-fat milk in TBST 0,1% and immunoblotted overnight at 4°C with different primary antibodies listed in the WB table together with their working dilutions. Chemiluminescent detection of proteins of interest was achieved using Immobilon™ Western Chemiluminescent HRP Substrate kit, WBKLS0500 manufactured by Millipore. Kit used as per the manufacturer's instructions. The Western blots were developed on X-ray film using a Konica Minolta SRX-101A medical x-ray film processor. Pixel intensity/quantification was performed using ImageJ.

Table 1: Primary and secondary antibodies used for western blotting including manufacturer details and titers used.

Primary Antibodies	Manufacturer details	Titer
Tom20 rabbit polyclonal IgG	Santa Cruz Biotechnology SC-11415	1:5000
Tom20 mouse monoclonal IgG	Santa Cruz BiotechnologySC-17764	1:5000

α-tubulin mouse monoclonal IgG	Abcam ab184613	1:5000
β-actin mouse monoclonal	Sigma Aldrich, A5441	1:5000
TCHP mouse monoclonal IgG	Santa Cruz Biotechnology G2 SC-515025,	1:100
Mitochondrial OXPHOS complexes cocktail – raised in mouse, monoclonal	Abcam/MitoProfiler®Total OXPHOS Blue Native WB antibody cocktail MS603-300, lot# J5259 –Mitosciences	1:5000
SQSTM1 rabbit polyclonal IgG	GeneTex, GTX100685-S	1:1000
LC3B rabbit polyclonal IgG	Cell Signalling, CS 2775s	1:2000
mTOR (7C10) Rabbit mAb	Cell Signalling CS 2983	1:1000
Phospho-mTOR (Ser2448) (D9C2) XP® Rabbit mAb	Cell Signalling CS 5536	1:1000
Phospho-p70 S6 Kinase (Thr389) (108D2) Rabbit mAb	Cell Signalling CS 9234	1:1000
Phospho-p70 S6 Kinase (Ser371) Antibody	Cell Signalling CS 9208	1:1000
Phospho-4E-BP1 (Thr37/46) (236B4) Rabbit mAb	Cell Signalling CS 2855	1:1000
CDKN2 Purified Mouse Anti-Human p16	DB Bioscience 551154	1:250
PARP1 policlonal anti Rabbit	Bethyl Laboratories A301-376A	1:1000
Poly (ADP-ribose) (10H) Mouse IgG MoAb	Immuno-Biological Laboratories 10407	1:1000

Secondary Antibodies	Manufacturer details	Titer
Anti-rabbit IgG	A0545 Sigma - Anti-Rabbit IgG (whole molecule)–Peroxidase antibody produced in goat, lot # 054M4812	1:10000
Anti-mouse IgG	A5906 Sigma - Anti-Mouse IgG (whole molecule)–Peroxidase antibody produced in sheep, lot # SLBJ3608VBC	1:10000

Native-PAGE of mitochondrial electron chain complexes

To assess the effect of TCHP knock-down on the electron transport chain (ETC) also referred to as OXPHOS complexes, Native-PAGE was used to separate the different complexes while in their native conformation followed by western blotting. All products were used according to manufacturer's instructions. The Novex® NativePAGE™ Bis-Tris gel system purchased from Thermo Fisher Scientific was used to separate the mitochondrial electron chain complexes. Kit included Invitrogen NativePAGE™ 3-12% Bis-Tris Gels, cat# BN1001BOX. NativePAGE™ 20X Cathode Buffer Additive, cat# BN2002, lot# 1772846. Native-PAGE™ 20X Running Buffer, cat# BN2001, lot# 1772822. As well as NativePAGE™ Sample Prep Kit, cat# BN008, lot# 1772859.

Mitochondrial isolation protocol

In order to separate OXPHOS complexes using Native-PAGE, mitochondria were isolated from control and TCHP know-down HUVECs. The mitochondrial isolation protocol used by (Frezza et al. 2007) to isolate mouse embryonic fibroblasts (page 289) was used as a starting point to develop the

protocol in HUVECs. Cells were harvested and suspended in ice cold IBc buffer (10 ml of 0.1M Tris-MOPS, 1 ml of EGTA/Tris, 20 ml 1M sucrose made to 100 ml in DH2O, pH = 7.4, Complete™ protease inhibitor added). Cells were then homogenised using a Teflon pestle. A number of centrifugation steps followed in order to isolate the mitochondria from the homogenate.

Solubilisation of mitochondria

Mitochondria isolates were solubilised as per the manual provided with the Native-PAGE system. Digitonin detergent provided in the sample prep kit was used at a final concentration of 2.5% v/v which was found to yield the best solubilization results.

Running Native-PAGE gels

Invitrogen NativePAGE™ 3-12% Bis-Tris Gels were loaded and run according to the manufacture's kit instructions. The gels were transferred onto PVDF membrane for western blotting and subsequent western blot pixel quantification using UN-SCAN-IT gel version 6.1.

Seahorse: Mitochondrial respiration stress test

The Seahorse XFe24, Extracellular Flux analyzer manufactured by Agilent Technologies was used to conduct a mitochondrial stress test to quantify key parameters of mitochondrial respiration under control and TCHP know-down conditions. The test included injecting predetermined volumes of a number of drugs onto cells and measuring oxygen consumptions throughout the time course.

Cell preparation for Seahorse

Control HUVECs and TCHP know-down were plated into Seahorse XF24 V7, 24 well microplate plates and grown to 70% confluence before analysis at

either day three and seven days after infection. Cells were washed three times with fresh culture media just prior to analsysis on the Seahorse system.

Seahorse Bio-analyzer XF Cell Mito Stress Test protocol

The Seahorse XF cell Mito Stress Test was performed on cell preparations using the Seahorse XFe24, Extracellular Flux analyzer. Cell were analyzed four and seven days after infection. Results shown for each day represent the data from individual Seahorse XF24 V7, 24 well microplates.

Flow cytometry

Both control and TCHP know-down cells were analyzed to determine total mitochondrial mass and relative levels of mitochondrial ROS.

Table 2: Fluorescent probes used to quantify mitochondrial mass and mitochondrial ROS.

Probe used in flow cytometry	Manufacture	Final conc. used
MitoTacker®Green FM – Mitochondrial probe (*used to determine mitochondrial mass*)	Life Technologies, cat# M7514	100 nM
MitoTracker®Red CM-H2XRos – Mitochondrial ROS probe (*used to quantification mitochondrial ROS*)	Life Technologies, cat# M7513	50 nM

Probes were incubated with cells for 30 minutes at 36°C prior to washing with PBS and subsequent detachment with trypsin before being analysed. A BD LSR Fortessa (5 laser) flow cytometry analyser was used for all flow cytometry experiments. A minimum of 10000 total events per sample analysed were recorded.

PROTEOSTAT® Aggresome

Cells were grown directly on glass slides previously coated with 10µg/ml Fibronectin and 0.2% gelatin from porcine skin (Sigma G1393. At the appropriate time cells were washed twice with 1X PBS and fixed with4% formaldehyde (Alfa Aesar #43368) for 30 minutes at room temperature. After carefully washed 2 times with PBS cells were permeabilized with Permeabilizing Solution (0.5% Triton X-100, 3 mm EDTA, pH 8.0 in Assay Beffer 1x) on ice, and gently shake for 30 minutes. Cells were then washed twice with 1X PBS and incubated with Dual Detection Reagent (1 µL of PROTEOSTAT® Aggresome Detection Reagent and 2 µL of Hoechst 33342 Nuclear Stain in 2ml of 1x Assay Buffer) for 30 minutes at room temperature protected from light. Carefully the cells were washed other 3-4 times with 1X PBS and the coverslips were mounted with 20 µl of Fluoromount-GR (SouthernBiotech#0100-01) on a microscope slide. Cells were analysed by wide-field fluorescence or confocal microscopy using a standard rhodamine filter set for imaging the cell aggresome signal and a DAPI filter set for imaging the nuclear signal.

Immunofluorescence

80,000 HUVECs cells were plated on fibronectin-coated glass coverslips in 24-well tissue culture plates. Twenty-four hours later, the slides were rinsed with PBS once and fixed for 15 min with 4% paraformaldehyde in PBS at room temperature. The slides were rinsed twice with PBS and cells were permeabilized with 0.05% Triton X-100 in PBS for 5 min. After rinsing twice with PBS, the slides were incubated with primary antibody in 3% BSA O.N. in a cold room, rinsed four times with PBS, and incubated with secondary antibodies diluted 1:1000 in 3% BSA for 45 min at room temperature in the dark and washed four time with PBS. Slides were mounted on glass coverslips using Vectashield (Vector Laboratories) and imaged on Zeis LSM-780 confocal or Zeis Axioskop HBO 50 florescence microscope equipped

with a Photometrics® coolSNAP HQ2 CCD camera and QImaging® CRI Micro*Color 2 RGB Liquid Crystal Tunable Filters were used to image fluorescently stained microtubules.

Table 3: Primary and secondary antibodies used for immunofluorescence including manufacturer details, and titers used

Primary Antibodies	Manufacturer details	Titer
SQSTM1 rabbit polyclonal IgG	GeneTex, GTX100685-S	1:1000
LC3B rabbit polyclonal IgG	Cell Signalling, CS 2775s	1:2000
Tom20 mouse monoclonal IgG	Santa Cruz BiotechnologySC-17764	1:2000
Caveolin-1 (D46G3) XP® Rabbit mAb	Cell Signalling, 3267	1:1000
Clathrin Heavy Chain (D3C6) XP®	Cell Signalling, 4796	1:1000
Rabbit mAb Rab5 (C8B1) Rabbit mAb	Cell Signalling,3547	1:1000
Rab11 (D4F5) XP® Rabbit mAb	Cell Signalling,5589	1:1000
EEA1 (C45B10) Rabbit mAb	Cell Signalling,3288	1:1000
Rab7 (D95F2) XP® Rabbit mAb	Cell Signalling,9367	1:1000
TFEB policlonal anti Rabbit	GeneTex, GTX33541	1:1000
Texas Red™-X Phalloidin	Molecular probes T7471	1:1000

Secondary	Manufacturer details	Titer
Alexa-Fluor ® 555 Goat anti-Rabbit IgG (H+L)	Molecular probes A32727	1:1000
Alexa-Fluor ® 488\ Goat anti-Rabbit IgG (H+L)	Molecular probes A-11008	1:1000
Alexa-Fluor ® 488\ Streptavidin Conjugate	1:1000	1:500

Immunohistochemistry

Samples were fixed in 4% formalin, embedded in paraffin wax and sectioning for histological staining. Sections were incubated overnight at 4 °C with TCHP (Abcam, ab-77622; 1:1000). Capillary and arteriole were stained with Alexa 488-conjugated isolectin-B4 (Molecular Probes, I2141, 1:100).

ImageJ and CellProfiler analysis

CellProfiler software was used to build a pipeline (predefined sequence of analyses) to quantify the localisation/distribution of fluorescent labelled mitochondria. Cells treated with either shRNA scramble (control) or shRNA TCHP were grown and stained with DAPI (to identify the nucleus) and Phalloidin (to labelled F-actin to identify the cell periphery). Tom20, a protein localised to the outer mitochondrial membrane, was labelled with a green Alexa Fluor® 488 conjugated antibody. With these organelles and structural components labelled CellProfiler was used to aid in quantifying the intensity of Tom20 signal on a large number of images/cells. The intensity of the Tom20 signal in sequential areas/rings from the nucleus were measured to quantify the distribution/localisation of the mitochondria. Analysis performed by Mr Gian-Marco Melfi .

Quantification of mitochondrial localization – CellProfiler

Quantification of mitochondrial localisation within defined areas/distance from the nucleus was achieved using CellProfiler. This software allows semi-automated analysis of batches of images. A pipeline was designed and constructed for this particular study .

RNA extraction and quantitative real-time analysis

Total RNA was extracted using miReasy kit (Qiagen). For mRNA analysis, cDNA was amplified by quantitative real-time PCR (qPCR) and normalized to 18S ribosomal RNA. Each reaction was performed in triplicate. Quantification was performed by the 2–ΔΔCt method (Schmittgen and Livak 2008). Primers are listed in table 4.

Table 4: Forward and Reverse primers for each gene assessed by quantitative PCR .

Gene	Forward	Reverse
TFE3	GCTTGATTGTGTACAGTAGTC	TGTGATTGTCTTTCTTCTGC
ULK1	TCAAAATCCTGAAAGGGGGAACTC	ACCAGGTAGACAAGGTTCAA
LAMP1	TAAGAAACATCATGGGTAAATA	GTCGGTAAATTTAAATTCCCAT
LAMP2	AACAAGAGTGACATAGGGAT	CAGCTCTCTCAAATTATGATA
CSTB	CCTTGATGAAGTAGTTTGTCC	AGAAAACAAGAAGTTCCCTT
LC3	ATAGAACGATACAAGGGTGAG	CTGTAAGCGCCTTCTAAATTATC
TFEB	CTATGGGAACAAGTTTGCTG	CAATGACATCATCCAACTCC
TFEC	GAGAATTGGAACACAGAGACAG	GAATTTTCTCAGCGCTGAAATG
PGC1α	GCAGACCTAGATTCAAACTC	CATCCCCTCGATCATAATCCTC
BECLIN	ATGTAGTTGGTATTTAGGGGG	AGTACATCTCTATTGACTGAAA
SQSTM1	GTAGCTGATGGTTTTAGGTAATT	ATGAGTAGCCATTCATTGGTAG
hTCHP	CAGCCGTTACTTCAGGATGTC	GCTGCTCCCGGATTCTTCTTT
mTCHP	TGCACGCCTACCATTGTGAG	GTCGTTCAGCAATCAGCTTCC
18S	CCGAGGGCCTATCATCAACC	CCCCAGTAAAGTGCGGGTCATAA
TBP	GCCAAGAGTGAAGAACAG	GAATGCTGCCAATGGAGCTG
ATF4	GTTCTTCCGATCTGAATCC	ATCCTCCTTGCTGCTGCTTAA
CHOP	AGAACCAGAACCGGAAACGGCAG	TCTCCTTTTCATGCGCTGCTTT
GRP78	GACCTGTTCTTCCTAATTATGTT	ATTGTTTAGGACCTTTATTCC
GRP94	AATAATCCAATTGGTCCTGC	GCCTGCCTGGGTTTATTTACG
HEDEM	GTAGTAGCTAGGTCGGATGAAA	AGTCACTCGTTAATGCTAGTA
XBP1	CTGAGTCCCGAATCAGGTCACAG	ATCCTGGGGAGATGTTTCTGG
CDKN1A	CAGACATGAGTAGGATGGGGAA	TCCCTTATCTTTATCCTTAATT
CDKN1B	TCCTAGTATGGGTTTAGGGTCA	GGCAGCAGTAGTCGTTAGGGG
CDKN2A	ATCATCATTTCAGAGCGCGTTA	CCTATATGATTTTGTTAAAAGG
CDKN2B	ACATGACTGAGGTGGTAGGTGG	GATGTAGCAGACAGATTTTATC
TP53	ACCTATGGAAACTAACTACTTCCTG	ACCATTGTTCAATATCGTCC
IL1A	TGTGAGTTTTGACAGTAGGTGG	TTATTAGATTTTCCTAAATCA

IL1B	CACGTCCCGGGACTCACA	TTACTTGATTGGATCACCATG
IL6	TTCTTCTTATTTCTTAGGGAT	GATGTAGTAATGGCATTGGAA
IL8	TGGCTCTCTTGGCAGCCTTC	CCTTGGGGTCCAGACAGAGC
MCP1	CCTCTCGTGCCTGCTGCTCA	TTGGGGGTCAGCACAGATCTCC
SNAIL	CTGCTGATGATGCATGATCT	ATGATGATTGGGGAAAGGTAA
TGFB1	GGAACACCCATAGGGGTCAGG	ACGCATCGGTTGTTCAATGC
TGFB2	ACCGGCCTTTCCTGCTTCTC	TTGTACACATGATTGCATCTC
VEGFA	CACCCATGGCAGAAGGAGGA	ACACACTCCAGGCCCTCGTC
VEGFR1	CGCTTGCCAGTCACGGTTTC	GGCGACGAATTGACCAAAGC
PDGFRA	TCTGGAGGCGAGCTGGAGAG	ACTRGCAGCGTTGCGGTTGTTG
PDGFRB	CCATCCTACTCATTCAATCCTA	AGAAGTAGTATTCCCATAAAA
CDH5	GCCTGCTTCTCTTCTCGGTCCAA	GTAGTTGATTTGAAATTTCTCCTC
CDH2	CGAGCAGATAGCCCGGTTTC	GAGGGCATTGGGATCAGTCAG
FGF2	GGAGTGTGTGCTAACCGTTACCTG	CTGCCCAGGTCCTGTTTTGG
TEK	GFTCGTCGTTACCTGAATGCAACC	TTGAGATGATCGGTAGGATG

Cells transfection, transduction and functional assays

HUVECs were transduced at 20 MOI using MISSION shRNA Controls or MISSION shRNA TCHP Lentiviral (SIGMA) particles. Cells were incubated with the viral supernatant for 12h. Transduced HUVECs were lysed for RNA extraction between 72h and 1week after transduction, as indicated in figure legends. Lipofectamine RNAiMAX (Invitrogen) was used to transfect HUVECs, with pre-miR-503, pre-miR-control (50nM final concentration), according to the manufacturer's instructions. The following functional assays were performed: BrdU incorporation assay using Cell Proliferation colorimetric assay (Roche); Caspase-activity assay using CaspaseGlo assay (Promega); migration assay was performed using wound healing assay as oreviously described (Caporali, Meloni et al. 2011). Matrigel assay with HUVECs was performed as previously described using BD Matrigel Basement Membrane Matrix (BD Biosciences)

ATP Colorimetric/Fluorometric Assay

1 x 106 cells were lysed in 100µl ATP Assay Buffer. Protein were removed by cell lysate using 10 kDa Spin Column (Cat. # 1997 Biovision). 50µl of sample were added to a 96-well plate. Standard Curve Preparation was

prepared for the colorimetric assay, diluting 10µl of the ATP Standard with 90 µl of dH2O to generate 1 mM ATP standard. 0, 2, 4, 6, 8, 10 µl were added into a series of wells and adjusted to 50 µl/well with ATP Assay Buffer to generate 0, 2, 4, 6, 8, 10 nmol/well of ATP Standard. To each well was added 50µl of Reaction Mix (ATP Assay Buffer 44µl, ATP Probe 2µl, ATP Converter 2 µl ,Developer 2 µl). After an incubation time of 30 min at room temperature, protected from light, were measured the absorbance (OD 570 nm) or fluorescence (Ex/Em = 535/587 nm) in a microplate reader. The signals are stable for over two hrs. Samples concentration was derived interpolating the respective OD to the standard curve values.

NAD/NADH Quantitation

Cellular content was extracted with 400µl of NADH/NAD Extraction Buffer by freeze/thaw two cycles (20 min. on dry ice, then 10 min. at room temperature), or by homogenization. Samples were centrifuged at 14000 rpm for 5 min and transferred in tubes. To detect total NADt (NADH and NAD), 50µl of extracted samples were transferred into labelled 96 well plates. To detect NADH, NAD needed to be decomposed before the reaction. To decompose NAD, extracted samples were heated to 60°C for 30 min in a water bath or a heating block. Under this condition, all NAD has been decomposed, while NADH was still intact. Cooled 50µl of NAD decomposed samples were transferred into labelled 96 well plate. 10pmol/µl standard NADH was generated by dilution and 0, 2, 4, 6, 8, 10 µl of the diluted NADH standard were added to a labelled 96 well plate in duplicate to generate 0, 20, 40, 60, 80, 100 pmol/well standard in a final volume of 50 µl with NADH/NAD extraction buffer. 100 µl of Reaction Mix (NAD Cycling Buffer 98µl ,NAD Cycling Enzyme Mix 2µl) was added to each well of NADH Standard and samples. After an incubation of 5min at RT to convert NAD to NADH, 10 µl NADH developer was added to each well and leaved from1 to 4 hours. The absorbance at 450 nm was measured for each samples and the

concentration of NADH was derived interpolating the respective OD to the standard curve values.

Luciferase assays

For 3'UTR stability assay, HEK 293 cells were transfected with pMIR-REPORTTM Luciferase and pMIR-REPORTTM Renilla constructs carrying TCHP 3'UTR and miR-503 or scrambled oligonucleotide sequence (control). using Lipofectmin 2000™ In Vitro DNA Transfection Reagent (LifeTechnology) Luciferase constructs. Cells were cultured for 48h and assayed with the Dual-Luciferase Reporter Assay System (Promega).

Animal experiments

Mouse experiments are reported in accordance with Animal Research Report of In Vivo Experiments (ARRIVE) guidelines. Experiments were performed in accordance with the Animal (Scientific Procedures) Act (UK), 1986 prepared by the Institute of Laboratory Animal Resources and under the auspices of UK Home Office Project and Personal License. CD-1 mice were made diabetic using streptozotocin (STZ) (Sigma) (Emanueli, Salis et al. 2002) or left normoglycemic after STZ buffer administration alone. STZ was delivered i.p. for 5 consecutive days (40mg/Kg in citrate buffer per each day). Fourteen days after the first STZ injection, glycaemia at fast and glycosuria were measured and only those mice with glycaemia above 200 mg/dL and overt glycosuria entered the protocol. Absence of hyperglycemia and glycosuria in buffer-injected non-diabetic mice was also verified. Animal experiments have been performed by Dr Marco Meloni.

Isolation of endothelial cells from mouse limb muscles

Adductor muscles at 3 mounts in diabetic and non-diabetic mice were rinsed and digested with collagenase II (Worthington) plus DNase I (Sigma) using gentleMACS™ Dissociator, following the manufacture's protocol. Next, ECs were immunomagnetic sorted using a CD31antibody (Miltenyi Biotech) as

reported in (Larsson, Fredlund Fuchs et al. 2009). Experiment performed by Dr Andrea Caporali.

Statistical analysis

Comparisons between different conditions were assessed using 2-tailed Student's t test. If the normality test failed, the Mann-Whitney test was performed. Continuous data are expressed as mean ± SEM of three independent experiments, each performed in triplicate or quintuplicate. P value <0.05 was considered statistically significant. Analyses were performed using GraphPad Prism V.

CHAPTER 3:

Does TCHP regulate EC function and senescence?

3.1 **Introduction**

Blood vessel formation by angiogenesis is a complex multistep process that requires control and coordination of ECs as well as the pericytes and other intra- and extra-vascular supporting cells.

In stable vessels, ECs typically form a monolayer of quiescent cells that line the luminal surface of vascular tubes. In response to pro-angiogenic stimuli, ECs loosen their cell–cell contacts, activate proteases that degrade the surrounding basement membrane and acquire extensively invasive and motile behaviour to initiate new blood vessel sprouting, followed by further vascular morphogenesis and maturation (Potente, Gerhardt et al. 2011). This disrupted balance of angiogenesis contributes to the pathogenesis of numerous disease states including tumour growth and metastasis (Carmeliet and Jain 2011). While it is desirable to block the growth of new blood vessels under these circumstances, the controlled stimulation of angiogenesis is beneficial in ischemic conditions, characterised by impaired local blood supply. Considering the potential clinical benefits of therapeutically manipulating blood vessel growth and blood flow, the mechanisms regulating the angiogenic process have formed a major focus for vascular research over the last two decades.

Disrupted integrity of ECs plays a significant role in the genesis of vascular complications due to diabetes, such as delayed wound healing, ischemia and accelerated atherosclerosis (Nishikawa, Edelstein et al. 2000, Sheetz and King 2002). Early during diabetes, intracellular hyperglycaemia causes EC dysfunction and structural changes in large and small arteries, with tissue hypo-perfusion and hypoxia. Death of ECs by apoptosis leads to a microvascular rarefaction, which favours the formation of peripheral vascular diseases (Brownlee 2001). The migration of ECs is crucial for their normal integrity and for the process of vessel healing. Different mechanisms have been proposed to explain this process, including regulation of endothelial NOS (eNOS) (Hamuro, Polan et al. 2002) and increased reactive oxygen species (Masotti, Miller et al.) production (Lamers, Almeida et al. 2011). Furthermore, diabetes impairs endogenous reperfusion mechanisms and

generation of vessels by angiogenesis, thereby worsening the recovery from an ischemic insult (Martin, Komada et al. 2003).

There is increasing interest in developing diabetes-targeted therapies, which would be more effective than currently available treatments. Thus, the discovery and characterization of novel genes and regulatory pathways in diabetes-induced vascular complication is of vital scientific interest.

Recently, our work demonstrated that microRNA-503 (miR-503) has a prominent role in diabetes-induced impairment of post-ischaemic reparative neovascularisation (Caporali, Meloni et al. 2015) (Caporali, Meloni et al. 2011). Recovery from ischaemic events is delayed in diabetic patients with critical limb ischaemia, due to impairment of reparative angiogenesis, and their plasma miR-503 levels are highly elevated. In addition, type-1 diabetes increases miR-503 in ECs of mouse ischaemic limb muscles (Caporali, Meloni et al. 2011, Caporali, Meloni et al. 2015). Among the targets of miR-503 that I identified, I decided to further characterize Trichoplein (TCHP) for two main reasons: It is a strong and consistent target of mir503 and its role in vascular biology is completely unknown.

TCHP (alias MITOSTATIN) is a cytosolic ubiquitously expressed 62 kDa protein recently identified like keratin-binding protein. Interestingly TCHP was shown to relocate during the epithelial differentiation from cytoplasmic localization to the cell-cell border, closely associated with desmoplakin (Nishizawa, Izawa et al. 2005, Ibi, Zou et al. 2011).

The highest levels of TCHP RNA expression were detected in the heart, skeletal muscle, kidney, liver, and testis (Vecchione, Fassan et al. 2009). The TCHP mature transcript consists of a 3.2 Kb mRNA while a larger 5.5 Kb transcript was observed in the heart and skeletal muscle, and a smaller of 1.24 Kb is usually detected in the heart (Vecchione, Fassan et al. 2009). TCHP binds the centrosomal proteins Odf2 and Ninein, regulating Ninein recruitment to the centrosome, and is, thus, indispensable to the microtubule-anchoring activity of Ninein at the centrosome (Ibi, Zou et al. 2011). It is noteworthy that Ninein appears to have a cytoplasmic distribution in pericyte and ECs with a markedly increased expression in tip versus stalk cells

(Matsumoto, Schiller et al. 2008). Migrating ECs have a highly polarized structure, with the appearance of membrane ruffles at the leading edge and asymmetrical localization of signalling molecules and the cytoskeleton (Lamalice, Le Boeuf et al. 2007). There is a growing body of evidence that the coordinated action of microtubules and actin filaments is necessary for the cell polarization and migration (Li and Gundersen 2008). Thus, the above evidence supports an important role for TCHP in regulating EC migration and angiogenesis.

Both Mir-503 and TCHP were shown to have an opposite effect on the cell cycle progression. In fact, mir-503 negatively regulates G1 to S phase progression (Caporali, Meloni et al. 2011). In contrast TCHP can promote the progression through the cell cycle, counteracting primary cilium formation through Aurora A kinase activation (Inaba, Goto et al. 2016). Defects in cell cycle progression or cilium re-adsorption are associated with cellular senescence. Premature senescence of ECs is recognized to play a key role in the pathogenesis of diabetic vascular complications (Palmer, Tchkonia et al. 2015). When ECs acquire a senescent phenotype, their homeostatic functions become impaired as indicated by a decrease in production of nitric oxide and an increase in expression of adhesion molecules such as ICAM-1 (Foreman and Tang 2003). These alternations lead to endothelial dysfunction, vascular inflammation, and impaired angiogenesis and vascular repair. Specifically, hyperglycaemia promotes senescence of ECs through persistent cell cycle arrest in the G1 phase, increasing senescence-associated β-galactosidase (SA-β-gal) activity and decreasing telomerase function. Moreover, senescent cells acquire the Senescence-Associated Secretory Phenotype (SASP), which is characterized by the activation of a pro-inflammatory transcriptional program (Acosta, Banito et al. 2013, Childs, Durik et al. 2015). According to a recent hypothesis, the build-up of cells expressing the SASP may promote the development of both diabetes and its vascular complications (Childs, Durik et al. 2015, Palmer, Tchkonia et al. 2015).

The identification of TCHP as target of miR-503 led us to examine the relationship between these two genes and whether if the miR-503 related phenotype described in ECs before is partially due to TCHP downregulation. The work herein will attempt to provide more clarity on the role of TCHP in ECs and its possible role in vascular function and senescence.

3.1.2 **Hypothesis**

Since TCHP expression might be negatively regulated by Mir-503 it would be interesting to determine whether TCHP loss may partially recapitulate the detrimental effects of Mir-503 up-regulation on EC function and whether they are modulated by the same stimuli.

Moreover, considering that TCHP is responsible for proper anchoring of microtubules to the centrioles and for Aurora A kinase activation, it seems likely that TCHP may play a role at least during ECs migration and proliferation; the work described in this chapter addressed the hypothesis that:

"*TCHP expression is regulated by mir-503 and TCHP loss has an impact on EC function.*"

3.1.3 **Aims**

In this Chapter, I aim to:

1. Analyze TCHP localization, and regulation by mir-503 and stimuli triggering its expression in ECs
2. Discover whether TCHP inhibition impacts on EC function
3. Discover whether TCHP inhibition promotes premature senescence in ECs

3.2 **Materials and Methods**

Cells and cell culture

Human Umbilical Vein ECs (HUVECs) and Human Micro Vascular ECs (HMVECs) (both from Lonza) were grown in EGM-2 (EBM-2 medium supplemented with growth factors and normal 5mM D-Glucose, NG) and 2% Foetal Bovine Serum (FBS) (Lonza). To mimic diabetes and ischemia *in vitro*, the ECs were maintained in EBM-2 (growth factor free medium) with 2% FBS and 25 mM D-glucose (high glucose, HG). L-Glucose was used as an osmotic control (Cont) at the concentration of 25 mM. HUVECs were used between P2 and P6 passage.

RNA extraction and quantitative real-time analysis

Total RNA was extracted using miReasy kit (Qiagen). For mRNA analysis, cDNA was amplified by quantitative real-time PCR (qPCR) and normalized to 18S ribosomal RNA. Each reaction was performed in triplicate. Quantification was performed by the $2^{-\Delta\Delta Ct}$ method (Schmittgen and Livak 2008). Primers are from Sigma (KiCqStart™ Primers).

Cells transfection, transduction and functional assays

HUVECs were transduced at 20 MOI using MISSION shRNA Controls or MISSION shRNA TCHP Lentiviral (SIGMA) particles. Cells were incubated with the viral supernatant for 12h. Transduced HUVECs were lysed for RNA extraction between 72h and 1week after transduction, as indicated in Figureure legends. Lipofectamine RNAiMAX (Invitrogen) was used to transfect HUVECs, with pre-miR-503, pre-miR-control (50nM final concentration), according to the manufacturer's instructions. The following functional assays were performed: BrdU incorporation assay using Cell Proliferation colorimetric assay (Roche); Caspase-activity assay using CaspaseGlo assay (Promega); Matrigel assay with HUVECs was performed as previously described using BD Matrigel Basement Membrane Matrix (BD Biosciences).

Impedance based scratch assays and barrier functions experiments

Infected cells were seeded on ECIS cultureware (8W1E array) and allowed to reach confluence. Then a wound in the cellular monolayer was generated in by applying a 3-mA, voltage pulse for 20 s, and recovery of the layer was monitored by measuring Resistance at 4000 Hz. The assessment of ECs barrier functions was performed with Electric Cell-substrate Impedance Sensing (ECIS) Zq instrument (Applied Biophysics). Briefly this instrument applies a small alternating current and records the impedance, and thus the resistance, of the cellular layer. VEGFA was used at 20nM concentration to open the endothelial monolayer.

Luciferase assays

For 3'UTR stability assay, HEK 293 cells were transfected with pMIR-REPORT™ Luciferase and pMIR-REPORT™ Renilla constructs carrying TCHP 3'UTR and miR-503 or scrambled oligonucleotide sequence (control). using Lipofectmin 2000™ In Vitro DNA Transfection Reagent (LifeTechnology) Luciferase constructs. Cells were cultured for 48h and assayed with the Dual-Luciferase Reporter Assay System (Promega).

Western-Blot analyses

Cells were rinsed once with ice-cold PBS and lysed with Chaps lysis buffer (0.3% Chaps, 10 mM b-glycerol phosphate, 10 mM pyrophosphate, 40 mM HEPES [pH 7.4], 2.5 mM MgCl2 and one tablet of EDTA-free protease inhibitor [Roche] per 25 ml) and 1% Triton X-100. Where specified in the Figureures, Chaps lysis buffer was supplemented with 12.5 mM EDTA. Western blot was performed as previously described (Caporali, Meloni et al. 2011). The following antibodies have been used: TCHP (Abcam); mTOR and p-mTOR (both Cell Signalling); tubulin (Cell Signaling) and β-actin (Sigma).

Animal experiments

Mouse experiments are reported in accordance with Animal Research Report of *In Vivo* Experiments (ARRIVE) guidelines. Experiments were performed in accordance with the Animal (Scientific Procedures) Act (UK), 1986 prepared by the Institute of Laboratory Animal Resources and under the auspices of UK Home Office Project and Personal License. CD-1 mice were made diabetic using streptozotocin (STZ) (Sigma) (Emanueli, Salis et al. 2002) or left normoglycemic after STZ buffer administration alone. STZ was delivered i.p. for 5 consecutive days (40mg/Kg in citrate buffer per each day). Fourteen days after the first STZ injection, glycaemia at fast and glycosuria were measured and only those mice with glycaemia above 200 mg/dL and overt glycosuria entered the protocol. Absence of hyperglycemia and glycosuria in buffer-injected non-diabetic mice was also verified.

Isolation of ECs from mouse limb muscles

Adductor muscles at 3 mounts in diabetic and non-diabetic mice were rinsed and digested with collagenase II (Worthington) plus DNase I (Sigma) using gentleMACS™ Dissociator, following the manufacture's protocol. Next, ECs were immunomagnetic sorted using a CD31antibody (Miltenyi Biotech) as reported in (Larsson, Fredlund Fuchs et al. 2009).

Immunofluorescence

80,000 HUVECs cells were plated on fibronectin-coated glass coverslips in 24-well tissue culture plates. Twenty-four hours later, the slides were rinsed with PBS once and fixed for 15 min with 4% paraformaldehyde in PBS at room temperature. The slides were rinsed twice with PBS and cells were permeabilized with 0.05% Triton X-100 in PBS for 5 min. After rinsing twice with PBS, the slides were incubated with primary antibody in 3% BSA O.N. in a cold room, rinsed four times with PBS, and incubated with secondary antibodies diluted 1:1000 in 3% BSA for 45 min at room temperature in the dark and washed four time with PBS. Slides were mounted on glass

coverslips using Vectashield (Vector Laboratories) and imaged on a Fluorescent Microscope.

β-Galactosidase staining

Senescence of ECs was measured using the Cellular Senescence Assay kit from Cell Biolabs, Inc. (Cat: CBA-230). The protocol was performed according to the manufacturer's guide. Briefly, TCHP KD and control ECs were plated in a 6 well plate. Upon confluency, cells were initially fixed and later incubated with SA-β-gal working solution for 16 hours in a non-humidified CO2 free incubator at 37°C.

Immunohistochemistry

Samples were fixed in 4% formalin, embedded in paraffin wax and sectioning for histological staining. Sections were incubated overnight at 4 °C with TCHP (Abcam, ab-77622; 1:1000). Capillary and arteriole were stained with Alexa 488-conjugated isolectin-B4 (Molecular Probes, I2141, 1:100).

Statistical analysis

Comparisons between different conditions were assessed using 2-tailed Student's *t* test. If the normality test failed, the Mann-Whitney test was performed. Continuous data are expressed as mean ± SEM of three independent experiments, each performed in triplicate or quintuplicate. *P* value <0.05 was considered statistically significant. Analyses were performed using GraphPad Prism v5.01.

3.3 **Results**

3.3.1 **TCHP localization in endothelia cells and vessels.**

Iassessed TCHP expression and localization by immunofluorescence in HUVECs. THCP localized prevalently in the cytoplasm and showed extensive overlap with the mitotraker stained mitochondria. However, Inoticed that in some cells TCHP displayed a diffuse cytoplasm distribution with no obvious localization, suggesting a dynamic regulation of TCHP (**Figure 3.1A**). Moreover, Iexamined the presence and localization of TCHP in vessels (**Figure 3.1B**). Double immunohistochemistry for TCHP and Isolectin-B4 (marker of ECs) in mouse limb muscle showed a strong signal for TCHP in correspondence of ECs in muscle-associated microvasculature (**Figure 3.1B**). A strong positive signal was also present in the myocytes.

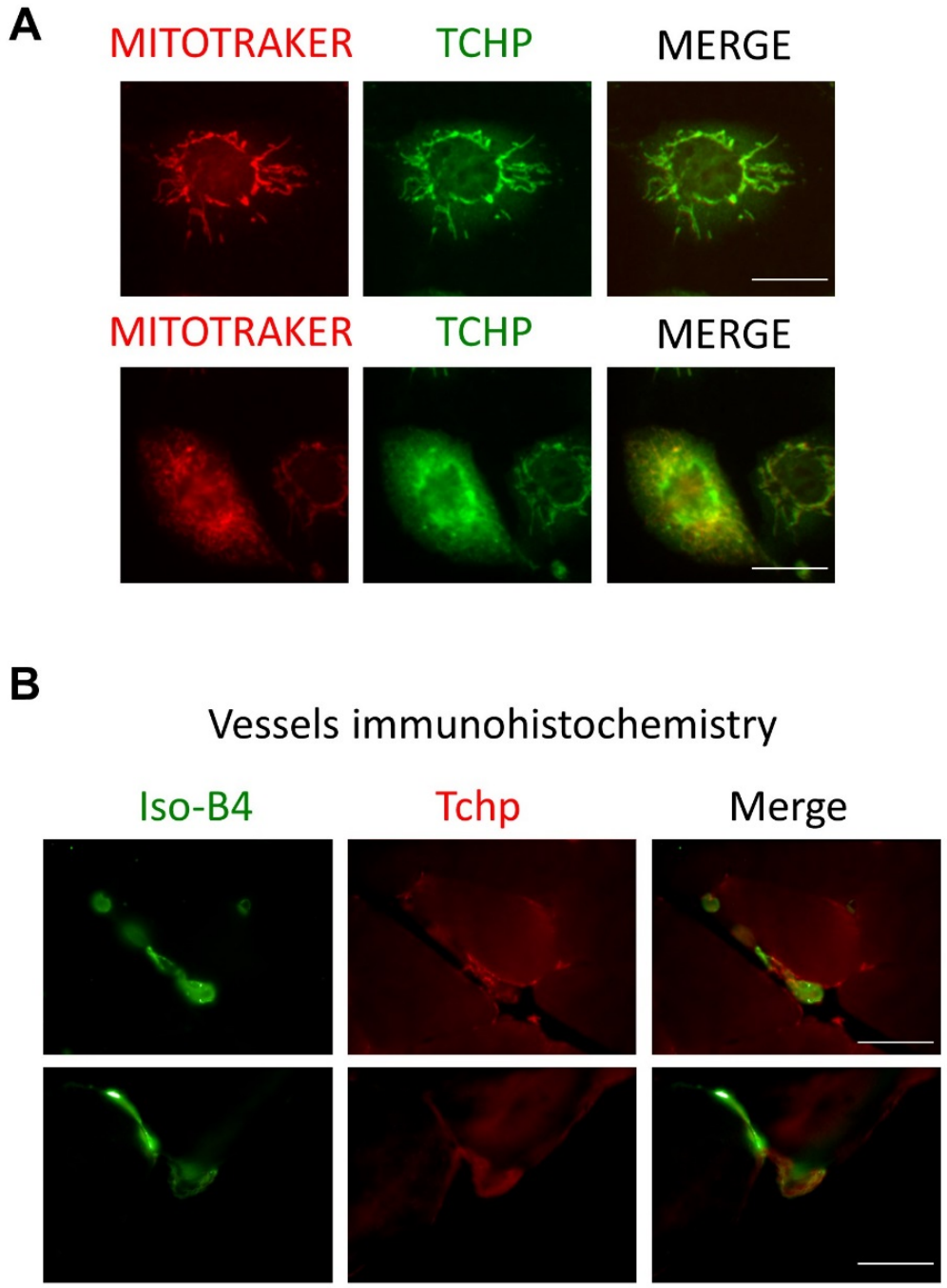

Figure 3.1: Localization of TCHP in Ecs and endothelium

A, Fluorescent microscope images show Mitotraker stained mitochondria and TCHP immunostaining in HUVEC cells. Upper panel represents an example of TCHP co-localizing with mitochondria, whereas lower panel is an example of TCHP distribution in the cytoplasm. Scale bar, 25 μm. **B**, Localization of TCHP in vessels of limb muscles. Scale bar, 50 μm

3.3.2 **TCHP is target of miR-503**

It was tested if the micro-503 may have TCHP among one of its targets. HUVECs were transfected with pre-miR503 and a scrambled oligonucleotide RNA as a control and harvested 72h later for western blot analysis. Interestingly TCHP protein level is reduced in HUVECs overexpressing mir-503 (**Figure 3.2A**). Next, the 3' untraslated region (3'UTR) of TCHP mRNA was confirmed to be a mir-503 target, by using an in vitro luciferase report assay (**Figure 3.2B**). HEK293T cells ectopically expressing a pMIR-Report plasmid carrying the TCHP 3'UTR downstream a luciferase reporter gene coupled with the constitutive housekeeping Renilla reporter gene, were transfected with either premiR-503 or a scrambled oligonucleotide sequence. Subsequently, the relative fluorescence was calculated using Dual-Glo® Luciferase Assay System.

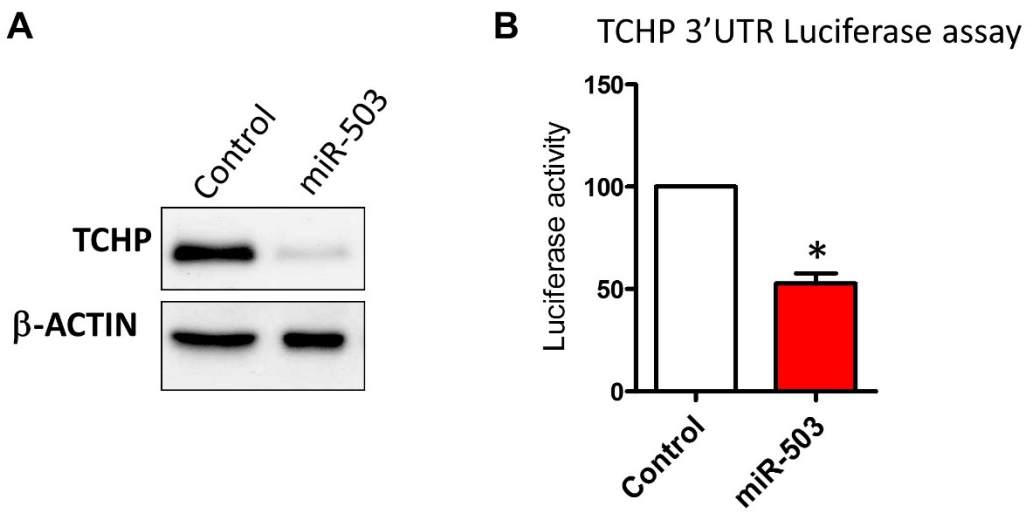

Figure 3.2: TCHP is target of miR-503

A, TCHP protein level in HUVEC transfected with control or miR-503 mimics oligonucleotides. **B**, Luciferase activity calculated in 293HEK cells co-transfected with Luciferase carrying 3'UTR TCHP and control RNA or miR-503 mimics oligonuncleotides. Data are means ± SEM, n = 3; *p < 0.05 vs control (Student's t test).

3.3.3 **TCHP regulation *in vitro***

Since micro-RNA 503 (mir-503) is known to be specifically up-regulated in HG/LGF condition (Caporali, Meloni et al. 2011), I investigated how TCHP is modulated in response to several stimuli. HUVECs and human microvascular ECs (HMVECs) (**Figure 3.3A-3.3D,** respectively) were cultured in condition of high glucose (HG, 25mM D-glucose) or low growth factors (LGF) or a combination of the two. The HG/LGF condition is intended to mimic advanced diabetes, when hyperglycemia is accompanied by cell starvation (Caporali, Meloni et al. 2011). The cells were harvested at 24h after treatment and TCHP expression was determined by Western Blot and qPCR; an additional time point of 5 days treatment was added for the high glucose condition. TCHP expression was slightly decreased after 24h in high glucose condition compared to the control (25mM non-metabolized stereoisomer L-glucose was used as an osmotic control) but sharply dropped down when cells were co-treated with HG and LGF. Yet HG alone was sufficient to trigger a clear TCHP down-regulation after 5 days (**Figure 3.3A and 3.3C**). TCHP mRNA levels followed the same trend of the protein level as shown in **Figure 3.3B and 3.3D.** Moreover, the expression of TCHP in hypoxic condition was also analyzed. TCHP protein levels dropped in HUVECs at 24h and more consistently at 48h of hypoxia (**Figure 3.3E**), while mRNA levels of TCHP increased at 24h of hypoxia and decreased at 48h (**Figure 3.3F**).

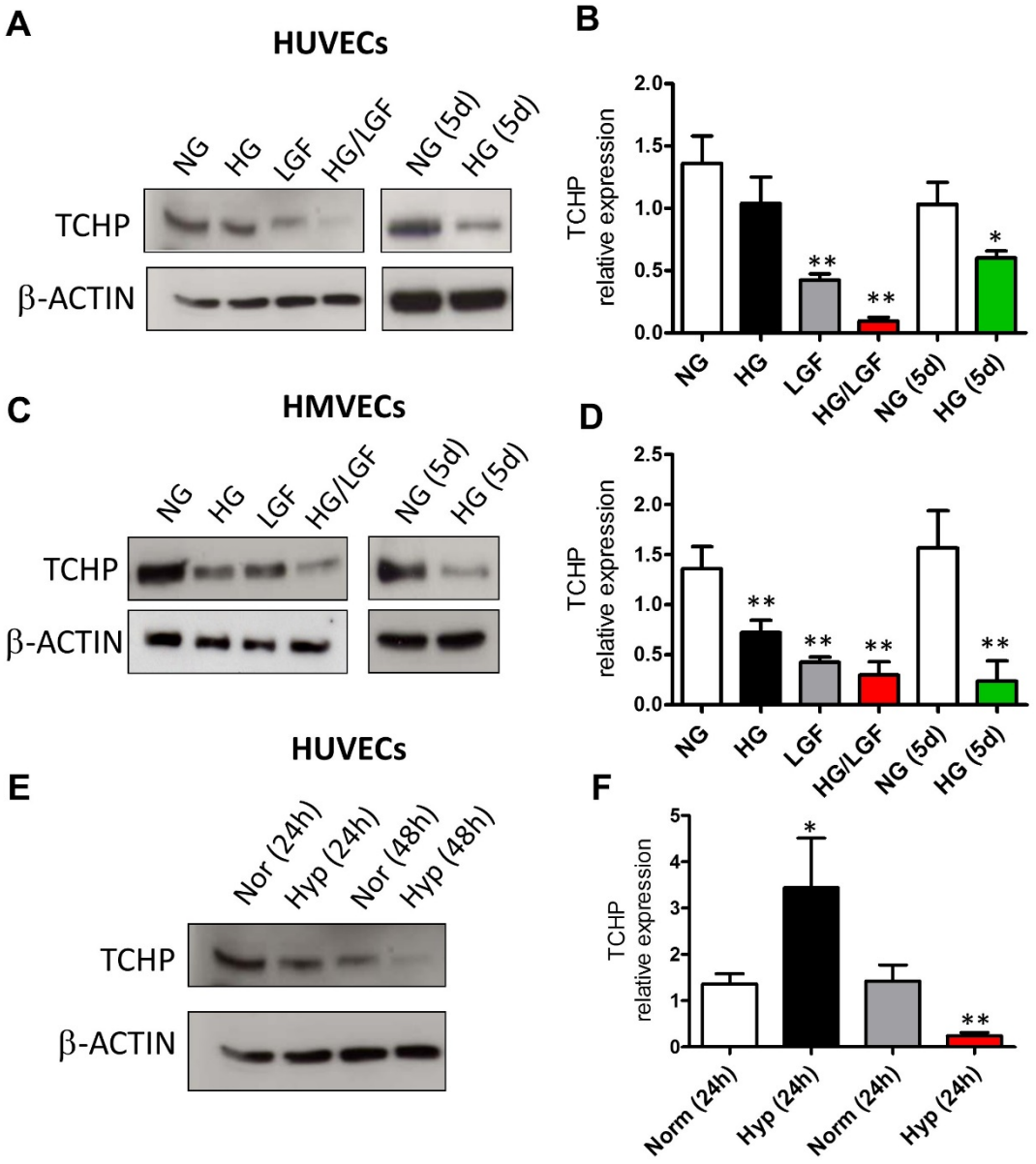

Figure 3.3: TCHP regulation *in vitro*

A and **C**, Protein expression of TCHP in HUVEC and Human Microvascular Endothelial Cells (HMVEC) cells under normal condition (Wang, Cano et al.), high glucose, low growth factor (LGF), HG/LGF for 24h or cultured in HG for 5 days. **E**, TCHP protein level in HUVECs under normoxia (21%O2) or hypoxia (1%) for 24h. **B, D** and **F**, TCHP mRNA expression of the conditions described above. Data are means ± SEM, n = 3; *p < 0.05 (Student's t test).

3.3.4 **TCHP regulation *in vivo***

I have examined TCHP expression in a streptozotocin-induced type-1 diabetes (12 weeks) (Caporali, Pani et al. 2008, Caporali, Meloni et al. 2011) and I found reduced level of TCHP expression in diabetic limb muscles (**Figure 3.4A**) as well as in CD31 sorted ECs from diabetic muscle compared to non-diabetic one (**Figure 3.4B**). Moreover, I found that TCHP expression is also reduced in ECs sorted from limb muscle of db/db mice (model of type-2 diabetes) compared to the control mice (**Figure 3.4C**), whereas TCHP expression is not affected in ECs sorted from aorta of db/db mice (**Figure 3.4D**).

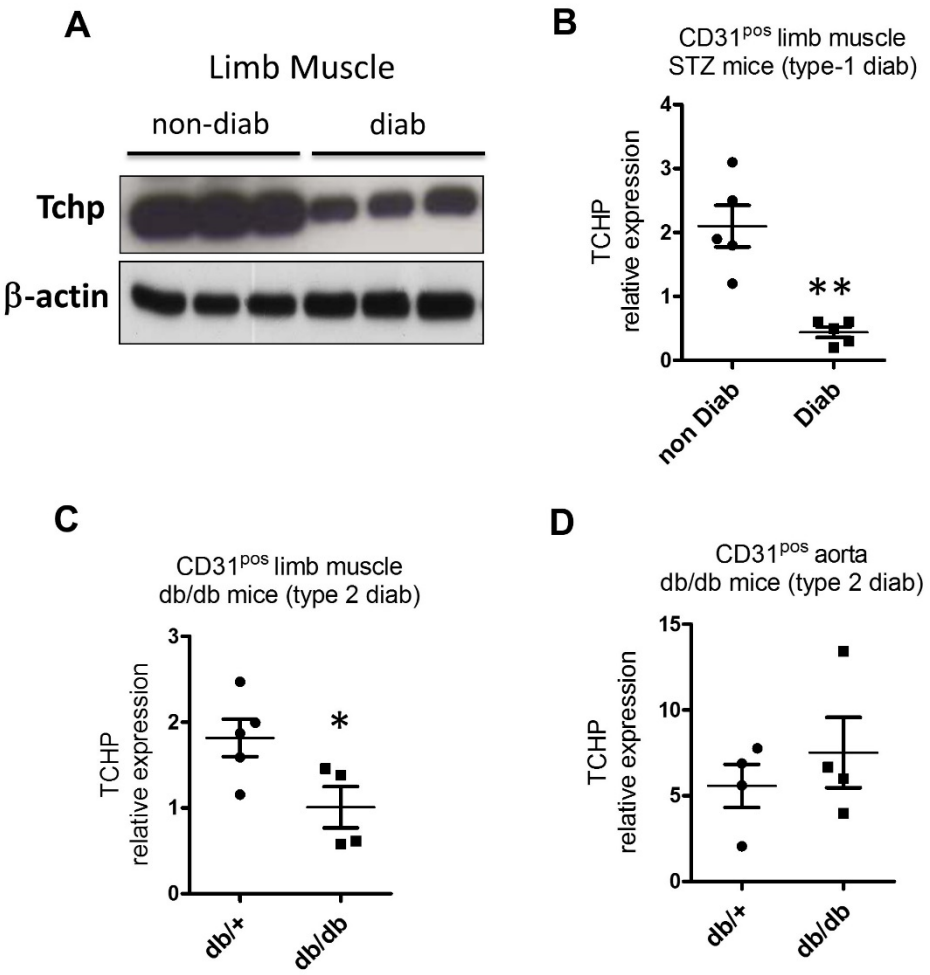

Figure 3.4: TCHP regulation *in vivo*

A, TCHP protein level in Limb Muscles of non-diabetic or type I diabetic mice. **B,** TCHP mRNA expression in $CD31^{pos}$ cells sorted from non-diabetic or diabetic limb muscles (type-1). **C,** TCHP mRNA expression in $CD31^{pos}$ cells sorted from non-diabetic or diabetic limb muscles (type-2). **D,** TCHP mRNA expression in $CD31^{pos}$ cells sorted from aorta of non-diabetic or diabetic mice (type-2). Data are means ± SEM, n= 3; **p < 0.01; *p < 0.05 (Student's t test).

3.3.5 **TCHP knockdown affects EC morphology**

To investigate the involvement of TCHP in the regulation of endothelial cell cellular physiology, Iknocked down TCHP in HUVECs. The down regulation of TCHP was obtained using a lentivirus based delivery of a short hairpin RNA targeting TCHP mRNA. Virus over-expressing a scrambled RNA sequence was used as control.

HUVEC were infected with shTCHP or control and subsequently TCHP expression was assessed at 3 and 7 days after transduction using quantitative real time PCR (qRT-PCR) (**Figure 3.5A**). The protein level of TCHP was markedly decreased at 7 days as showed by Western blot (**Figure 3.5B**). Notably, TCHP knock down cells (elsewhere referred as TCHP KD) undergo to a remarkable phenotypic alteration even noticeable by light microscopy. Specifically, they manifested an enlarged flattered round shaped morphology with extensive lamellipodia formation and increased cytoplasmic vacuolization (**Figure 3.5C**).

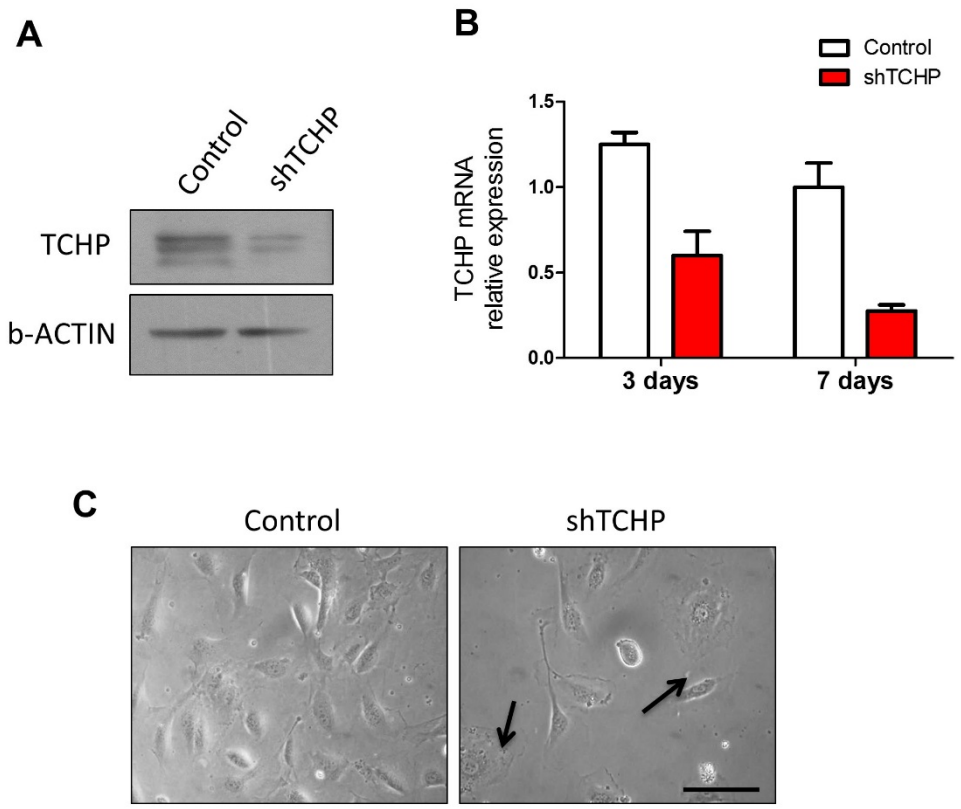

Figure 3.5: Characterization of TCHP knockdown endothelial cells

A, TCHP protein level in HUVEC transduced with control or shTCHP lentivirus one week after infection. **B**, Relative mRNA level of TCHP in HUVEC transduced with control or shTHP lentivirus after one week from infection. **C**, Bright field images of shTCHP KD or control HUVECs. Scale bar, 50 mm. Data B are means ± SEM, n = 3; **p < 0.001 vs control (Student's t test).

3.3.6 **Lack of TCHP impairs EC angiogenesis, migration and barrier function in vitro**

To examine the impact of TCHP down-regulation on endothelial function, it was performed an *in vitro* Matrigel tubule formation assay. TCHP down regulation severely affects the tubule forming capacity of HUVECs, mainly reducing the total length of tubule-like structures (**Figure 3.6A and 3.6B**). Coherently, it was observed that reduced level of TCHP also affects HUVECs migration properties as measured by wound healing assay (**Figure 3.6C**). Finally, the barrier function of TCHP KD cells was measured by the analysis of impedance. Cell were cultured as monolayer on specific array of the ECIS machine and treated with VEGFA at the concentration of 20ng/ml. Through the real-time analysis of the impedance, it was possible to detect the change in permeability of the EC monolayer. TCHP KD treated with VEGFA showed a significant drop of resistance compared to control cells (**Figure 3.6D**).

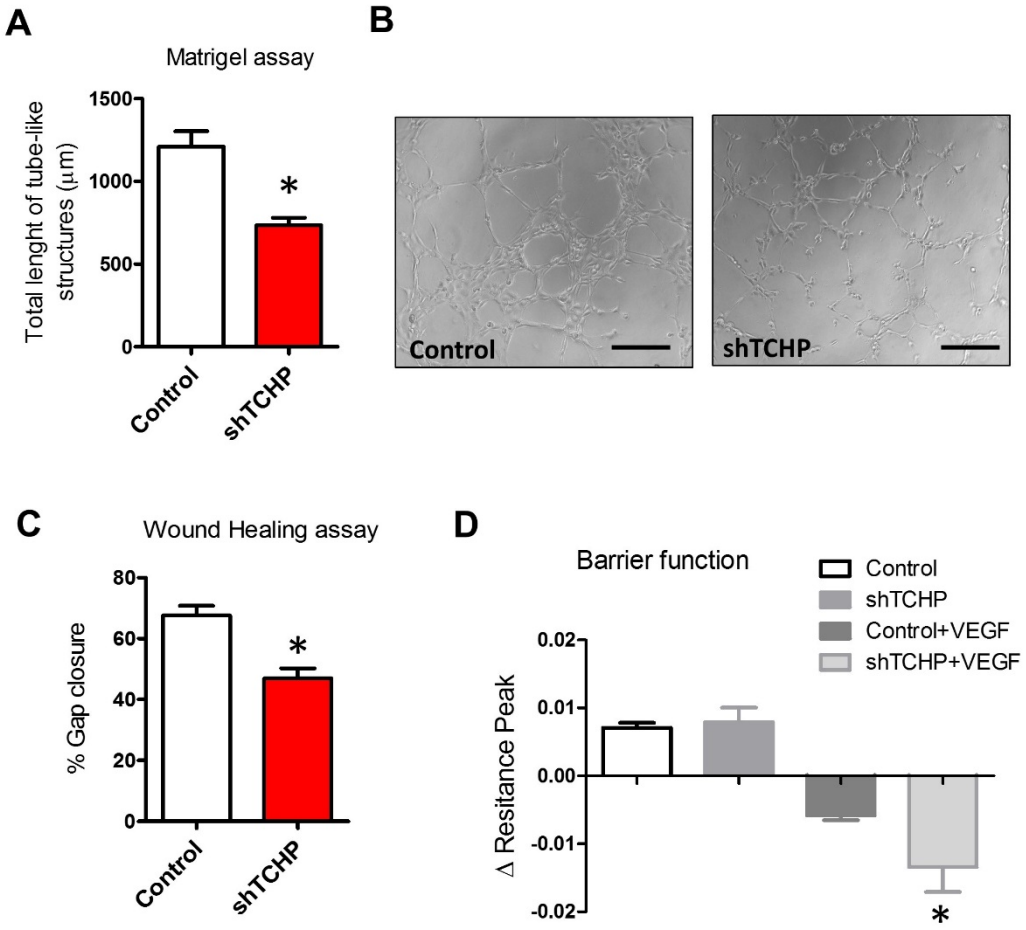

Figure 3.6: Knockdown of TCHP inhibits *in vitro* angiogenesis, migration and endothelial cell barrier function

A, Endothelial network formation on Matrigel was quantified at 24 h from cell seeding and analyzed by quantification of the total length of tubule-like structures. **B**, Representative microphotographs from Matrigel assay. Original magnification 10X; scale bar: 100 mm. **C**, Wound healing assay. **D**, Barrier function analysis in TCHP knockdown cells treated with VEGF (20ng/ml). Data are expressed as difference in cell resistance. Data (A, C and D) are means ± SEM; n=3 ; *p < 0.05 vs control, (Student's t test).

3.3.7 **TCHP KD affects microtubule density and actin localization**

Next, it was examined by immunofluorescence the microtubule cytoskeleton, being itself, a fundamental component of the cell migrating machinery. In accordance to previous findings demonstrating TCHP participation in microtubules binding at the centrosome of epithelial cells (Sarkar, Korolchuk et al. 2011), TCHP KD cells presented a decreased density in the microtubule network at the microtubule-organizing center (MTOC) and the absence of the centrosomal anchored microtubule aster (**Figure 3.7A**). Moreover, actin filaments (stained by phalloidin) were localized in the periphery of the cells in TCHP KD cells (**Figure 3.7B**) leaving fewer actin stress fibers stretching across the cell ‘s body.

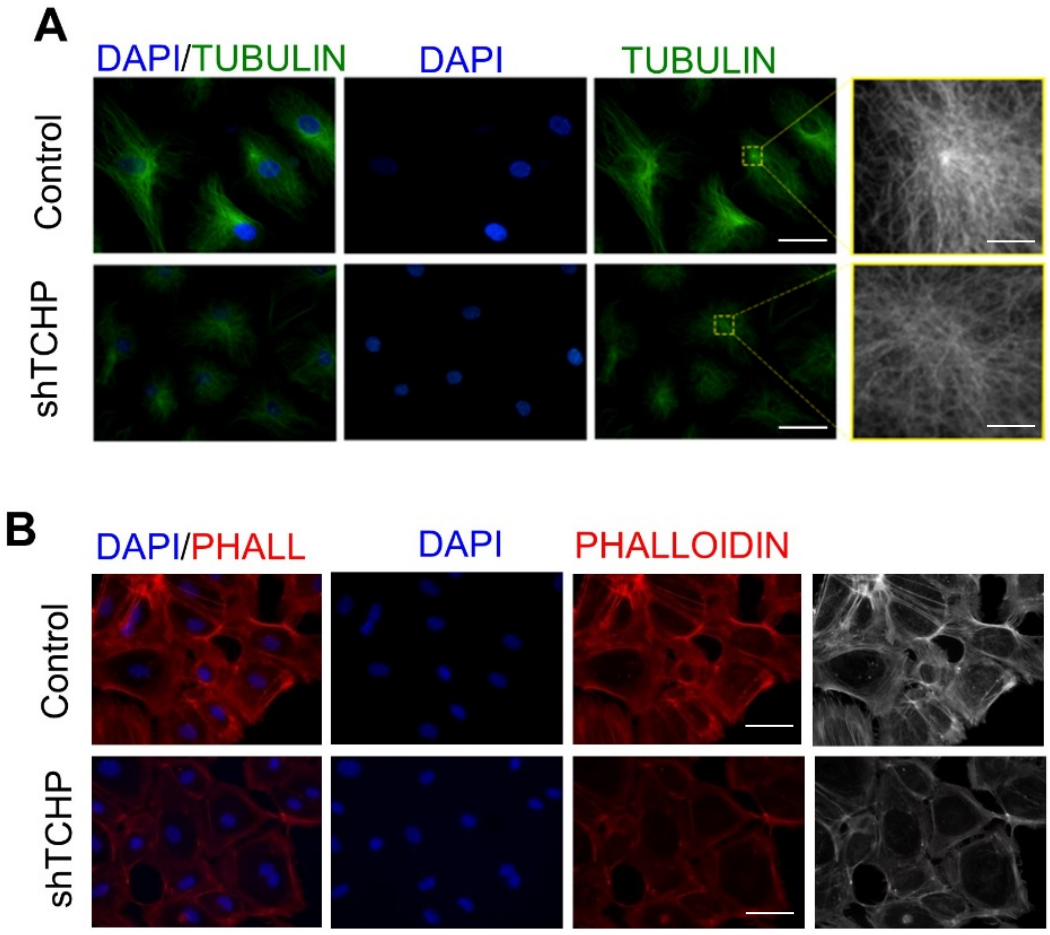

Figure 3.7: Analysis of microtubule and actin localization in TCHP knockdown cells.

A, Immunofluorescence images of b-tubulin (green) and **B**, actin (phalloidin staining) in control and TCHP KD cells. Nuclei are stained in Dapi (blue). Scale bar, 25 µm
In **A**: magnification showing the centrosomes inside of a 10 μm^2 yellow square are presented in black and white. Scale bar, 2.5 µm

3.3.8 **TCHP is required for cell cycle progression**

Analysis of 5-bromo-2'-deoxyuridine (BrdU) incorporation assay showed that TCHP downregulation negatively affected cell cycle progression, showing a decrease in the number of cells undergoing S phase progression (**Figure 3.8A**). Furthermore, analysis of the cell cycle progression by Propidium Iodide (Bonora, Wieckowski et al.) staining showed a significant accumulation of cells in the phase G2/M of the cell cycle (**Figure 3.8B**).

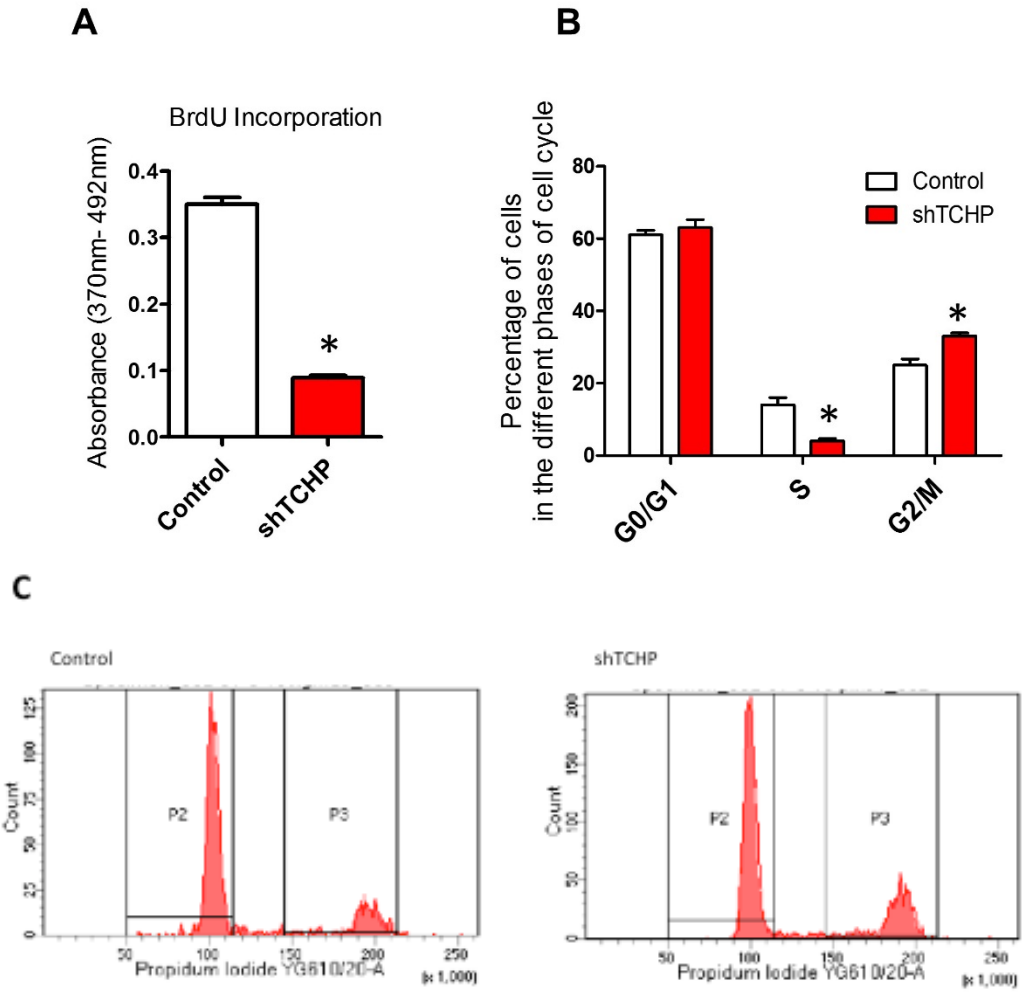

Figure 3.8: TCHP knockdown impairs cell cycle

A, Proliferation of Control and TCHP KD HUVECs was measured by BrdU incorporation assay. The Absorbance between 370 and 490 nm is shown for both cell populations. **B,** Flow cytometric analysis of cell cycle using PI staining. Chart shows percentage of the cell in different phases of cell cycle. Data are means ± SEM; n=3; *p < 0.05 versus control, (Student's t test). **C,** FACS plot from B

3.3.9 **TCHP knockdown sensitizes ECs to cell death in response to different cell death inducing stimuli**

To further unravel the phenotype behind TCHP knock down, was tested the apoptotic response to different stimuli using Annexin-V/ 7AAD double staining. TCHP KD cells displayed significantly higher number of both Annexin-V and 7AAD positive cells compared to the control population (**Figure 3.9A)**. This difference was further increased when cells were exposed 16h to Homocystein (**Figure 3.9B)**. Homocystein is known to induce ROS production (Topal, Brunet et al. 2004) and consequently ER stress response (Elanchezhian, Palsamy et al. 2012). In agreement, overnight treatment of 2 μM Thapsigargin or 5μg/ml Tunicamycin, two known drugs inducing ER stress (Oakes and Papa 2015), increased cell death respect to control but at a slightly lower level than the treatment with Homocystein (**Figure 3.9C-D)**. Notably, Homocysteine, Thapsigargin and Tunicamycin were reported to induce not only ER stress but for some extend also autophagy (Yorimitsu, Nair et al. 2006, Qin, Wang et al. 2010, Vacek, Vacek et al. 2012). This consideration leads us to investigate cell death in response to Rapamycin a well-known mTOR inhibitor and inducer of autophagy (Kim and Guan 2015). Interestingly, after 16h treatment with 10μM Rapamycin, it was observed a sharp increase in cell death in TCHP KD cells. The difference in the percentage of death cells was higher than with any other stimulus reaching more than 60% cell death for TCHP KD cell population (**Figure 3.9E)**.

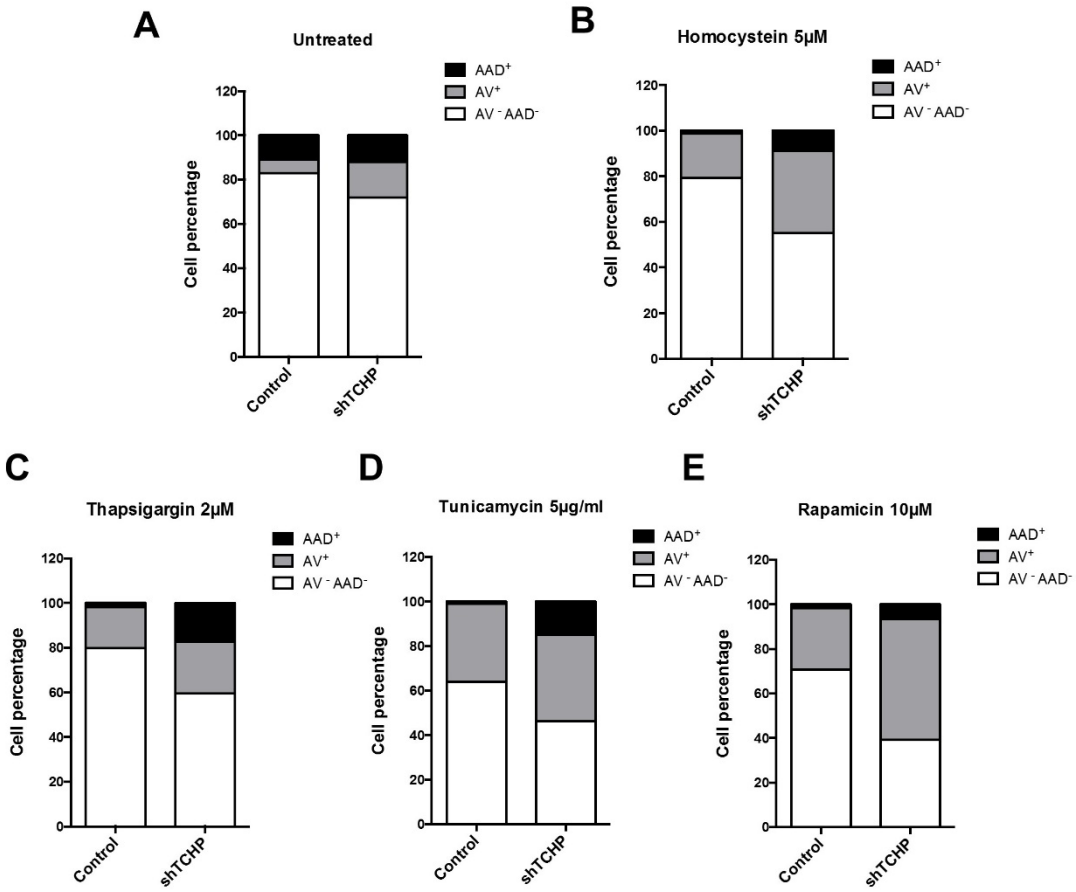

Figure 3.9: TCHP knockdown triggers apoptosis in response to cell death stimuli

A Flow cytometry analysis of Annexin V and 7AAD co-stained cells of control cells **A**, or after 16h of treatment with 5µM Homocystein **B**, 2µM Thapsigargin **C**, 5µg/ml Tunicamycin **D** or 10µM Rapamycin **E**. Graphs show the percentage of cells for different drug administration conditions and for both Control and shTCHP (n=2).

3.3.10 **Gene expression regulation by knockdown of TCHP**

To further dissect the TCHP KD cell phenotype, different subsets of genes were screened by qPCR. Performing two-time point, one at 72h and the other at 7 days post transduction gave us the possibility to analyze the early and late effects driven by TCHP down regulation. At the beginning were selected some of the key angiogenic driving genes, underling fundamental process as survival, proliferation and differentiation of ECs. However, no significant change in gene expression was detected (**Figure 3.10A**). Since it has been shown that Thapsigargin and Tunicamic increase ER stress, among others was introduced a group of gene up-regulated during ER stress condition; yet without substantial significant differences in comparison with control cells, apart GRP94 gene (**Figure 3.10B**). Only when a broad spectrum of negative cell cycle regulators was tested was possible to undercover a substantial increase of CDKN2A (p12) at 3 days and of CDKN2B (p16) at 1 week after transduction, thus possibly explaining the marked decrease of proliferation in TCHP KD cells (**Figure 3.10C**). Moreover, it was also assessed a subgroup of genes linked with senescent induced inflammatory processes (Davalos, Coppe et al. 2010). Interestingly IL6, IL8, MCP1 and TGFβ2 were differentially up-regulated after TCHP downregulation (**Figure 3.10D**). These considerations prompted us to investigate whether TCHP KD cells might display any features of senescence.

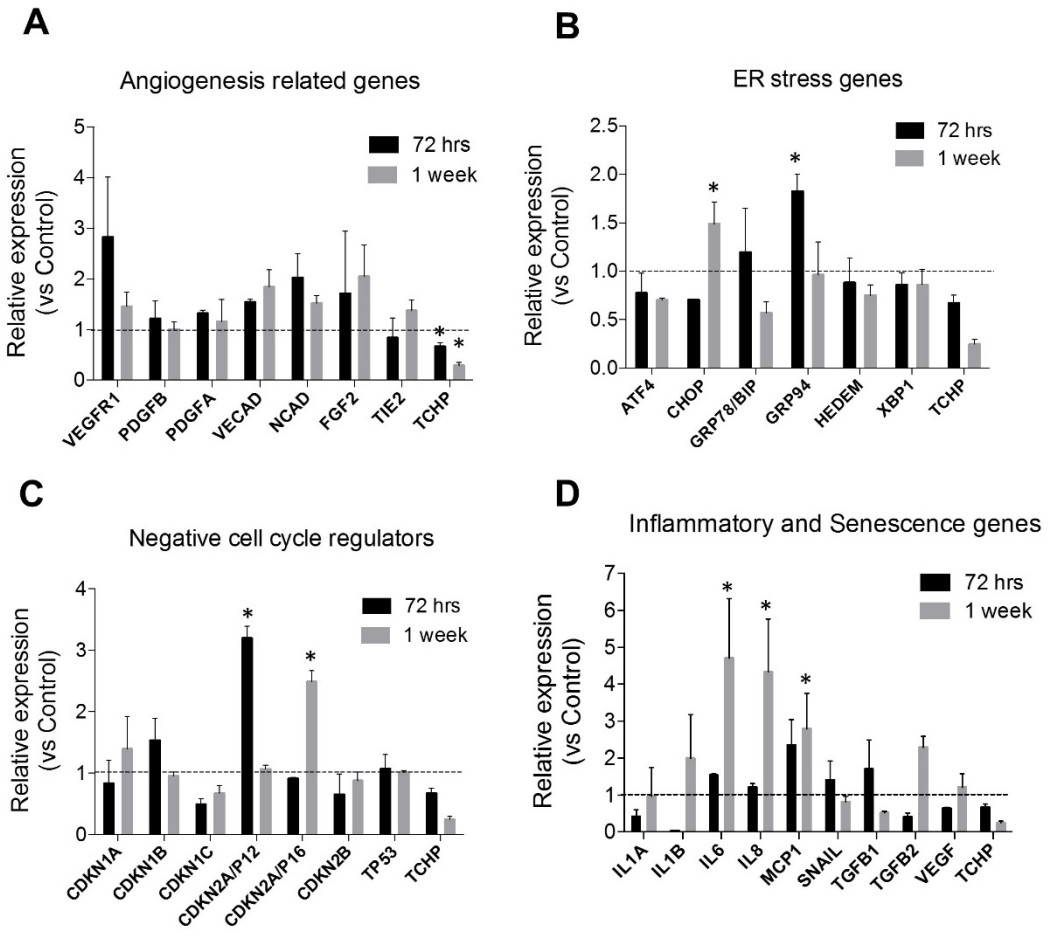

Figure 3.10: Gene expression regulation in TCHP knockdown cells

Relative mRNA levels of TCHP and panel of **A,** angiogenic genes; **B,** endoplasmic reticulum (ER) stress genes; **C,** cell cycle regulator gene; or **D,** inflammatory and senescent genes. Graphs represent transcripts measured at 72 h and 7 days post TCHP shRNA transduction. n = 3; Data are means ± SEM; *p < 0.05 vs control, (Student's t test).

3.3.11 **Analysis of the senescence associated phenotype after TCHP downregulation**

Control and TCHP KD cells were assessed for Senescence-associated beta-galactosidase (SA-β-gal) (**Figure 3.11A**) and p16 (**Figure 3.11B**), two well-characterized senescence markers (McHugh and Gil 2018), using X-gal staining on fixed cells and WB, respectively. Interestingly KD cells exhibited strong β-Gal activity and a sharp increase of p16 protein level at 7 days post-infection. Moreover, in TCHP KD cells mTOR was phosphorylated (S2448), showing the possible involvement of mTOR pathway in the senescence process (**Figure 3.11B**). Another well-defined hallmark of senescence is the senescence-associated secretory phenotype (SASP) whose principal components are pro-inflammatory cytokines and chemokines (McHugh and Gil 2018). Finally, the expression and release of IL8 and IL6 were investigated using ELISA and the results showed that TCHP down-regulation augmented the production and secretion of those two cytokines (**Figure 3.11C**).

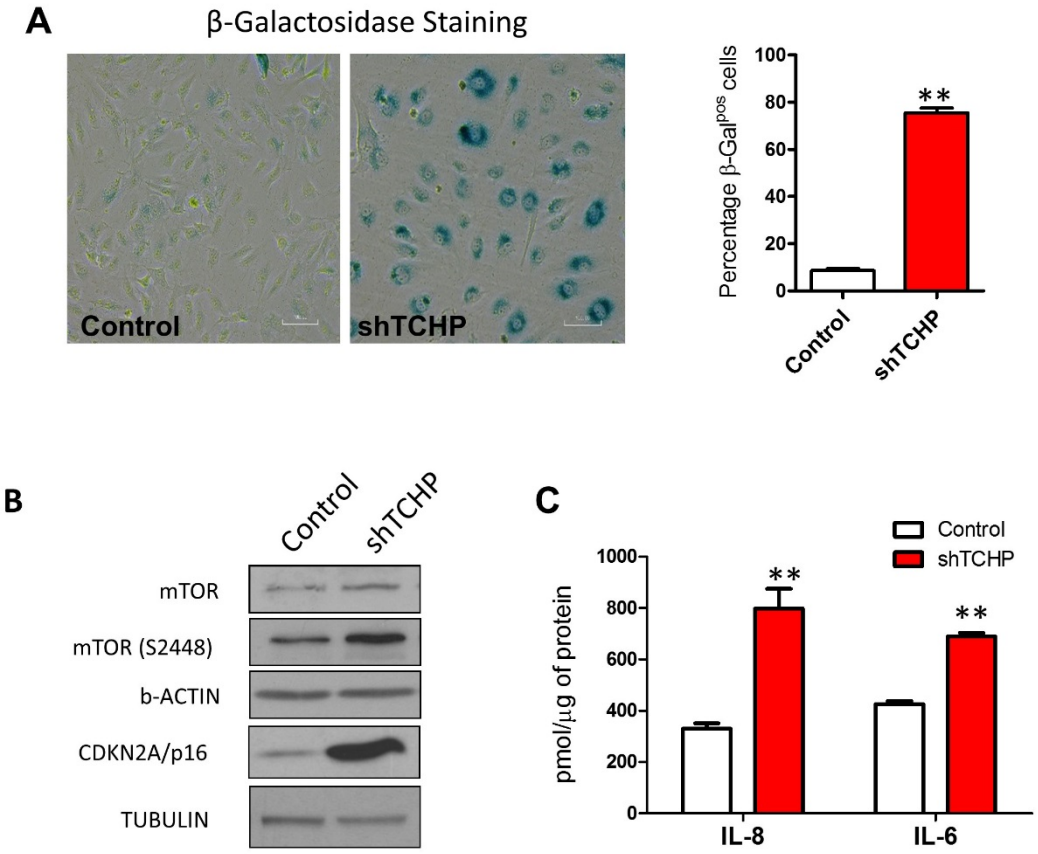

Figure 3.11: TCHP knockdown induces a senescence-like phenotype
A β-Galactosidase activity as reveal by the chromogenic β-Gal substrate X-Gal in control and TCHP KD cells. **B** Western Blot assessing the CDK inhibitor p16, mTOR, p-mTOR (S2448) in control and KD cells. Analysis of **C** IL8 and IL6 in control and TCHP KD cells determined by ELISA detection kit. All the experiments were performed 7 days after viral transduction. Data are means ± SEM, n=3; **p< 0.01 vs control (Student's t test). Scale bars, 25 μm.

3.4 **Discussion**

Our findings reveal for the first time a new mechanism through which TCHP preserve EC homeostasis by regulating an important biological process such as senescence.

I shed light on the regulation of TCHP providing evidence for stimuli that negatively affect TCHP expression in vitro and in vivo. I demonstrated that lack of TCHP alters ECs functions sensitize cells to apoptosis, is associated with an increase of senescence associated proinflammatory cytokines.

3.4.1 **TCHP localization and regulation**

It has been previously reported that endogenous or expressed TCHP shows a punctuate pattern, partly overlapping with mitochondria (Nishizawa, Izawa et al. 2005, Vecchione, Fassan et al. 2009). Using a commercial antibody, THCP localization is prevalently in the cytoplasm and showed a strong overlap with the mitotraker stained mitochondria. As TCHP lacks a canonical mitochondrial targeting sequence or a clear transmembrane domain for insertion into the mitochondrial membrane (Vecchione, Fassan et al. 2009), I can assume that TCHP doesn't bind directly mitochondria but it can shift from mitochondrial localization to cytoplasm, thus suggesting a dynamic regulation in the cells. This kind of regulation could be due to a different repositioning of TCHP during different cell cycle stages or under the effect of cellular stimuli or stressor. Moreover, THCP localization in different subcellular compartment may mirror different functional role played by the same protein.

TCHP expression in normal human tissues was previously examined using two multiple normal-tissue northern blots. All tissues examined (brain, heart, skeletal muscle, colon, thymus, spleen, kidney, liver, small intestine, placenta, lung, peripheral blood leukocyte, prostate, testis and ovary) demonstrated the presence of the 3.2 kb TCHP transcript, albeit at different levels. The highest RNA expression was detected in heart, skeletal muscle, kidney, liver and testis. A larger 5.5 kb transcript was observed in heart and skeletal muscle. A smaller RNA transcript of 1.24 kb was also detected in heart mRNA (Vecchione, Fassan et al. 2009). I have analysed the

localization of TCHP in the vessels of limb muscles, showing a strong correlation between TCHP antibody and Isolectin-B4 (marker for ECs) and diffuse staining for TCHP in the myocytes.

Recently, Caporali lab demonstrated that microRNA-503 (miR-503) has a prominent role in diabetes-induced impairment of post-ischaemic reparative neovascularisation (Caporali, Meloni et al. 2011, Caporali, Meloni et al. 2015). Recovery from ischaemic events is delayed in diabetic patients with critical limb ischaemia, due to impairment of reparative angiogenesis, and their plasma miR-503 levels are highly elevated. In addition, type-1 diabetes increases miR-503 in ECs of mouse ischaemic limb muscles (Caporali, Meloni et al. 2011, Caporali, Meloni et al. 2015). Using different approaches I have identified TCHP as target of miR-503.

Overexpression of miR-503 decreased TCHP protein level in a TCHP 3'UTR dependent manner, showing that TCHP is a *bona fide* target of miR-503.

Moreover, I have demonstrated that TCHP expression is decrease in ECs by HG and LGF conditions and during hypoxia. Moreover, TCHP expression is down-regulated in the muscles and ECs from a type I diabetic mouse model. Again, our data defined a direct down-regulation of TCHP expression orchestrated by miR-503 and showed also an inverse correlation between TCHP and conditions known to increase miR-503 expression.

3.4.2 **TCHP knockdown impairs EC functions**

The function of TCHP in ECs is still unknown, although its cellular localization, expression and function in other cell lines suggest its role in regulation of migration, proliferation and angiogenesis. In this Chapter, I have provided evidence for impaired endothelial capacity to form tubule-like structure in vitro, decrease migration and proliferation as well as appearance of abnormal microtubule structure arising from TCHP reduction.

Silencing TCHP in ECs using lentiviral vector impairs tubulogenesis (assessed by in vitro Matrigel assay). To determine whether the observed inhibitory effect of TCHP silencing on EC migration and proliferation may be a consequence of alterations in the microtubule structure, I examined the

morphology of tubulin networks in HUVECs by immunofluorescence staining for α-tubulin. In the control, cytoplasmic tubulin filaments showed normal appearance, radiating from a central point to the cell periphery. Silencing of TCHP in HUVECs, however, produced marked changes in the tubulin cytoskeleton organization showing a marked loss of microtubules.

The profound effects of TCHP depletion on microtubules suggests that downregulation of TCHP could compromise EC migration and barrier function of ECs. To address this, I treated ECs with shRNA to TCHP and I used ECIS machine. The ECIS machine allows the measurement of EC behaviour by measuring the complex impedance spectrum of adherent cells growing on gold electrodes (Szulcek, Bogaard et al. 2014). Analysis of migration showed a significant decreased in percentage of gap closure in TCHP KD cells. In the barrier function assay, confluent TCHP KD cells and control cells were treated with high concentration of VEGFA (20ng/ml) in order to observe the opening of adherent and tight junction (AJ and TJ respectively). VEGFA is a potent and powerful permeability inducing cytokine and has profound effect on adherent and tight junction (AJ and TJ respectively) acting on multiple pathways and at different points of each signal transduction cascade (Weis and Cheresh 2005, Claesson-Welsh 2015). TCHP KD cells were subjected to an increased VEGF-induced permeability respect to the control. Hyper-permeability is characteristic of compromised endothelial function in different advanced cardiovascular diseases (Weis and Cheresh 2005) and the result in TCHP KD cells seems to suggest a similar dysfunction. VEGFA stimulates actin cytoskeleton remodelling at the cell-cell membrane contact site in a RAP1 and ROCK-RHO dependent pathway (Rho, Ando et al. 2017), therefore is possible that TCHP deficiency may interfere with those events since TCHP KD results in defective MTOC and altered actin organization and distribution. A second important event occurring at the AJ after VEGFA stimulation is the phosphorylation mediated internalization and rerouting of VE-Cadherin to the recycling endosomes (RE) (Fukuhara and Mochizuki 2010) and even in this setting is possible that the absence of TCHP might

exacerbate the hyper-permeability seen in TCHP KD because of the alteration caused to the RE, better described in the next chapter.

Finally, since TCHP has been previously associated with the regulation of cell cycle (Vecchione, Fassan et al. 2009), I have analysed BrdU incorporation and PI staining in cells lacking TCHP and controls. BrdU incorporation mark the number of cells in S-phase of cell cycle and PI staining determined if there is any delay/accumulation in the different phases of cell cycle. TCHP KD cells showed a decrease of BrdU incorporation and consequently an accumulation on G2/M. This results are in apparent conflict with those shown by others in cancer cells (Vecchione and Fassan 2009),where the absence of TCHP stimulates the progression of the cell cycle whereas TCHP overexpression block it. However it is not surprising that cancer cells behave in a complete different way than primary cells having them lost sensitivity to tumour suppressing pathways and resistance to oncogene driving signals. Moreover the abovementioned studies used cancer cells adapted to survive to high degree of aneuploidy and genotoxic stress, on the other hands HUVEC like many others primary cells are more sensitive to ploidy alteration and DNA damage response.(Bautista-Nino, Portilla-Fernandez et al. 2016)

3.4.3 **TCHP knockdown sensitizes ECs to apoptotic death**

The partial mitochondrial localization would also explain its potential involvement in apoptosis. Mitochondria are central organelles in the regulation of apoptosis, mainly by amplifying death signals by the release of cytochrome c and other protein cofactors from the inter-membrane space to the cytosol, where they activate effector caspases (Tait and Green 2013). The mechanisms by which increased expression of TCHP facilitates apoptosis remain to be resolved, but it is conceivable that this occurs through a mechanism dependent on mitochondria and ER tethering and the subsequent calcium efflux from ER to the mitochondria (Cerqua et al. 2010).

As mentioned previously, the mechanisms through which hyperglycemia initiates apoptosis include oxidative stress, increased intracellular Ca2+ and

mitochondrial dysfunction, otherwise known as activation of the mitochondrial apoptotic pathway (Duchen 2004). To address if TCHP silencing could affect apoptosis in ECs, I tested whether TCHP influences apoptotic responses to cell death stimuli. For this purpose, HUVECs were infected with shRNA for TCHP or control vector and treated with Homocysteine, Thapsigargin, Tunicamycin or Rapamycin. ECs lacking TCHP display increase sensitivity to cell death by stimuli triggering an autophagic response and ER stress, showing that these two pathways could be involved in the observed phenotype. Rapamycin, a well-known mTOR inhibitor, was the most effective apoptosis inducer among the treatments. This might reflect a stronger reliance for the KD cells on mTOR dependent survival signals, other than a defective modulation of the autophagy response. It would be interesting a more in depth analysis in order to dissect the between normal apoptosis and other kind of programmed induced cell death, like autophagy or ER-induced cell death.

In the end seems that both the gain and loss of function of TCHP might affect cells' viability, although for different reason; while the former increases the sensitivity to Ca^{2+} induced apoptosis, the latter probably affects the capacity of the cells to resist to stressful conditions, such as autophagy, ER stress or loss of survival signals (mTOR inhibition), resulting in increased cell death.

3.4.4 **TCHP knockdown induces premature senescence phenotype**

Based on the data collected on the characterization of TCHP KD cells, I was prompted to investigate whether lack of TCHP can influences expression of key genes involved in angiogenesis, inflammations, ER stress and cell cycles.

Accordingly, to the presence of defective cell cycle progression, cells with decreased levels of TCHP showed a senescent-like phenotype characterized by elevate levels of p16 and p12 and transcription and secretion of senescent associated pro-inflammatory cytokines, such as IL-6 and IL-8. No significant regulation of genes involved in angiogenesis or ER stress has been observed.

The senescent phenotype was further confirmed by staining for β-Galactosidase activity and western blot for p16 and mTOR phosphorylation.

3.5 **Conclusion**

In conclusion, I have for the first time functionally characterized TCHP in ECs. I have further provided the first evidence that loss of TCHP protein expression may play a role in angiogenesis. Our findings support the hypothesis that TCHP is critical for EC function. Furthermore, I demonstrate, for the first time, that TCHP is implicated in the control of cell growth, apoptosis and that lack of TCHP protein induces a premature senescent-like phenotype in ECs after 7 days of culture.

There two key points that I will be investigated further in the next Chapters of this Thesis; first the increase of number of vacuoles observed at TEM, the strong response to Rapamycin stimulation and the involvement of mTOR pathway encouraged us to investigate the role of autophagy in TCHP KD cells. Second, the partial localization of TCHP with the mitochondria brought us to test the mitochondrial metabolism in TCHP cells and the possible involvement of TCHP in ROS production and apoptosis.

CHAPTER 4:

Does TCHP regulate the autophagy process?

4.1 **Introduction**

Autophagy is a complex intracellular process that delivers cytoplasmic constituents for degradation into lysosomes. Three main types of autophagy have been described: (i) microautophagy (Mizushima and Komatsu 2011), comprising direct engulfment of cytoplasmic material by lysosomes *via* inward invaginations of the lysosomal membrane, (ii) macroautophagy (Feng, He et al. 2014), characterised by the formation of double-membrane sequestering compartments termed autophagosomes that fuse with lysosomes for delivery of cytoplasmic cargo, and (iii) chaperone-mediated autophagy (Klionsky, Abdalla et al. 2012), defined by the association of a chaperone complex with a lysosomal-associated membrane protein type 2A to degrade cytosolic proteins with a specific targeting motif. Autophagy occurs at basal levels in most tissues to allow constitutive turnover of cytosolic components but is stimulated by environmental stress-related signals (e.g. nutrient deprivation and oxidative injury) to recycle nutrients and to generate energy for maintenance of cell viability in adverse conditions (Klionsky, Abdalla et al. 2012). In addition to cellular stress, basal autophagy can be intensified by specific drugs, indicating that the autophagic machinery is a potential therapeutic target for diverse diseases. Indeed, given that autophagy is involved in the prevention of different human pathological conditions, including heart and liver disease, cancer, neurodegeneration, as well as infectious and metabolic disorders, the development of highly specific autophagy modulators has become a major clinical priority.

Basal autophagy also mediates proper cardiovascular function. A variety of cardiovascular risk factors cause defective autophagy due to accumulation of unfolded proteins within the cells. This induces high levels of metabolic stress and impairs functionality of ECs, reducing levels of NO (Bravo-San Pedro, Kroemer et al. 2017). Recent studies suggest that autophagy plays a protective role for other aspects of endothelial function. For example, autophagy has been shown to regulate the release of von Willibrand factor from ECs and angiogenic activity as reflected by endothelial sprouting, proliferation, and tube formation (Torisu, Torisu et al. 2013). Currently, the

pharmacological modulation of autophagy by blocking mTOR function has shown beneficial effects on plaque phenotype. Specifically, local stent-based delivery of rapamycin (known as sirolimus for clinical use) showed antirestenotic activity and improved vascular healing (Garg, Bourantas et al. 2013). Therefore, pharmacotherapy with compounds to re-establish physiological levels of autophagy and restore EC function in the vasculature is an emerging concept for cardiovascular disease, even though a direct univocal link between autophagy reactivation and therapeutic benefits is still to confirm (Galluzzi, Bravo-San Pedro et al. 2017). Interestingly, the potential cardiovascular effect of certain nutraceuticals and common supplements has also been linked to an upregulation of endothelial autophagy (Galluzzi, Bravo-San Pedro et al. 2017, Bonora, Wieckowski et al. 2018).

The parameter that is most appealing is that rates of autophagy are coupled to rates of vascular aging. Clearly, age is the major risk factor for cardiovascular disease and autophagy is increasingly being implicated as a modulator of longevity (Gewirtz 2013). Indeed, global gain of function approaches demonstrate that autophagy induction can extend murine life span (Pyo, Yoo et al. 2013). Analysis of ECs from old versus young mice, as well as analysis of ECs from old versus young patients, reveals that older ECs have lower levels of BECN1 and higher levels of SQSTM1/p62 (LaRocca, Henson et al. 2012). Since SQSTM1/p62 is largely cleared through autophagy, these results are at least consistent with the notion that the aging vasculature has reduced autophagic flux. The notion that this might be more than a correlation is supported by pharmacological interventions that attempt to increase autophagy. The addition of trehalose (LaRocca, Henson et al. 2012) or spermidine (LaRocca, Gioscia-Ryan et al. 2013), two agents that stimulate autophagy, appears to reverse aspects of arterial aging. Interesting results in terms of SASP suppression have been obtained with the mTOR inhibitor rapamycin (Laberge, Sun et al. 2015), which has long been known to extend lifespan and health span in mice (Laberge, Sun et al. 2015). mTOR controls SASP protein secretion by enhancing IL-1α and MAP kinase

activated protein kinase 2 (MAPKAP2) translation (Herranz, Gallage et al. 2015).

4.1.2 **Hypothesis**

Given the activation of the mTOR pathway and the premature senescent phenotype in TCHP KD cells, observed in Chapter 3 and the causal link between them and autophagy, I have been interested in analyzing the possible involvement of TCHP in regulating the autophagic flux in ECs.

4.1.3 **Aims**

The work described here aims to address the hypothesis that:
"*Lack of TCHP impairs autophagic flux in ECs"*

In this Chapter, I aim to:

1. Analyze the autophagic flux in TCHP KD cells
2. Determine and characterize the role of TCHP in ECs from patients with pre-cardiovascular disease

First, the TCHP KD cells will be assessed in order to check critical autophagy proteins and determine the autophagic flux in basal and in autophagy induced condition. Second, the role of TCHP in ECs from patients with pre-cardiovascular disease will be explored, matching the expression of TCHP with key features described previously in our model of TCHP KD cells.

4.2 **Materials and Methods**

Cells and cell culture

Human Umbilical Vein ECs (HUVECs) were grown in EGM-2 and 2% Foetal Bovine Serum (FBS) (Lonza). HUVECs were used between P2 and P6 passage.

RNA extraction and quantitative real-time analysis

Total RNA was extracted using miReasy kit (Qiagen). For mRNA analysis, cDNA was amplified by quantitative real-time PCR (qPCR) and normalized to 18S ribosomal RNA. Each reaction was performed in triplicate. Quantification was performed by the $2^{-\Delta\Delta Ct}$ method (Schmittgen and Livak 2008). Primers are from Sigma (KiCqStart^{TM} Primers).

Cells transduction

HUVECs were transduced at 20 MOI using MISSION shRNA Controls or MISSION shRNA TCHP Lentiviral (SIGMA) particles. Cells were incubated with the viral supernatant for 12h. Double reporter retrovirus was developed using pBABE-puromCherry-EGFP-LC3B (Plasmid #22418) from Addgene.)

Western-Blot analyses

Total protein extracts were obtained resuspending and vortexing cell pellets in small volumes of RIPA buffer containing 1 mM sodium orthovanadate and Complete Protease Inhibitor Cocktail (Roche Applied Science) and quantified with BCA assay. Equal amounts of proteins were loaded onto SDS-Polyacrilamide gels and transferred to PVDF membrane. The membranes were then blocked with 5% non-fat milk in TBST 0,1% and immunoblotted overnight at 4°C with different primary antibodies.

Immunofluorescence

80,000 HUVECs cells were plated on fibronectin-coated glass coverslips in 24-well tissue culture plates. Twenty-four hours later, the slides were rinsed

with PBS once and fixed for 15 min with 4% paraformaldehyde in PBS at room temperature. The slides were rinsed twice with PBS and cells were permeabilized with 0.05% Triton X-100 in PBS for 5 min. After rinsing twice with PBS, the slides were incubated with primary antibody in 3% BSA O.N. in a cold room, rinsed four times with PBS, and incubated with secondary antibodies diluted 1:1000 in 3% BSA for 45 min at room temperature in the dark and washed four time with PBS. Slides were mounted on glass coverslips using Vectashield (Vector Laboratories) and imaged on a Fluorescent Microscope.

ECIS migration

Migration assay was performed using ECIS machine using 8W1LE. 60,000 cells are grown on the arrays on top of opposing, circular gold electrodes. A constant small alternating current is applied between the electrodes and the potential across is measured. The insulating properties of the cell membrane create a resistance towards the electrical current flow resulting in an increased electrical potential between the electrodes. The basis for the measurement of the electrical impedance of cells is Ohm's law, a basic electro-technical principle, which describes the relation between resistance (R), current (I) and voltage (U) in an electrical circuit at a given time (t). The gap in the monolayer is performed increasing the voltage on the electrodes. Speed is determined as the time the cells re-establish the monolayer.

Aggregates staining

Aggregates of ECs was measured using the PROTEOSTAT kit from Enzo (ENZ-51035-0025). The protocol was performed according to the manufacturer’s guide.

Endothelial cells from patients

The study was performed with the approval of the South-East Scotland Research Ethics Committee, in accordance with the Declaration of Helsinki and with the written informed consent of all participants. Patients with

premature coronary artery disease and a family history of premature coronary artery disease (n = 8) were identified from the outpatient department, Royal Infirmary of Edinburgh, Scotland, UK. A control group of healthy age- and sex-matched subjects (n = 8) with no evidence of significant coronary artery disease following computed tomography coronary angiography (CTCA) was recruited from the Clinical Research Imaging Centre, Royal Infirmary of Edinburgh. Subjects attended the Clinical Research Facility at the Royal Infirmary of Edinburgh for vascular assessment and tissue sampling. Vessel wall endothelial cells were isolated by wire biopsy for in vitro expansion.

Statistical analysis

Comparisons between different conditions were assessed using 2-tailed Student's *t* test. If the normality test failed, the Mann-Whitney test was performed. Continuous data are expressed as mean ± SEM of three independent experiments. *P* value <0.05 was considered statistically significant. Analyses were performed using GraphPad Prism v5.01.

4.3 **Results**

4.3.1 **TCHP KD affects autophagy homeostasis**

Transmission Electron Microscope (TEM) revealed a significant increase in the number of autophagic vesicles when TCHP is down-regulated in HUVECs. Autophagosome were identified as double membrane enclosed vesicles while autolysosome as single membrane vacuoles containing partially degraded cytoplasmic content (**Figure 4.1 A**). Immunocytochemistry staining revealed an increased number of LC3 and Sequestosome1 (SQSTM1) positive puncta (**Figure 4.2 A**). As the other ATG8 family members, LC3b undergoes two subsequent post translational modifications, cleavage of the C-terminus exposing Gly120 (LC3b I) and conjugation to the phosphatidylethanolamine' s head group (LC3b II), enabling to its decoration of autophagyc vacuoles (Mercer, Gubas et al. 2018). Western blot analysis showed an increased level of the lipidated form of LC3b (LC3b II) and an increase of SQSTM1 protein levels in TCHP KD cells compared to control (**Figure 4.2 C**). SQSTM1 is an ubiquitin binding protein and an ATG8 binding protein. SQSTM1 acts as an autophagosome cargo targeting protein and organelles for autophagic degradation. Since cargo receptors are degraded by autophagy, increased SQSTM1 stability might indicate a decreased autophagic flux (Klionsky, Codogno et al. 2010). Moreover, a time course was performed to follow up the accumulation of LC3 and SQSTM1 during the time and the samples analyzed by Western blot (**Figure 4.3 A**). Interestingly, it was possible to notice the accumulation of an additional band cross-reacting with SQSTM1 antibody and with a higher electrophoretic mobility than SQSTM1 at the early time point of 4 days. Even if the nature of this second SQSTM1 band was not investigated it was reported a second SQSTM1 isoform lacking the first 84 amino acids at the N-terminal with comparable electrophoretic mobility(Wang, Cano et al. 2014). Alternatively it might have been a cleavage of the full length SQSTM1 by means of Caspase 6 or 8 (Norman, Cohen et al. 2010).

To confirm these data, was used as a complementary strategy the tandem monomeric red fluorescent protein (mRFP)-GFP-LC3 assay. In this assay,

autophagosomes are labeled with a yellow signal (mRFP-GFP-LC3), and their maturation into autolysosomes is attested by a red signal as a result of the quenching of GFP fluorescence in lysosomes. As shown in **Figure 4.3 B**, RFP fluorescence was lower in TCHP KD cells compared with control, attesting to a decrease in autolysosome formation and a slower autophagic flux in cell lacking TCHP.

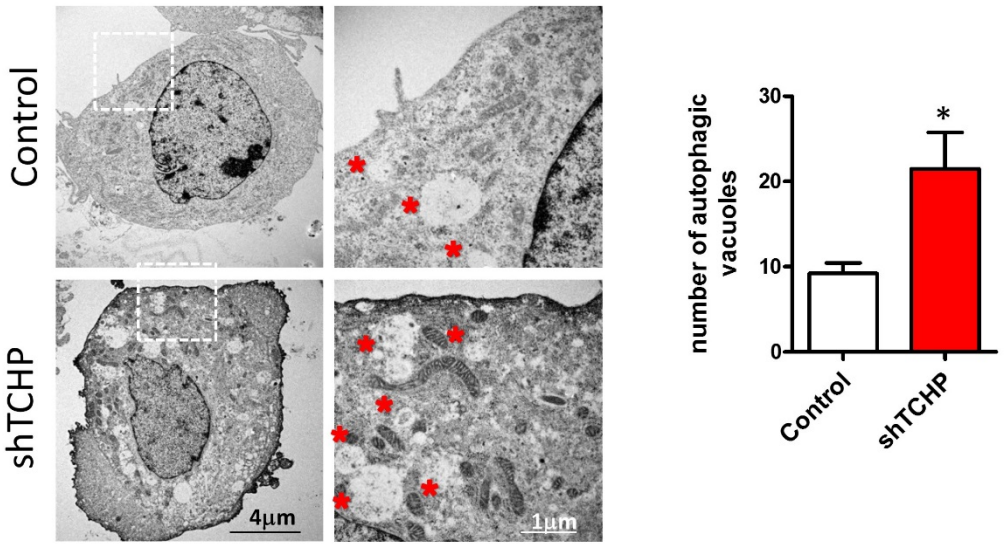

Figure 4.1: Analysis of autophagic features in TCHP KD endothelial cells

Representative pictures from Transmission Electron Microscopy analysis. Red stars are indicating autophagic vacuoles. Chart bars showed the number of autophagic vacuoles in TCHP KD and Control cells from 30 cells. Data are means ± SEM; *p<0.05 vs. control; n=30. (Student's t test).

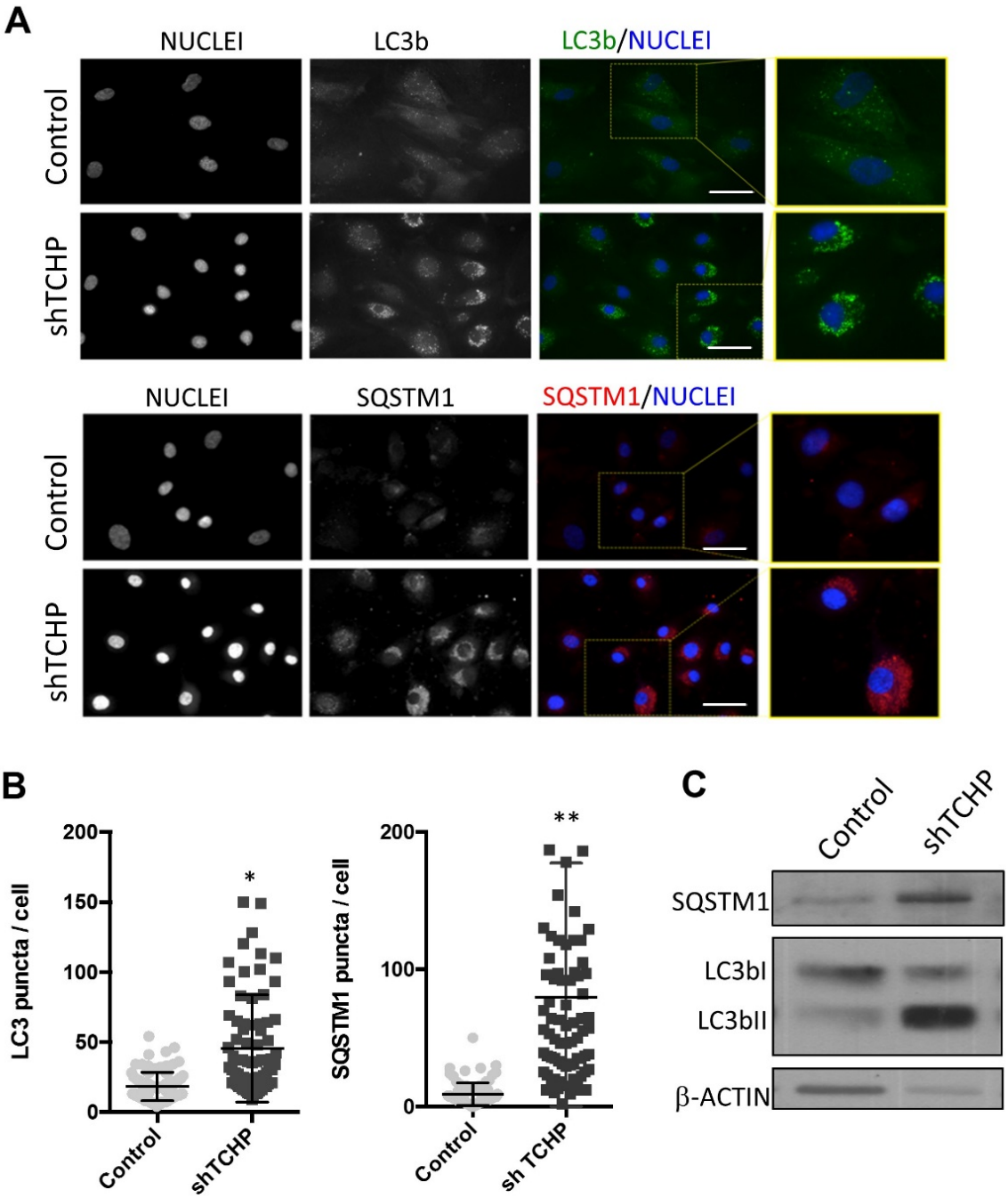

Figure 4.2: Analysis of LC3 and SQSTM1 accumulation

A, Immunofluorescent staining for LC3b and SQSTM1. Scale bar=25μm; **B,** LC3b and SQSTM1 puncta per cell were counted using ICTN plugin from ImageJ from >80 cells for each condition; **C,** Western Blot showing LC3b and SQSTM1 protein levels in transduced samples at 6 days. Data are means ± SEM; *p<0.05, **p<0.001 vs. control; (Student's t test).

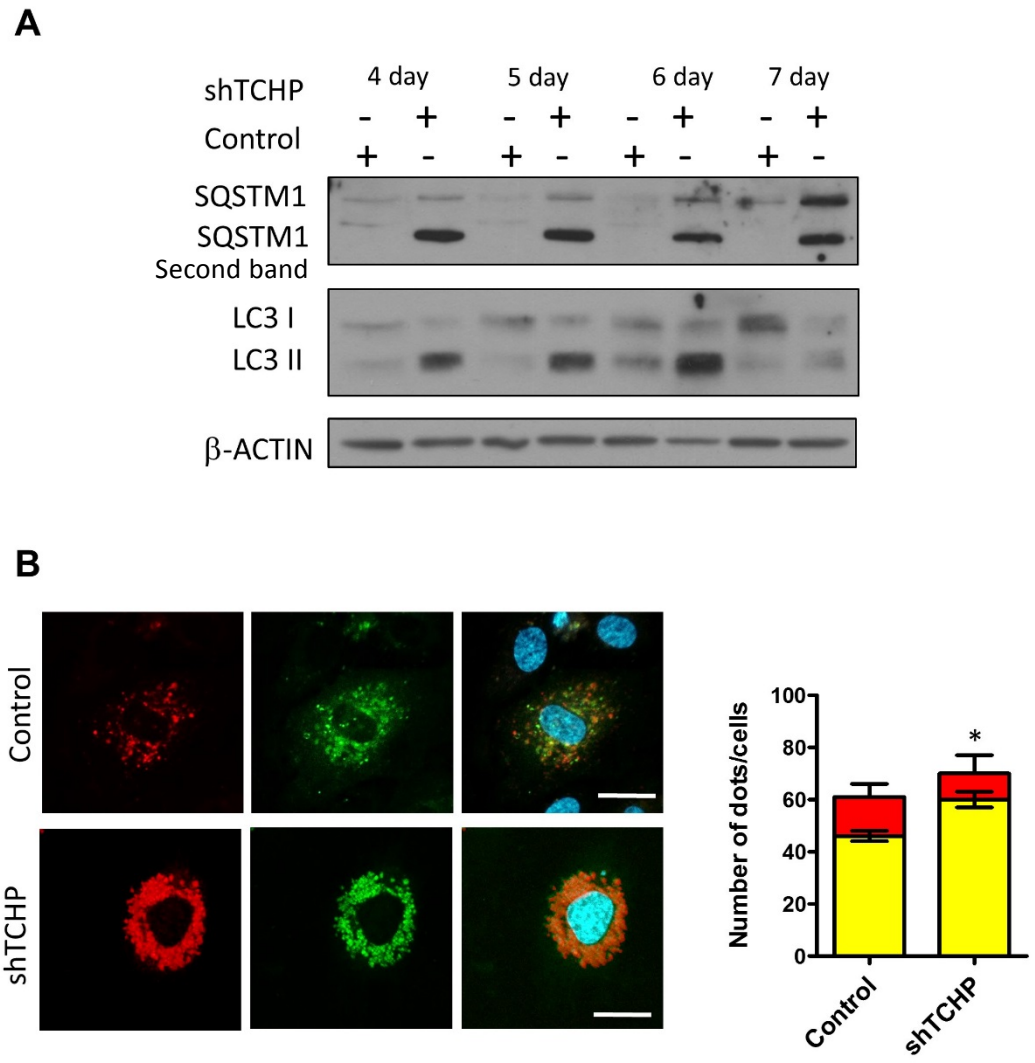

Figure 4.3: Analysis of autophagic flux
A, Western Blot showing time course of LC3b and SQSTM1 protein levels in transduced samples. **B**, Quantification of HUVECs infected with the tandem mRFP-GFP-LC3 lentivirus and infected with shRNA TCHP and Control virus. Yellow bars represent autophagosomes, and red bars represent autolysosomes. Images are representative of three independent experiments in which more than 60 cells were observed. Autophagosomes are labeled with a yellow signal, whereas autolysosomes are labelled with a red signal. (Scale bar, 10 μm.). *p<0.05 vs. control; (Student's t test).

4.3.2 **Regulation of autophagic flux in TCHP KD cells**

To analyze the regulation of the autophagic flux in TCHP KD cells, were performed a set of experiments using an inhibitor of autophagic flux such as Bafilomycin and activators of autophagy such as basal medium or HBSS. The ionophore Bafilomycin was in fact used to stop the flux at its late stage because blocking the lysosome acidification abolishes the digestive power of the lysosomes and at the same time prevents the fusion between autophagosome and lysosome. As shown in **Figure 4.4 A**, A time course treatment of TCHP KD cells with Bafilomycin further increased the level of SQSTM1, showing that the autophagic flux is not completely compromised. In fact if the flux was completely impaired already, adding bafilomycine to stop the lysosome function would not have had any effect on the total amount of SQSTM1.

To further understand if the partial block of autophagic degradation was reversible, control and TCHP KD cells were starved in naked medium (EBM2) and the SQSTM1 protein abundance was compared with cells growing in full medium (EGM2). SQSTM1 decreased after 24 h of starvation and completely disappear at 48 h in TCHP KD samples, showing that the autophagic block possibly affects basal autophagy and not starvation induced autophagy (**Figure 4.4 B**). To biochemically analyze the autophagic flux dynamically during the time the abundance of LC3b and SQSTM1 were analized by Wester Blot in normal and HBSS starved condition with or without bafilomycin. During basal condition, after complete autophagic block, control cells accumulated more SQSTM1 than TCHP KD cells, while this difference was blunted after autophagy induction. Lipidated Lc3b on the other hand appeared to accumulate in KD cells at basal condition whereas the lipidation rate increase more in control cell than in the KD after autophagy stimulation. Finally, the treatment with HBSS re-activated the autophagic flux in TCHP KD cells as demonstrated by strong degradation of LC3b II and reduction of SQSTM1 (**Figure 4.4 C**). Indeed, those results were coherent with slower flux speed in KD cells under basal condition.

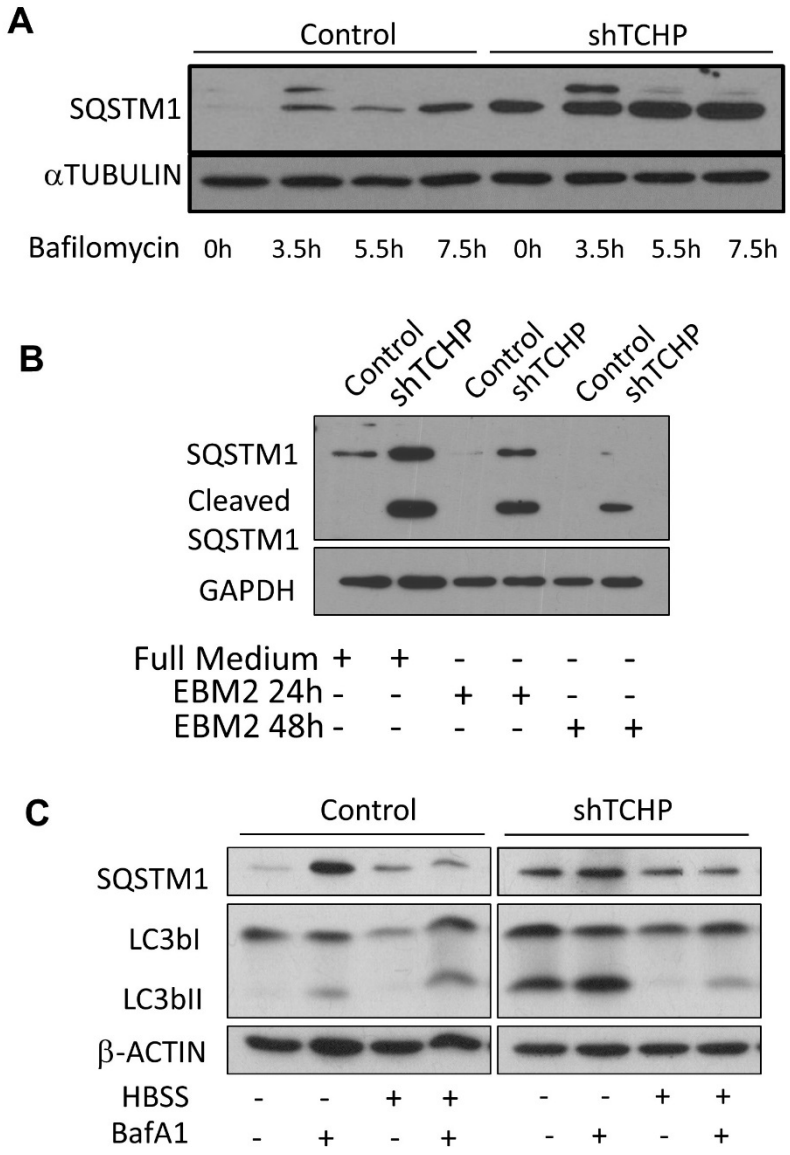

Figure 4.4: Control of autophagic flux in TCHP KD endothelial cells
A, Western blot showing SQSTM1 protein levels in the absence (DMSO) or presence of 200 nM BafilomycinA1 (BafA1) for the indicated time points in Control and TCHP KD **B**, Western blot showing SQSTM1 protein levels under normal culture condition (EGM2) or after serum and growth factors starvation (EBM2) for the indicated time points in Control and TCHP KD cells. **C**, Western blot of the autophagic flux assessment during 2 hours time point under normal culture condition or starved condition (HBSS) or the presence of BafA1.

4.3.3 **TCHP knockdown regulates lysosomal function**

During lysosomal stress or starvation conditions, the transcription factor TFEB relocates from the cytoplasm to the nucleus to activate a transcriptional program promoting autophagy and lysosomal biogenesis and function (Settembre, Di Malta et al. 2011). To test the activation state of TFEB in TCHP KD cells were performed immunofluorescence staining using an antibody targeting TFEB. In TCHP knockdown cells, but not in the control cells TFEB was detected inside the nucleus suggesting a possible activation of the transcription factor (**Figure 4.5 A**). To reinforce this observation, was analyzed the expression of a set of genes known to be regulated by TFEB at 3 and 7 days after knockdown of TCHP (Settembre, Dormitzer et al. 2011). Accordingly, most of these genes were up-regulated in TCHP KD cells and showed a dynamic regulation between the time points. For example, BECLIN1, LC3, CtsB and TFEB genes were highly expressed at 3 days and then decreased at 7 days post-infection, whereas ULK1, LAMP1 and LAMP2 were regulated in the opposite fashion (**Figure 4.5 B**). Interestingly TFEC and TFE3 were also up-regulated: TFEC followed the same trend of TFEB while TFE3 reached the highest expression at 7 days post-transduction.

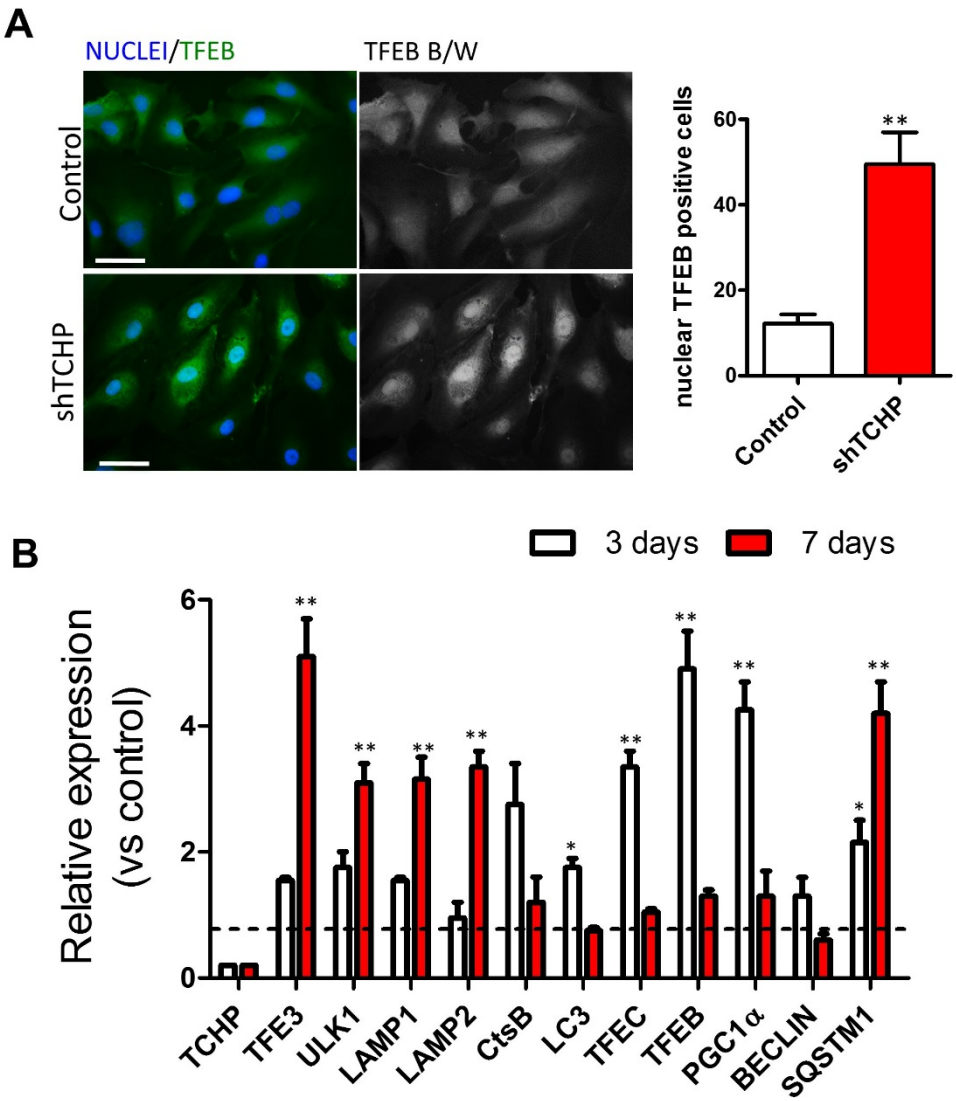

Figure 4.5: Activation of autophagic regulators in TCHP KD endothelial cells

A, Staining and quantification for nuclear TFEB in TCHP KD and control cells at 7 days. **B,** Autophagy regulator and effector genes were assessed by qPCR in control and TCHP KD HUVECs at 72h and 7 days after TCHP KD; Relative expression values to the control are means ± SEM. *p<0.05; **p<0.01 vs. control (n=3); (Student's t test).

4.3.4 **TCHP knockdown affects endo-lysosomal pathway**

The abnormalities affecting the autophagic flux in TCHP deficient cells may suggest a block during terminal stage of autophagy, when autophagosomes fuse with late endosome or lysosome (Klionsky, Codogno et al. 2010) (Klionsky, Abdalla et al. 2012). These observations prompted us to investigate the endosomal and lysosomal compartments as they play a fundamental role in the last step of autophagy (Shen and Mizushima 2014). Immunostaining analysis using anti CAVEOLIN1 (CAV1), RAB11, RAB5, EEA1, RAB7, LAMP1 and LAMP2 antibodies shown a discrete alteration in shape and/or distribution for all the endosomal and lysosomal markers tested (**Figure 4.6 A-F).** For example, CAV1 localization to the rear edge of the plasma membrane of a proliferating ECs was lost in TCHP KD cells, and instead was relocated to large and scattered membrane domains (**Figure 4.6 A**). After TCHP KD the centrosomal fraction of RAB11 appeared to enlarge in comparison to control cells (**Figure 4.6 B**). Both RAB5 and EEA1 vesicles showed similar perinuclear enrichment in TCHP KD cells. Moreover, in TCHP KD cells both proteins identified considerably enlarged vesicle than in the control (**Figure 4.6 C-D**), perhaps reflecting an increase in the active form RAB5-GTP. Control and TCHP KD cells displayed a similar positioning of the RAB7 positive structures around the nuclei (**Figure 4.6 E**). However, in TCHP KD cells the signal was more intense, possibly denoting an increase in RAB7 recruitment to late endosomes or the presence of other RAB7 positive structures like autophagosomes among late endosome vesicles. Finally, TCHP KD dramatically affected the cellular positioning of lysosomes as showed by LAMP1 and LAMP2 staining, inducing a sharp perinuclear clustering of these organelles (**Figure 4.6 F**).

To confirm the activation of endo-lysosomal pathway was performed the Epidermal Growth Factor (EGF) Receptor (EGFR) degradation assay (Pinilla-Macua and Sorkin 2015). Endocytosis and subsequent lysosomal mediated degradation are the major regulators of EGFR stability after activation by the ligand. EGFR degradation kinetic is the prototypic experimental system for studying the molecular mechanisms of stimulus-induced and constitutive

endocytic trafficking. As shown in **Figure 4.7**, in TCHP KD cells, was detected a significant increase of EGFR degradation when cells were stimulated with EGF.

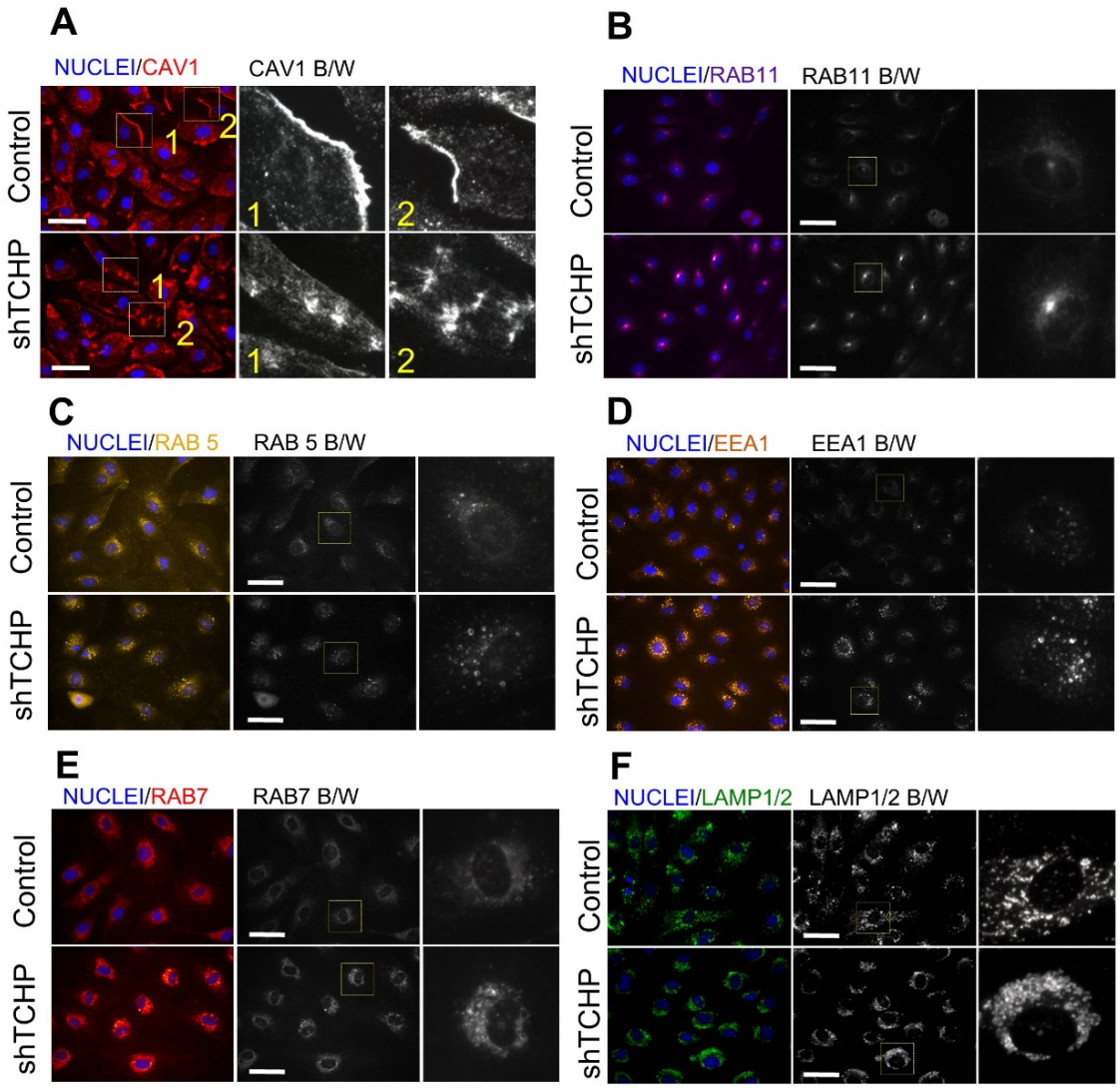

Figure 4.6: Analysis of endo-lysosomal pathway
The endo-lysosomal compartments from Control and TCHP KD cells are analyzed by immunofluorescence. **A,** Endocytic vesicles (CAVEOLIN1) **B**, recycling (RAB11) **C-D**, early (RAB5, EEA1); **E,** late (RAB7) endosomes and markers were detected by immunostaining. Representative image of 10 different fields; n=2; Scale bar 25µm

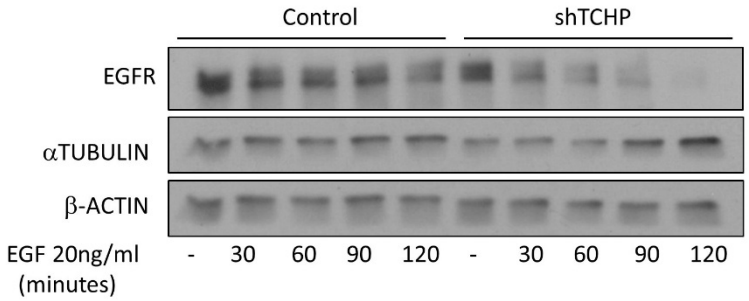

Figure 4.7: TCHP KD increases endo-lysosmal activity
Representative western blot showing Epidermal Growth Factor Receptor (EGFR) expression during pulse chase experiment: after 5 hours of growth factor deprivation Control and TCHP KD HUVECs were stimulated with 20ng/ml EGF for the indicated times. Cells were lysed and processed by SDS-PAGE and immunoblotted for EGFR (n=2).

4.3.5 **Accumulation of aggregates in TCHP KD cells**

Protein aggregates called aggregosome are formed in cells with defective proteostasis due to inefficient Ubiquitin Proteasome system (UPS) or defective autophagy. Aggresomes accumulate in cytoplasmic inclusion bodies and are generated in response to aggregates of misfolded proteins (Johnston, Ward et al. 1998, Kopito 2000), and depending on the cell types and associated misfolded proteins, aggresomes may contain a variety of chaperones. Aggresome composition was shown to varying depending on the cell types the causes at the base of their origin and the associated misfolded proteins for examples most but not all aggresome-associated proteins have been shown to be ubiquitinated or they may contain a variety of chaperones, proteasome subunits or autophagy related proteins(Wigley, Fabunmi et al. 1999, Markossian and Kurganov 2004). Using Proteostat dye, which becomes highly fluorescent upon binding to the amyloid-type b-sheet tertiary structure of protein aggregates (Garcia-Mata, Bebok et al. 1999) revealed increase number of protein aggregate in KD cells respect to control (**Figure 4.8 A**). The aggresome structure in TCHP KD cells was further characterized by immunofluorescence and surprisingly no co-localization between SQSTM1 and the protein aggregates was found (**Figure 4.8 B**).

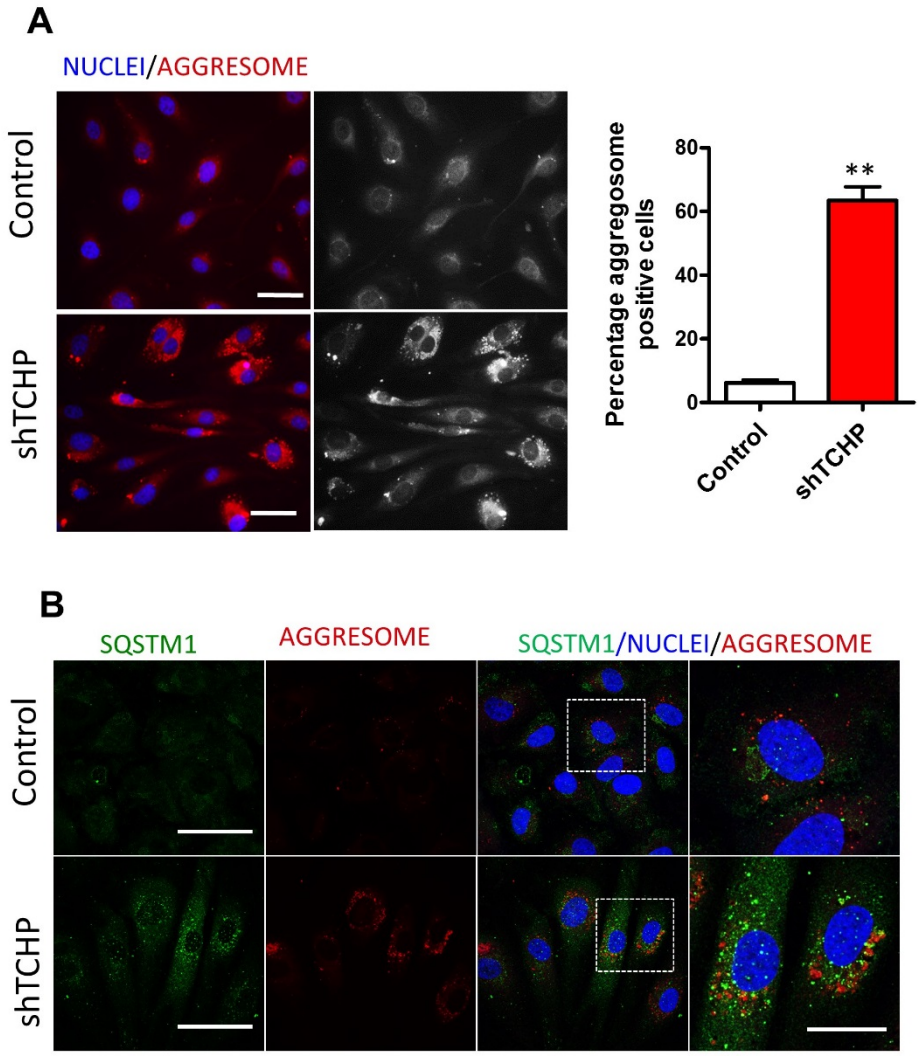

Figure 4.8: Analysis of aggregosomes
A, Aggresome staining and quantification of protein aggregates in Control and shTCHP cells using PROTEOSTAT® Aggresome Detection kit; Picture is a representative image of 8 different fields; n=3. Scale bar 25µm. **B,** Co-localization between aggregates (red) and SQSTM1 (green). Scale bar 25µm and 10µM for the inset. Data are means ± SEM; **p<0.01 vs. control (n=3); (Student's t test)

4.3.6 **Activation of autophagic flux in TCHP KD cells restores migration and decrease inflammation**

To confirm that decrease of autophagic flux is involved in the TCHP-dependent phenotype observed in ECs, I have used Torin-1 to reduce mTOR phosphorylation and consequently its negative activity on the autophagic flux. Torin-1 is a potent and selective ATP-competitive mTOR inhibitor (Thoreen, Kang et al. 2009); therefore Torin 1 treatment of cells leads to the dephosphorylation of mTOR downstream targets including p70 S6 kinase, S6 Ribosomal Protein, and 4E-BP1 (Peterson, Sengupta et al. 2011). Indeed, in our experiments, is shown a reduction in mTOR and p70S6K phosphorylation and a decrease a p16 in TCHP KD cells treated with Torin-1 for 8 hours (**Figure 4.9 A**). Interestingly, also SQSTM1 is downregulated by the Torin-1 treatment (**Figure 4.9 B**). In agreement with previous studies (Herranz, Gallage et al. 2015, Laberge, Sun et al. 2015), I have demonstrated that mTOR inhibition also decrease SASP transcription and improved cell migration (**Figure 4.9 C-D**).

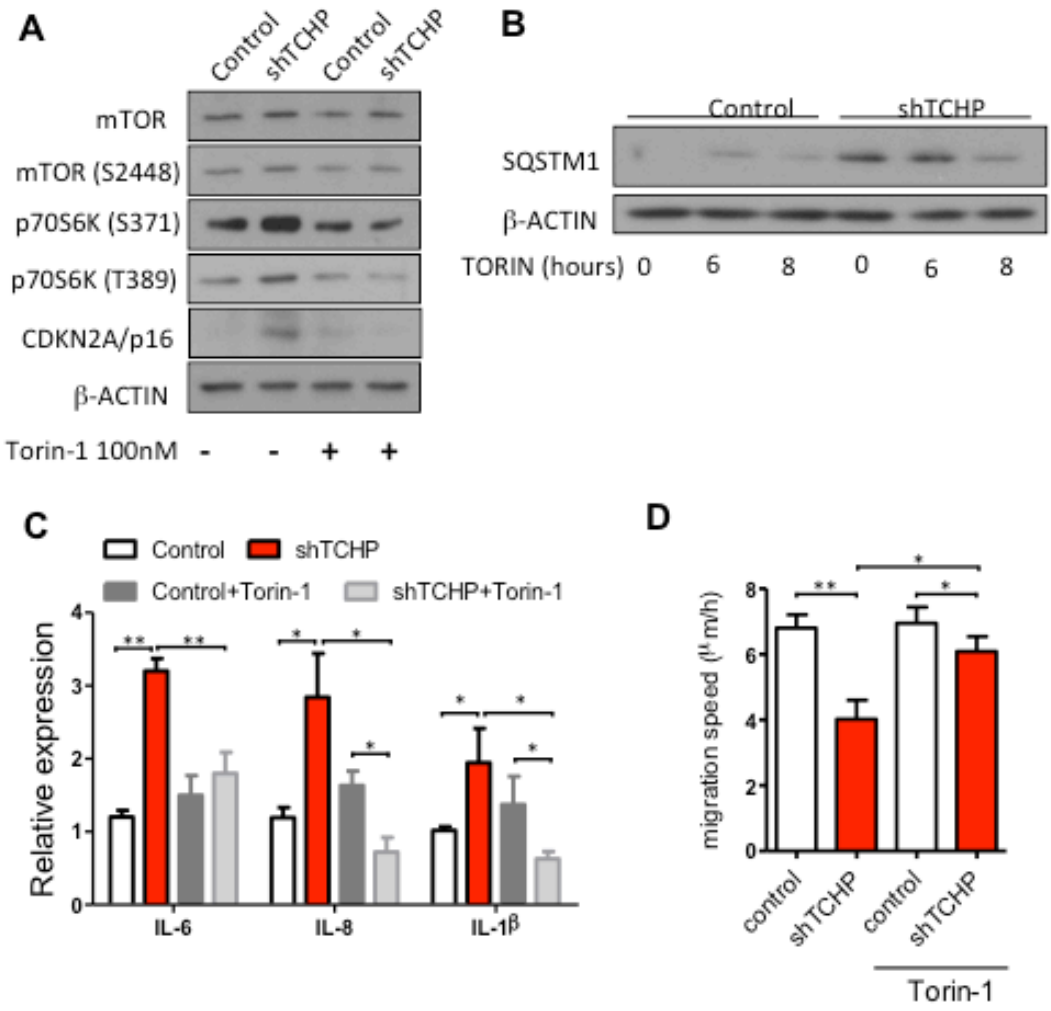

Figure 4.9: Activation of autophagic flux in TCHP KD cells restores migration and decrease inflammation
A, Western blot for mTOR, p-mTOR, p-S6K and p16 of transduced cells treated with DMSO or 100nM Torin1 for 8 hours. n=2. **B,** Representative Western blot showing SQSTM1 protein levels in the absence (DMSO) or presence of 100 nM Torin-1 for the indicated times in Control and TCHP KD HUVEC cells. **C,** IL-6, IL-8, IL-1β were assessed by qPCR in control and TCHP KD HUVECs either treated with vehicle (DMSO) or 100nM Torin-1. **D,** Migration speed of control and TCHP KD were measured by ECIS Zθ. Data are means ± SEM; **p<0.01 vs. Control;(n=3); (two-way Anova test for C and D).

4.3.7 **ECs from patients with premature coronary artery disease have low level of TCHP and express SAPS gene**

I have then analysed the expression of TCHP, SQSTM1 and SASP genes in the ECs from patients with premature coronary artery disease. These ECs have been obtained from vessel wall from patients with endothelial dysfunction had significant impairments in proliferation, adhesion and migration (Brittan, Hunter et al. 2015). Gene expression analysis showed that ECs from patients express low level of TCHP and high level of SQSTM1 and SASPs genes in comparison of ECs from healthy donors (**Figure 4.10**).

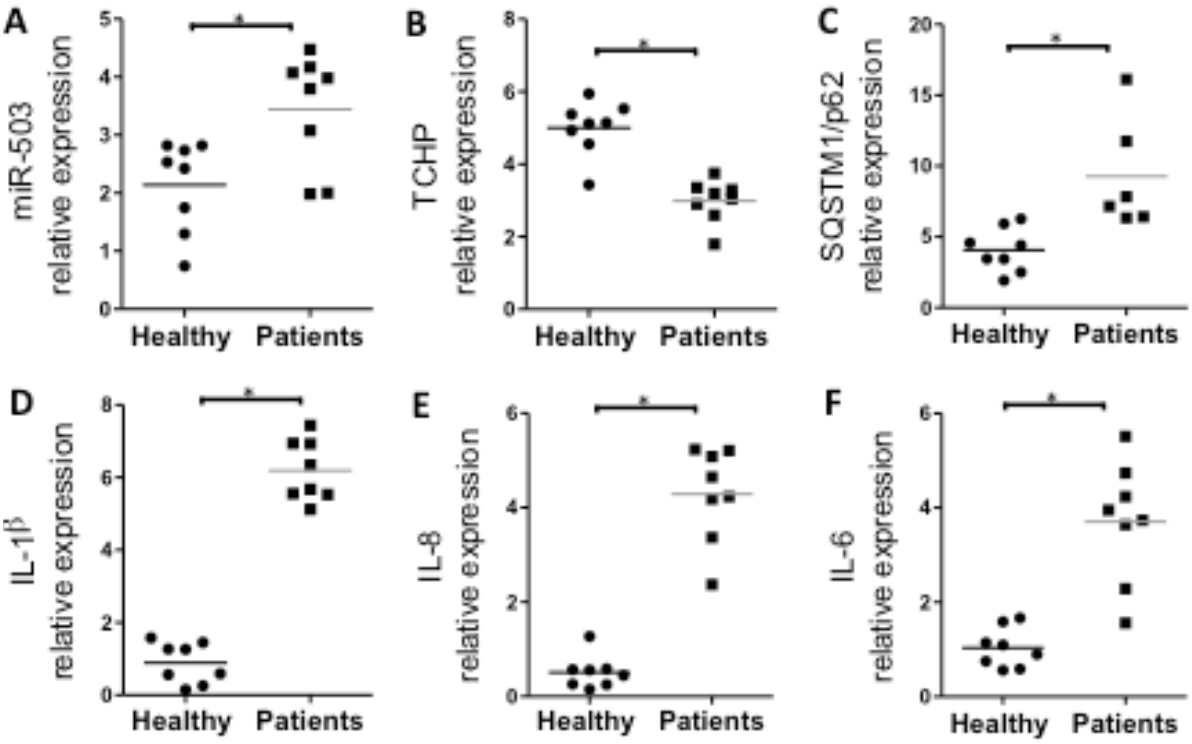

Figure 4.10: Analysis of TCHP, SQSTM1 and SASP genes in ECs from patients with premature coronary artery disease
Expression assessed by qPCR of **A**,miR-503, **B**, TCHP, **C**, SQSTM1 **D**, IL-1β, **E** IL-8 and **F** IL-6 in ECs from vessels wall from patients with premature coronary artery disease. *p<0.05 vs. Healthy subject. Data are means ± SEM (n=8).

4.3.8 **Torin-1 restores EC functionality in ECs from patients with premature coronary artery disease**

To confirm that the downregulation of TCHP in ECs from patients contribute to the similar phenotype observed in TCHP KD cells, I have treated the cells with Torin-1 and analysed SASP gene transcription and migration. As shown in **Figure 4.11 A-B**, Torin-1 treatment for 8 hours reduced cytokines transcription and improved the migration of ECs from patients. Moreover, I have demonstrated that ECs from patients has an accumulation of aggregates compared with ECs from healthy donors. Treatment with Torin-1 also reduced the accumulation of aggregates within the ECs from patients (**Figure 4.11 C-D**).

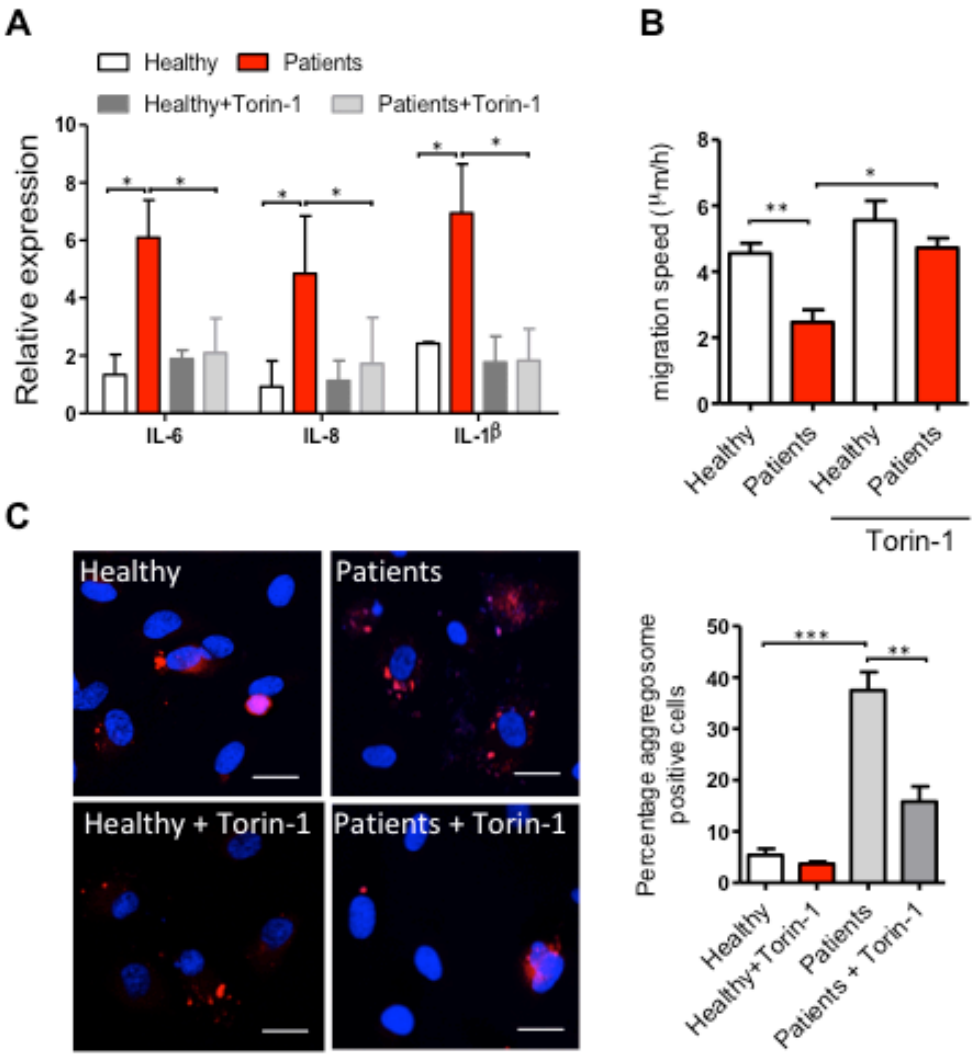

Figure 4.11: Activation of autophagic flux in ECs from patients with premature coronaric artery disease restores migration and decrease inflammation

A, The expression of selected genes SQSTM1, IL-6, IL-8 and IL-1B was measured by qPCR in ECs from healthy subject and patients either treated with vehicle (DMSO) or 100nM Torin1. **B,** Migration speed from healthy and patients ECs either treated with vehicle (DMSO) or 100nM Torin1 were measured by ECIS Zθ,. **C**, Staining and quantification of aggregates in ECs from healthy subject and patients either treated with vehicle (DMSO) or 100nM Torin1. Scale bar 25μm. Data are means ± SEM; *p<0.05; **p<0.01 (n=3); two-way Anova test for A,B and C.

4.3.9 **Characterization of TCHP knockout mice**

In collaboration with the Wellcome Trust-Sanger Institute, I have obtained a set of tissues from Tchp knock out mice and relative wild-type control (age-matched). IHC from different tissues were performed using SQSTM1 and CD31 to identify vessel. Preliminary analysis of the myocardial tissue from TCHP knockout mice at 16 week-of-age exhibited a reduced heart vascularization and significant accumulation of SQSTM1/p62 in the cardiomyocytes (Figure 6.1).

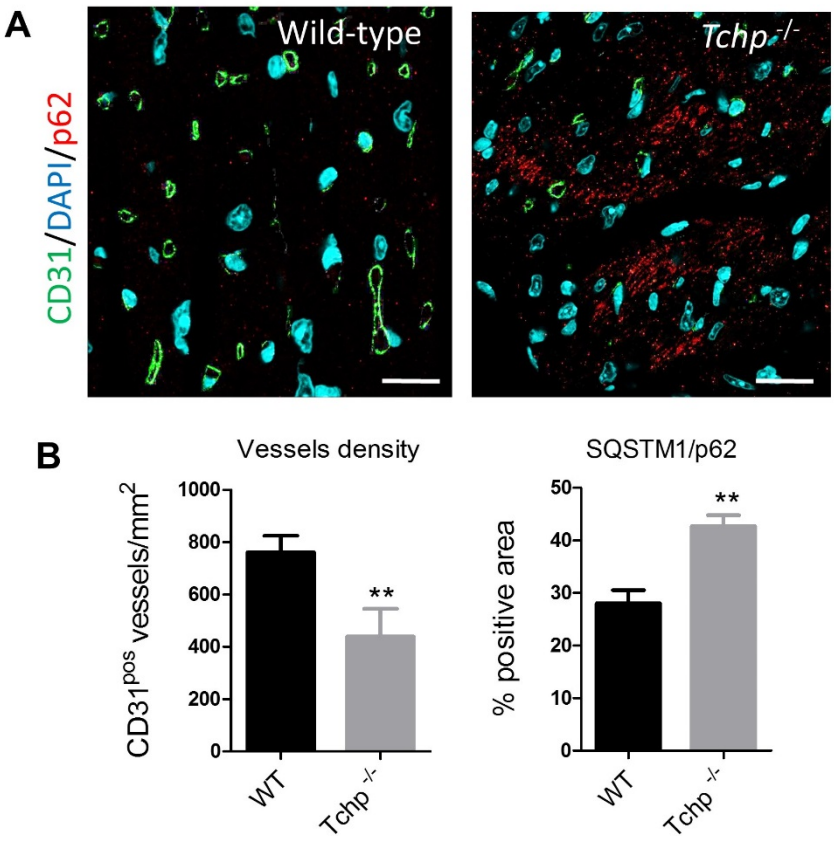

Figure 4.12 Expression of SQSTM1 in TCHP KO mice

A, Detection of SQSTM1 in the heart of Wild-type (WT) and TCHP KO (Tchp -/-) mice; B, Vessel density and quantification of SQSTM1 staining. **p<0.01 vs WT.

4.4 **Discussion**

Our findings highlight an unexpected role for TCHP in EC homeostasis by regulating cellular proteostasis. I demonstrated that lack of TCHP are found in dysfunction EC and are accompanied by the appearance of a senescence-like phenotype. Here I have shown that TCHP KD in HUVECs impairs basal autophagy leading to the accumulation of unresolved autophagosomes, SQSTM1 and protein aggregates.

4.4.1 **Regulation of autophagic flux by TCHP**

In order to analyse the autophagy in TCHP KD and to interpret autophagic flux in the cells were performed transmission electron microscopy, immunocytochemistry, Western blot and the use of LC3 double reporter (Klionsky, Abdelmohsen et al. 2016). Altogether, the assays performed reported a reduced autophagic flux in TCHP KD cells. Analysis of the LC3 and SQSTM1 showed that lack of TCHP can influence the accumulation of these two proteins in ECs. The results obtained using the LC3 double reporter vector reinforce the concept that autophagic flux is reduced in TCHP KD cells.

An interesting follow up of these results would be the identification of the specific point where the autophagic flux is delayed. Several experiments will be necessary to understand if the reduction of autophagic flux is due to an impairment of the autophagosome formation, closure or fusion with lysosomes. Interestingly, SQSTM1 did not co-localize with aggregates and this might play a role in the impaired degradation of protein aggregates through SQSTM1. Analysis of the ubiquitination and association with HDAC6 may provide a more complete set of information about the nature of these aggregates and their formation explaining whether there is any impairment in the binding of SQSTM1 or in the labelling tagging the aggregates for the destruction route.

Finally, I have also assessed that the autophagic flux in these conditions is not completely blocked but it is reversed by starvation, opening the possibility that TCHP-dependent reduction of autophagy could be pharmacologically re-activated.

4.4.2 **Regulation of endolysosomal pathway**

TCHP KD cells showed an interesting change in the localization and intensity of components of endo-lysosomal pathway.

CAV1 is the principal scaffolding protein of caveolae on the plasma membrane with a critical role in endocytosis and in EC polarization and directional migration (Beardsley, Fang et al. 2005). CAV1 was recently identified as a negative regulator of autophagy and lysosomal function through two different mechanisms: one dependent on the interaction with the ATG12-ATG5 autophagic regulatory system and the other by maintaining lipid rafts integrity (Chen, Cao et al. 2014, Shi, Tan et al. 2015). Because the role of CAV1 in ECs as transported of eNOS and VEGFR, the loss of CAV1 positive vesicles on plasma membranes in TCHP KD cells need further investigation and

RAB11 resides in the recycled endosome structure and participates in a number of cellular processes comprising primary cilium assembly, phagophore formation, autophagosome maturation and fusion with MVB/LE or lysosome (Longatti and Tooze 2012). After TCHP KD the centrosomal fraction of RAB11 appeared to enlarge in comparison to control cells.

RAB5 and EEA1 are early endosomal proteins, although while EEA1 has a more close and specific localization, RAB5 can be present in the plasma membrane, clathrin-coated vesicles, and early endosome that mediates fusion of endocytic vesicles to form early endosomes (Ao, Zou et al. 2014). RAB5 after activation by its GEF, Rabex-5, binds EEA1 and other effectors to promote endosome fusion.(Mizuno-Yamasaki, Rivera-Molina et al. 2012). Rab5 is part of a macromolecular complex containing Beclin1 and Vps34, and participates in autophagosome formation (Tanida 2011). Both RAB5 and EEA1 vesicles are enlarged and showed similar perinuclear enrichment in TCHP KD cells.

Rab7 is located on late endosome and promotes microtubule plus-end-directed transport and fusion of autophagosomes with lysosomes. Rab7 when in its active GTP-bound form, binds to Rab7-interacting lysosomal protein (RILP) regulating the microtubule minus-end-direct transport of late endocytic vesicles and phagosomes by recruiting the dynein–dynactin motor complex (Lamb, Longatti et al. 2016). TCHP KD cells the signal was more intense, possibly denoting an increase in RAB7 recruitment to late endosomes or the presence of other RAB7 positive structures like autophagosomes among late endosome vesicles.

LAMP1 and LAMP2 specifically reside on the lysosome membrane. LAMP2 is a core component of chaperone mediate autophagy, a process that involves chaperon assisted loading of target protein directly in the lysosome through a LAMP2 core complex (Cuervo and Wong 2014). TCHP KD cells an increase of lysosomal intensity and a change of position of these organelles. Coherently to the repositioning of the different intermediates of the endosomal pathway the EGFR pulse chase kinetics revealed a faster degradation of EGFR in KD than control cells. The endolysosomal pathway seems in fact more active in the absence of TCHP and a possible reason for that is the attempt of the KD cells to cope with the stall of basal autophagy, potentiating parallel sources of nutrient like endocytosis or micro-autophagy, both relying on the endolysosomal pathway.

4.4.3 **Regulation of TCHP-related phenotype by mTOR inhibitor**

The pharmacological modulation of autophagy by blocking mTOR function has shown beneficial effects on several diseases (Galluzzi, Bravo-San Pedro et al. 2017). Since I have determined that mTOR pathway is strongly activated in our experimental model, I decide to use Torin-1 in order to inhibits mTOR pathway and activate the autophagic flux in the cells.

The mTOR kinase inhibitor Torin-1 blocks the phosphorylation of all mTORC1 substrates more efficiently than rapamycin does, and as a result Torin-1 elicits stronger autophagy induction in both mouse and human cell lines (Thoreen, Kang et al. 2009). Reduction of p16 accumulation and SASP

transcription was previously reported on seminal studies on senescence and mTOR regulation (Herranz, Gallage et al. 2015, Laberge, Sun et al. 2015). As expected, 8 hours treatment of Torin-1 reduced SQSTM1 accumulation; moreover, Torin-1 strongly reduced accumulation of p16 in TCHP KD cells, decreased the transcription of inflammatory cytokine, thus improving EC migration.

Finally, I have further confirmed these results using ECs from the vessel wall from healthy subjects and from patients with premature coronary artery disease. These patients with endothelial dysfunction were identified and selected by measurement of forearm blood flow using venous occlusion plethysmography before and during intra-arterial infusions of endothelial-dependent and -independent vasodilators (Brittan, Hunter et al. 2015). Moreover, the methods for the expansion and maintenance in culture of vessel wall endothelial cells from both patients and healthy controls was adapted from an endothelial biopsy protocol and allow long-term in culture of the cells (Brittan, Hunter et al. 2015).

The traditional paradigm of vascular repair is based on the proliferation and migration of existing mature ECs from the adjacent vasculature (Psaltis and Simari 2015). The vessel wall ECs from patients with endothelial dysfunction have reduced proliferation, adhesion and migration suggest that local mechanisms of vascular repair are impaired in patients who develop premature coronary artery disease. Treatment with Torin-1 for 8 hours reduced the transcription of inflammatory cytokines, increase proliferation and reduced the protein aggregates within the cells. Although Torin1 is able to trigger a strong autophagic response its use in clinic results improbable because of its non specific action on mTOR1 and mTOR2 and potential dangerous side effects. Rapamycin and its derivates (Rapalogs) may represent a better option since maintains mTOR2 active and preserve the capacity to activate autophagy. For reason concerning the cytostatic and anti inflammatory action exerted by rapamycin, rapalogs eluting stent are currently on trials for anti re-stenosis therapies. Although there are beneficial

effects on smooth muscle cells and immune cells, the cytotoxic effect on endothelial cells is still source of preoccupation. At this regard it should be noted that the positive effect induced by TORIN1 to TCHP KD and PCAD EC comes from a transient treatment with the drug and thus free from the cytotoxic side-effect associated with long exposure. Furthermore it would be valuable taking in consideration a different strategy and try to increase TCHP expression to improve patients' EC functions. For example a possible approach might involve Decorin stimulation to increase TCHP level (Neill,T.et al 2014).

4.4.4 **Tchp *in vivo* study**

Immunohistochemistry microscopy was performed on paraffin embedded tissue from Tchp KO mice kindly donated by the Wellcome Trust-Sanger Institute. Results from this *in vivo* study confirmed one of the major finds already observed during the *in-vitro* and *ex-vivo* study that is the strong increased of SQSTM1 after TCHP loss. More importantly IHC on myocardial tissue of KO mice showed for the first time the detrimental effect of TCHP loss on the vasculature network. Decrease capillary density in Tchp KO in partially anticipated by the results coming from *in vitro* studies, is of fundamental importance not only because it is the first example of organ dysfunction linked to TCHP deficiency and remarks the critical role of this protein in the cardiovascular system, but also it opens other interesting perspective like the role the endothelial specific knock-out of Tchp during high-fat diet or post-ischaemic angiogenesis after myocardial infarction or limb ischemia.

4.4.5 **Conclusion**

In this Chapter, I have demonstrated that insufficient levels of TCHP leads to inefficient autophagy and this in turn contributes to the development of endothelial dysfunction. Defective endothelial autophagy, driven by TCHP

attenuation, not only curbs endothelial migration, but also promotes an inflammatory and senescent phenotype. Importantly. *Ex-vivo* study showed that pharmacological activation of autophagy in ECs from patient's vessel wall with premature coronary disease, improved EC migration and reduce inflammation. Altogether, these findings underline the role of TCHP in endothelial autophagic flux control and suggest autophagy activation by Torin-1 as a protective mechanism in TCHP deficient cells, thus showing that stimulation of autophagy may be an attractive strategy in the prevention of endothelial dysfunction associated to TCHP loss.

CHAPTER 5:

Does TCHP regulate mitochondrial function in ECs?

5.1 **Introduction**

Mitochondria have often been described as the energy factories of the cell. In numerous cell types, mitochondria produce large amounts of cellular energy required by the cell in the form of adenosine triphosphate (ATP). ATP is also produced in large quantities in the cytosol via the process of glycolysis. However, other major ATP producing metabolic processes are contained within the mitochondrial membranes namely, the Krebs cycle and oxidative phosphorylation (OXPHOS) via the electron transfer chain (Giedt, Pfeiffer et al. 2012). It is important to note that in previous years mitochondria have been shown to be highly functionally dynamic organelles with many non-bioenergetic roles. These roles include the regulation of intracellular Ca2+ homeostasis as well as in the production of reactive oxygen species (Masotti, Miller et al.) related to oxidative stress (Gutierrez, Ballinger et al. 2006, Davidson and Duchen 2007, Murphy 2012). The ability of mitochondria to produce ROS has emphasized their importance in influencing cell signalling pathways including the importance of ROS in apoptosis inducing pathways specifically (Willems, Rossignol et al. 2015).

It has been shown that ECs produce the majority of their cellular energy via glycolysis in the cytosol (Xu and Erzurum 2011) as opposed to in the mitochondria. These finding have lead researchers to identify the importance of non-biogenetic roles endothelial mitochondria play in the vasculature specifically.

Mitochondria are highly mobile organelle and evidence suggests that their spatial localization changes according to the needs of the cell (Murphy 2012). Therefore, their non-bioenergetic roles can be modulated by the localization of the organelles which has significant implications in the context of the mitochondria's involvement in signalling pathways.

One of the most important functions of mitochondria within cardiovascular cells, particularly ECs, is their ability to produce ROS (Caja and Enriquez 2017). Excessive production of these species has been linked to mitochondrial dysfunction, which is often an important factor in the

development and/or the progression of many cardiovascular pathologies. It was first thought that ROS were predominantly produced because of mitochondrial dysfunction and solely contributed to cell death via their effect on apoptosis pathways. More recent work has pointed to the importance of ROS as important secondary messengers, regulating several cellular signalling pathways present at basal levels. ROS have been shown to be produced by the oxidative phosphorylation (OXPHOS) complexes I and III via single electron reduction of oxygen (Tang, Luo et al. 2014). This production does occur at a basal level but is often increased during mitochondrial dysfunction. The reactive oxygen species produced is predominantly superoxide and, if produced in sufficiently high quantities, can overwhelm the ECs endogenous antioxidant defences leading to an increased oxidative stress state (Li, Dietz et al. 1997). Endothelial dysfunction in diabetic patients has been linked to increased ROS and reactive nitrogen species (Silvander, Kvarnstrom et al.) (Son 2012). ROS can directly modify mitochondrial (OXPHOS) proteins and in so doing exacerbate ROS production and its potential detrimental effects on the cell at high levels.

Mitochondrial ROS production has been implicated in hypoxia signalling/gene expression regulation in the nucleus. Specifically, the combined effect of the localization of mitochondria around the nucleus and increased oxidative stress results in the increased concentration of ROS inside the nuclear envelope. The co-localization of mitochondria and the nucleus results in a smaller total distance necessary for ROS to diffuse into the nucleus. The increased intra-nuclear ROS has been shown to stabilize oxygen-sensitive pro-hypoxia transcripts (Al-Mehdi, Pastukh et al. 2012).

Since recent studies indicate that TCHP plays an important role in the physiology of mitochondria (Vecchione, Fassan et al. 2009, Cerqua, Anesti et al. 2010), in this chapter, I have taken different approaches to analyse the effect of lack of TCHP has on mitochondria position and function. This study will try to provide for the first time whether TCHP promotes a fission-like phenotype of mitochondria and a redistribution of mitochondria near the

nuclear membranes. Moreover, analysis of ROS production and mitochondrial bioenergetics will be investigated.

5.1.2 **Hypothesis**

Since TCHP is partially localize with the mitochondria, thus possibly effecting ROS production and mitochondria functionality; the work described in this Chapter aims to address the hypothesis that:

“Lack of TCHP impairs mitochondrial function and bioenergetics in ECs”

5.1.3 **Aims**

In this Chapter, I aim to:

1. Analyse the effect of the downregulation of TCHP on the localization of mitochondria
2. Investigate the effects of the lack of TCHP on mitochondrial functionality and ROS production in ECs

5.2 **Materials and Methods**

Cells and cell culture

Human Umbilical Vein ECs (HUVECs) (Lonza) were grown in EGM-2 (EBM-2 medium supplemented with growth factors and normal 5mM D-Glucose, NG) and 2% Foetal Bovine Serum (FBS) (Lonza). HUVECs were used between P2 and P6 passage.

Western blot

Proteins were transferred to polyvinylidene difluoride (PVDF) blotting membrane. Membranes were hybridized with the following antibodies: Mitochondrial OXPHOS complexes cocktail (Abcam/MitoProfiler®Total); anti-PARP1 (Abcam); Anti-Rabbit IgG (whole molecule)–Peroxidase antibody produced in goat; Anti-Mouse IgG (whole molecule)–Peroxidase antibody produced in sheep. Chemiluminescent detection of proteins of interest was achieved using Immobilon™ Western Chemiluminescent HRP Substrate kit (Millipore). The Western blots were developed on X-ray film and quantified using UN-SCAN-IT gel™ version 6.1.

Native-PAGE of mitochondrial electron chain complexes

To assess the effect of TCHP KD on the electron transport chain (ETC) also referred to as OXPHOS complexes, Native-PAGE was used to separate the different complexes while in their native conformation followed by western blotting. All products were used according to manufacturer's instructions. The Novex® NativePAGE™ Bis-Tris gel system purchased from Thermo Fisher Scientific was used to separate the mitochondrial electron chain complexes. Kit included Invitrogen NativePAGE™ 3-12% Bis-Tris Gels. NativePAGE™ 20X Cathode Buffer Additive. Native-PAGE™ 20X Running Buffer. As well as NativePAGE™ Sample Prep Kit.

Mitochondrial isolation protocol

To separate OXPHOS complexes using Native-PAGE, mitochondria were isolated from control and TCHP know-down HUVECs. The mitochondrial isolation protocol used by (Frezza et al. 2007) to isolate mouse embryonic fibroblasts was used as a starting point to develop the protocol in HUVECs. Cells were harvested and suspended in ice cold IBc buffer (10 ml of 0.1M Tris-MOPS, 1 ml of EGTA/Tris, 20 ml 1M sucrose made to 100 ml in H2O, pH = 7.4, Complete™ protease inhibitor added). Cells were then homogenised using a Teflon pestle. A number of centrifugation steps followed in order to isolate the mitochondria from the homogenate. Mitochondria isolates were solubilised as per the manual provided with the Native-PAGE system. Digitonin detergent provided in the sample prep kit was used at a final concentration of 2.5% v/v which was found to yield the best solubilisation results.

Seahorse: Mitochondrial respiration stress test

The Seahorse XFe24, Extracellular Flux analyser manufactured by Agilent Technologies was used to conduct a mitochondrial stress test to quantify key parameters of mitochondrial respiration under control and TCHP know-down conditions. Control HUVECs and TCHP know-down were plated into Seahorse XF24 V7, 24 well microplate plates and grown to 70% confluence before analysis at either day three and seven days after infection.

Flow cytometry

Both control and TCHP know-down cells were analysed to determine total mitochondrial mass and relative levels of mitochondrial ROS. MitoTacker®Green FM – Mitochondrial probe (used to determine mitochondrial mass) Life Technologies, (100nM). MitoTracker®Red CM-H2XRos – Mitochondrial ROS probe (used to quantification mitochondrial ROS) (50nM). Probes were incubated with cells for 30 minutes at 36°C prior

to washing with PBS and subsequent detachment with trypsin before being analysed.

Immunofluorescence

HUVECs cells were plated on fibronectin-coated glass coverslips in 24-well tissue culture plates. Twenty-four hours later, the slides were rinsed with PBS once and fixed for 15 min with 4% paraformaldehyde in PBS at room temperature. The slides were rinsed twice with PBS and cells were permeabilized with 0.05% Triton X-100 in PBS for 5 min. After rinsing twice with PBS, the slides were incubated with primary antibody in 3% BSA O.N. in a cold room, rinsed four times with PBS, and incubated with secondary antibodies diluted 1:1000 in 3% BSA for 45 min at room temperature in the dark and washed four time with PBS. Slides were mounted on glass coverslips using Vectashield (Vector Laboratories) and imaged on a Fluorescent Microscope. Antibodies: Tom20 mouse monoclonal IgG (Santa Cruz Biotechnology/(FL10); Phalloidin; Green fluorescent Alexa Fluro® 488 anti-mouse. A Zeis Axioskop HBO 50 florescence microscope equipped with a Photometrics® coolSNAP HQ2 CCD camera and QImaging® CRI Micro*Color 2 RGB Liquid Crystal Tunable Filters was used to acquire imaging.

ImageJ and CellProfiler analysis

CellProfiler software was used to build a pipeline (predefined sequence of analyses) to quantify the localisation/distribution of fluorescent labelled mitochondria. Cells treated with either shRNA scramble (control) or shRNA TCHP were grown and stained with DAPI (to identify the nucleus) and Phalloidin (to labelled F-actin to identify the cell periphery). Tom20, a protein localised to the outer mitochondrial membrane, was labelled with a green Alexa Fluor® 488 conjugated antibody. With these organelles and structural components labelled CellProfiler was used to aid in quantifying the intensity of Tom20 signal on a large number of images/cells. The intensity of the

Tom20 signal in sequential areas/rings from the nucleus were measured to quantify the distribution/localisation of the mitochondria. Quantification of mitochondrial localisation within defined areas/distance from the nucleus was achieved using CellProfiler. This software allows semi-automated analysis of batches of images.

Statistical analyses

All statistical analyses were performed using GraphPad Prism v5.01. The predominant test used was the students paired t-test, which was used to assess the difference between the mean values of paired data sets throughout this study.

5.3 **Results**

5.3.1 **Lack of TCHP does not affect mitochondria localization**

The general rearrangement of endolysosomal vesicle systems identified in the previous Chapter persuaded us to further investigate the mitochondrial localization. The mitochondria's localisation with respect to the nucleus was assessed by immunoflorescence using The MitoTracker™ Green FM probe to label specifically mitochondria, followed by ImageJ and CellProfiler analysis (**Figure 5.1**). The median fluorescent intensity (MFI) is reported as a percentage of the total MFI measured in the full area analysed (nucleus/0 – 16 μm). By expressing the MFI as a percentage of the total an impression of the distribution/localisation of all mitochondria analysed per cell is described (**Figure 5.1 C**). The experiments were performed on samples labelled 7 days after infection. TCHP KD and control cells seemed to have similar mitochondrial positioning with respect to the nuclear membrane.

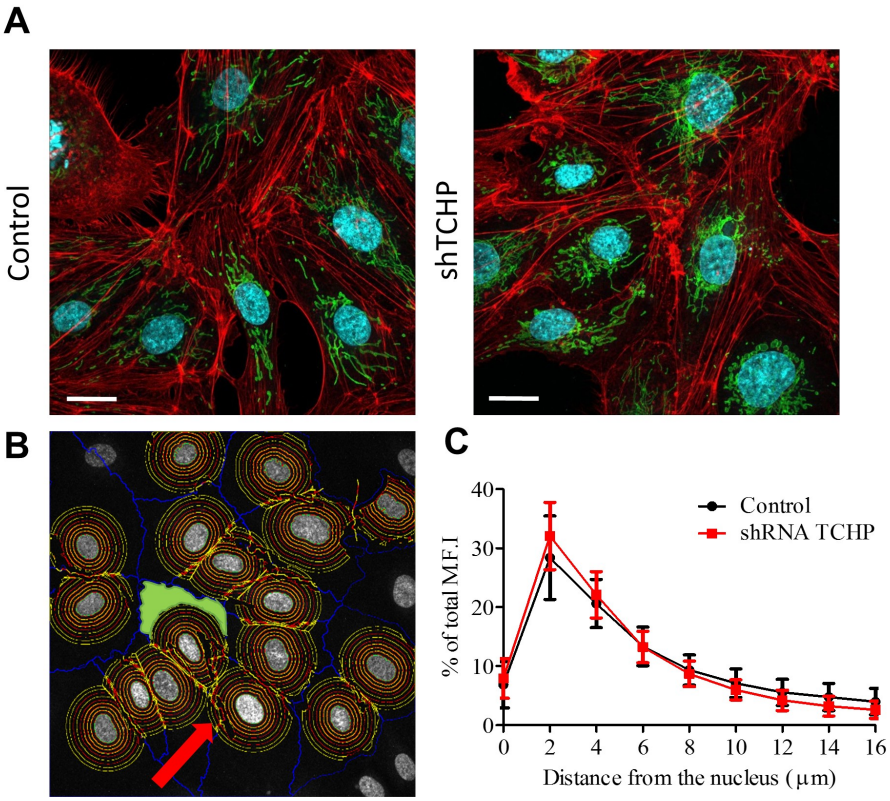

Figure 5.1: Analysis of mitochondrial localization in TCHP KD and control cells

Assessing the localisation/distribution of mitochondrial using confocal microscopy and CellProfiler image analysis software. TCHP KD and control cells were analysed at 7 days after transduction. **A,** Cell stained for Tom20 (green) and Phalloidin/F-actin (red) Scale bar 25µm. **B, F**inal output image generated by the CellProfiler pipeline. After nuclei were identified, the cell periphery was identified using the red/F-actin (Phalloidin) channel. Each nucleus then acted as a seed for subsequent 2 µm rings to be draw radiating from its periphery. **C,** MFI of mitochondria in 2 µm rings from the nucleus expressed as a percentage of the total MFI measured in the 0 – 16µm area analysed. More than 30 cells from 3 different field per experiment were analyzed. Data are means ± SEM, n=3; *p < 0.05 (Student's t test).

5.3.2 **Quantification of total mitochondrial mass and ROS in TCHP KD cells**

Mitochondria are highly dynamic organelles that can change their subcellular redistribution to redirect ROS signal into the nucleus during hypoxia (Al-Mehdi, Pastukh et al. 2012)**.** The total mitochondrial mass of HUVECs infected with control or shRNA TCHP lentivirus respectively was assessed using flow cytometry. The MitoTracker®Green FM probe was used to label mitochondria specifically, irrespective of membrane potential. No significant effect on mitochondrial mass due to TCHP KD was detected at 3 or 7 days post infection using this method (**Figure 5.2 A**). The MitoTracker™ Red CM-H2XRos fluorescent mitochondrial ROS probe was used and HUVECs were analysed at 3 days and 7 days after infection. A significant increase in mitochondrial ROS production was detected at 7 days after infection (**Figure 5.2 B**). Finally, using CellROX™ probe to analyse the level of total ROS in the cells, was shown that the total ROS in the cells are not affected in TCHP KD cells (**Figure 5.2.C**).

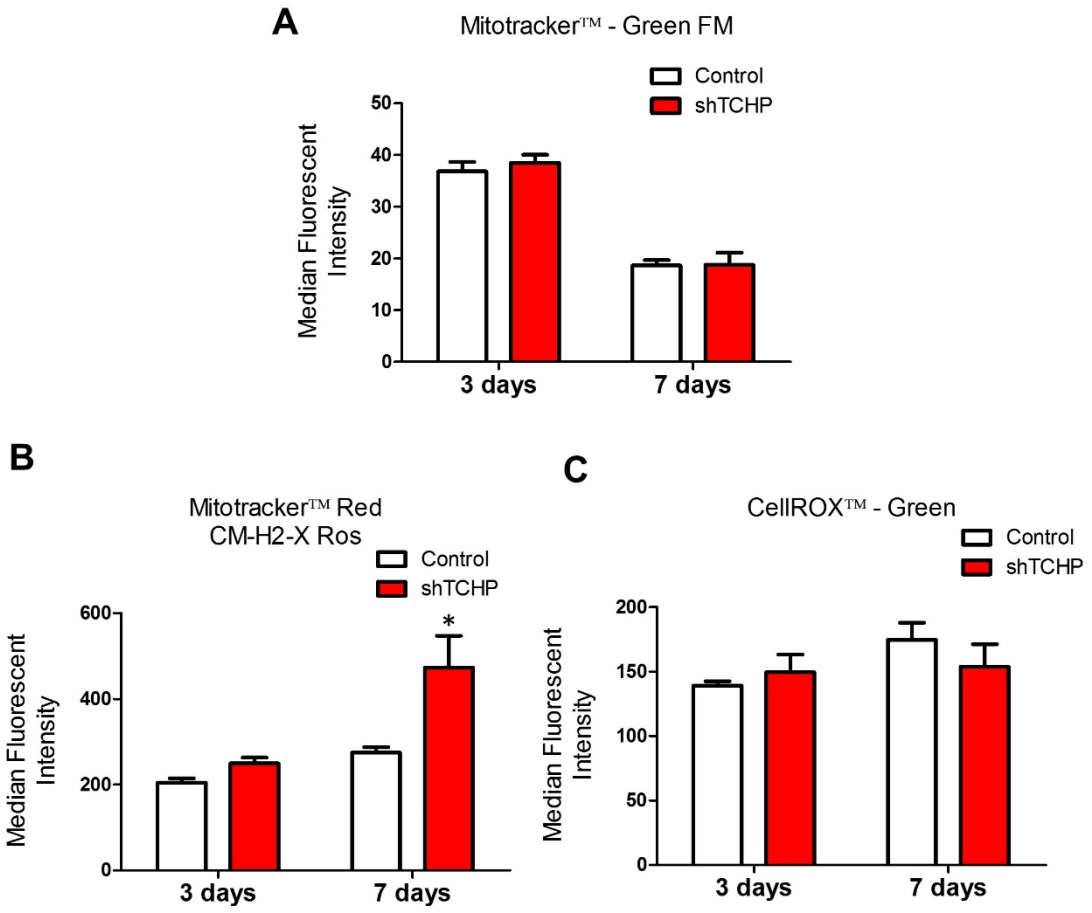

Figure 5.2: Quantification of total mitochondrial mass and ROS
TCHP KD and control cells were labelled at 3 and 7days after infection. **A.** Quantification of total mitochondrial mass using flow cytometry; graph showing total MFI values. **B.** Mitochondrial ROS were determined by MitoTracker™Red CM-H2XRos (emission spectra at wavelength 610 nm). **C,** Total cell ROS analysis were determined by CellROX™ (emission spectra at wavelength 520 nm). Data are means ± SEM, n=2; *p < 0.05 (Student's t test).

5.3.3 **Analysis of mitochondrial function with respect to mitochondrial respiration in cell lacking TCHP**

To evaluate the effect of the lack of TCHP on mitochondrial respiration, the Seahorse mitochondrial stress tests were performed on control and TCHP KD cells. The stress test was performed on cells 7 days after infection and results are shown in **Figure 5.3 B**. The Seahorse XF24 extracellular flux analyser provides cellular respiration in steady-state conditions and after the addition of specific inhibitors for selected mitochondrial electron transport chain complexes. Oxygen consumption rate over time was measured in control and TCHP KD cells. Cellular respiration was calculated and dissected into mitochondrial and non-mitochondrial respiration using Rotenone and Antimycin A inhibitors of complex I and complex III, respectively (**Figure 5.4 A-B**). Mitochondrial respiration was further dissected into proton leak as the residual oxygen consumption after R/A treatment (**Figure 5.4 D**) and ATP-linked respiration (**Figure 5.4 E**) using the ATP-synthase inhibitor, Oligomycin. The portion of spare respiratory capacity was obtained by subtracting basal respiration from maximal respiration rates induced by the FCCP drug treatment. Interestingly reserve capacity of TCHP KD cells was significantly lower than reserve capacity of control cells (**Figure 5.4 C**).

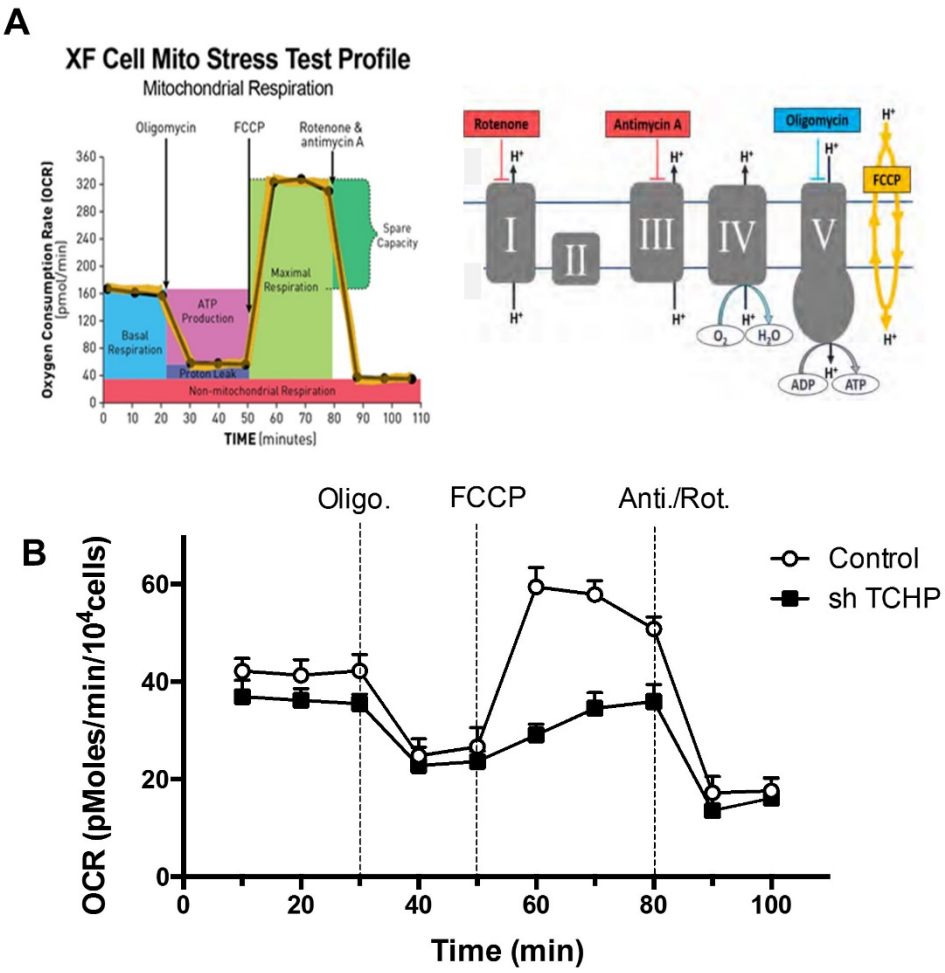

Figure 5.3: Seahorse XF Cell Mito Stress Test analysis of cell lacking TCHP

A. Exemplifying image of Seahorse XF Cell Mito Stress Test response profile (Sutendra, Dromparis et al.) and picture (left) describing the respective drugs used and which ETC complex/s they inhibit Source image available at https://www.agilent.com/en/products/cell-analysis/mitochondrial-respiration-xf-cell-mito-stress-test. **B,** Oxygen Consumption Rate (OCR) over time from control and TCHP knockdown cells calculated using a SeaHorse X24 extracellular flux analyzer.

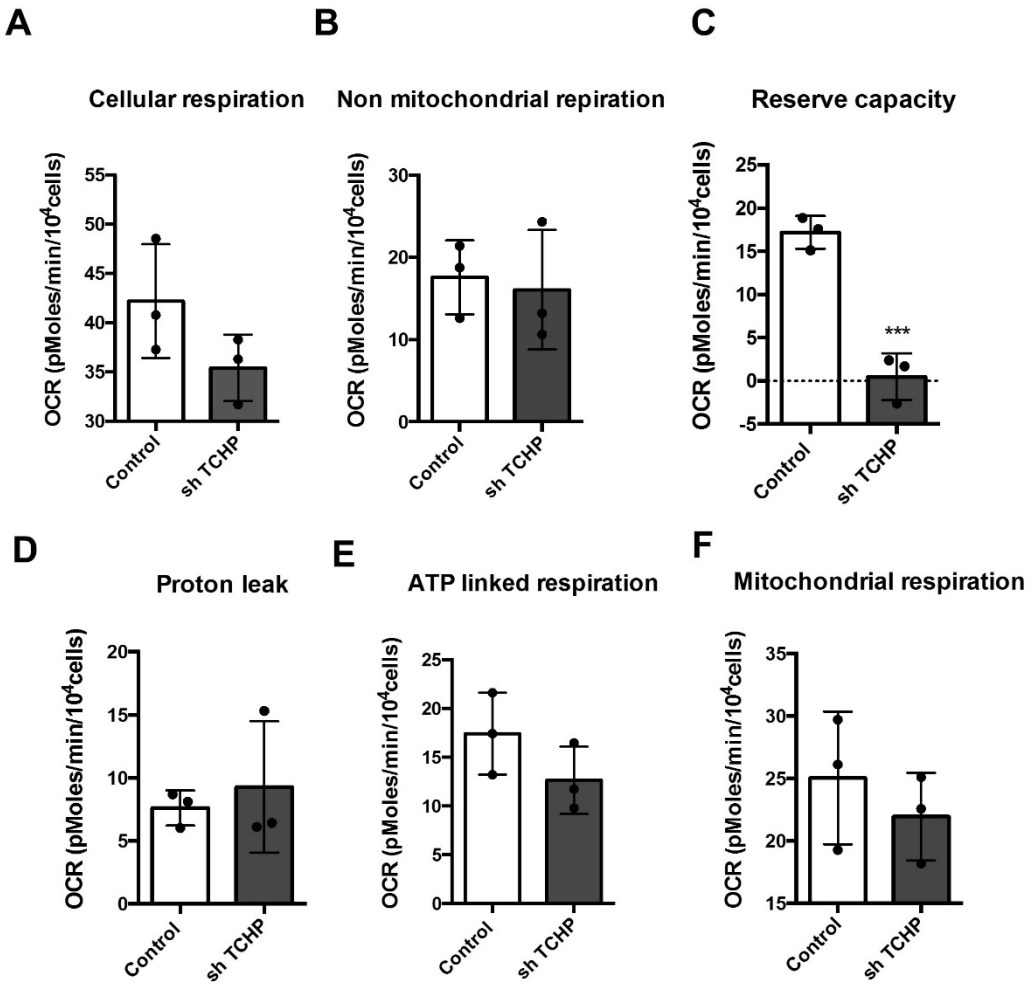

Figure 5.4: Analysis of Seahorse experiments parameters
Oxygen consumption rates (OCR) for cellular respiration **A**, mitochondrial and **B**, non-mitochondrial; **C,** reserve capacity, **D**, proton leak, **E**, ATP linked respiration and, **F,** mitochondrial reserve capacity were analyzed using specific electron transport Chain ETC inhibitors; Data are means ± SEM, n=3; *p < 0.05 (Student's t test).

5.3.4 **Analysis of relative abundance of electron transport chain complexes in TCHP KD cells**

Decreased mitochondrial spare capacity is often due to a reduced expression of one or more components of the Electron Transport Chain (ETC). Native-PAGE was specifically employed to ensure the complexes were kept in their native conformation (intact tertiary and quaternary structures) to better visualise potential changes to these complexes under TCHP KD conditions. **Figure 5.5** is representative of three replicate experiments in which aliquots of mitochondria solubilised with 2.5% v/v digitonin were run on a Native-PAGE gel. The pixel intensities of the Native-western blots were normalised using the Red Ponceau of the correspondent SDS-PAGE gels as well as being normalised against complexes levels from control cells (**Figure 5.5 B**). Interestingly, ETC complexes revealed an overall trend of increasing levels of mitochondrial ETC machinery present under TCHP KD conditions 7 days after infection. However, every precaution was taken to insure accurate loading of the Native-PAGE wells by means of BCA total protein analysis. A second precaution was taken to correct for potential loading error. The SDS-PAGE gels were loaded with the same amount of total protein per lane, 2 µg, as the Native-PAGE gels. These SDS-PAGE gel lanes were used to normalize for any loading error via pixel intensity quantification.

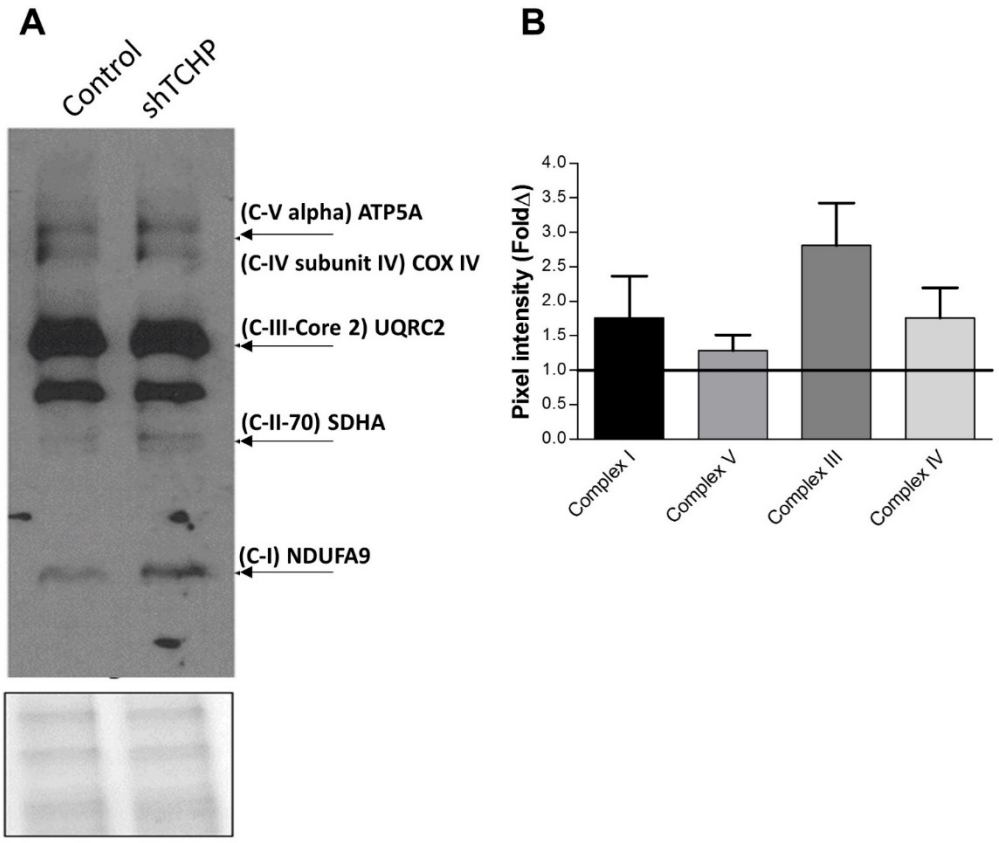

Figure 1 **Figure 5.5**: **Analysis of mitochondrial ETC/OXPHOS protein complexes**

HUVECs were transduced with either shRNA scramble (control) or shRNA TCHP lentivirus analyses was perfeormed at 7 days after transduction **A**. Western blot analysis of 5 different proteins representing the 5 different multisub-units complex enzymes constituting the ETC. **B,** Pixel quantification of all complexes detected in western blots. The solid line at 1 across the Y-axis indicates the normalised control FoldΔ. The labelled bars on the graph represent the relative abundance of each complex visualised through pixel intensity quantification. Data are means ± SEM, n=3.

5.3.5 **TCHP KD affects energy balance in ECs**

Potentially a deficit in the mitochondrial reserve capacity may be due to problems that affect one or more of the components of the ETC or may be related to a lack of intermediates fuelling the chain with their electrons (Dranka, Hill et al. 2010). In this section it was considered the latter option. I assessed the levels of total Nicotinamide adenine dinucleotide NADt (NAD+ and NADH) (**Figure 5.6 C**) at 3 and 7 days after transduction and detected a marked fall at 3 days in KD cells and was only partially recovered at the later time point (**Figure 5.6 A**). Since NAD is a cofactor for GAPDH, a decrease in its bioavailability might affect the glycolytic process. Three days post-infection was observed an initial decrease in ATP in KD cells, followed by a sharp drop at 7 days compared to controls (**Figure 5.6 B**). Moreover, to understand the reasons for NAD decline, I separated nuclear and cytoplasmic fractions from control and KD cells, which revealed that the most prominent reduction was restricted to the cytoplasm (**Figure 5.6)**. NAD is consumed by three classes of cellular proteins: CD38, Sirtuins and members of the Parp family (Canto, Menzies et al. 2015). To further investigate the causes behind the NAD decrease I have checked two of the most likely potential consumers of NAD: SIRT1 and PARP1. In TCHP KD cells SIRT1 expression as determined by qRT-PCR was slightly increased at 3 days but subsequently decreased at 7 days (**Figure 5.7 A**). PARP1 levels and activity were examined by WB and were strongly decreased in TCHP KD samples at 7 days post-infection (**Figure 5.7 B-C**). Therefore, if our observed effect was not due to NAD exhaustion I proposed that it may be a result of a recycling defect, as the NAD recycling pathway takes place in the cytoplasm. Consequently, I decided to test the expression of Nicotinamide phosphoribosyltransferase (NAmPRTase or **Nampt**), the rate limiting enzyme involved in NAD recycling. However, I noticed significantly higher levels of NAMPT in TCHP KD cells than in controls (**Figure 5.7 D**).

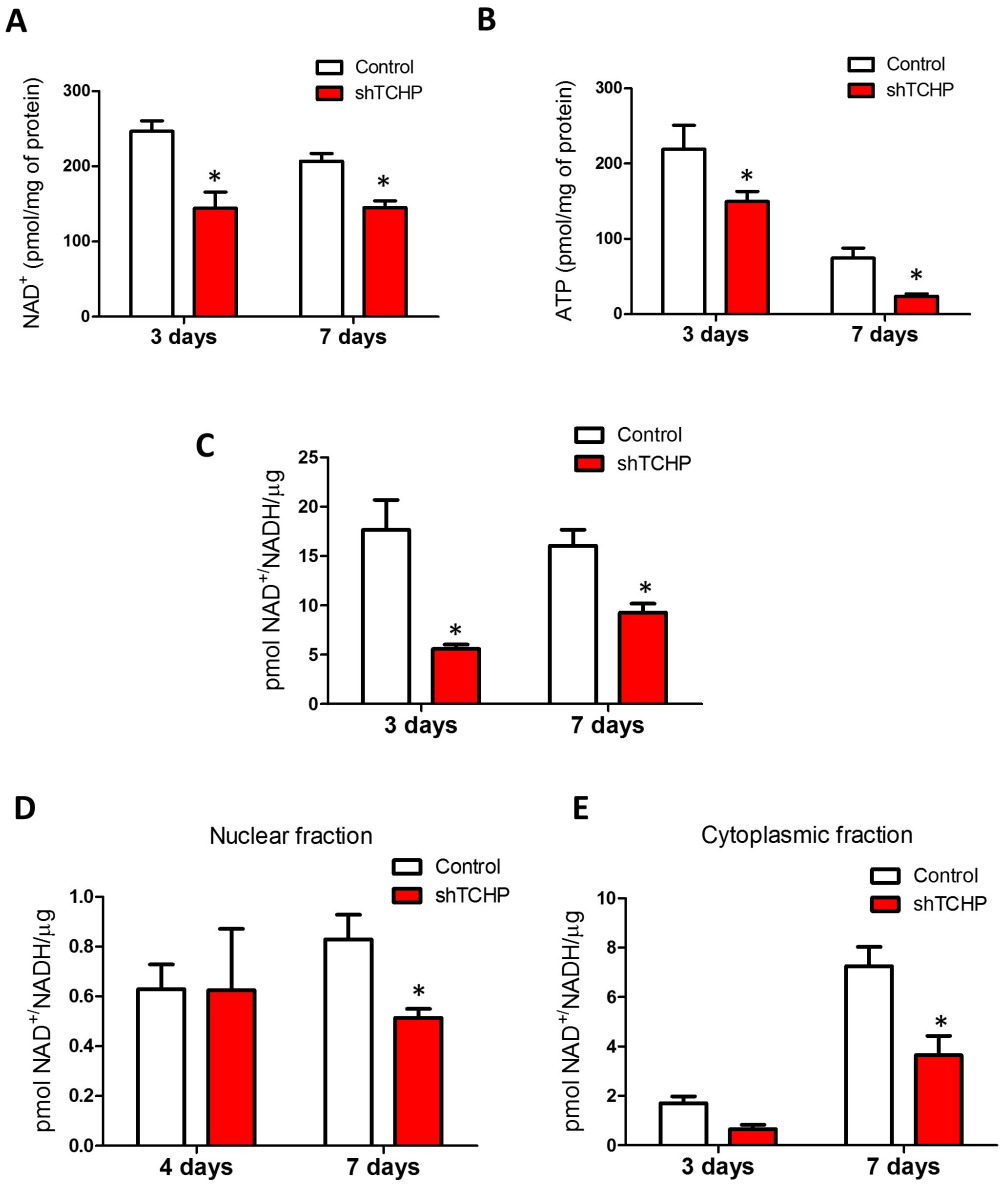

Figure 5.6: TCHP KD affects energy balance of the cells
Quantification of **A,** total NAD+ and **B,** ATP in Control and TCHP KD using a bioluminescent (StayBrite ATP Assay Kit) and a colorimetric (NAD+/NADH Quantification Colorimetric Kit) kit respectively; **C**, Quantification of total NAD [NADt (NAD+ and NADH)]. **D,** Nuclear and **E**, cytoplasmic quantification of both NADH and total NAD [NADt (NAD+ and NADH)] in Control and in TCHP KD cells; Data are means ± SEM, n=2; *p < 0.05 (Student's t test).

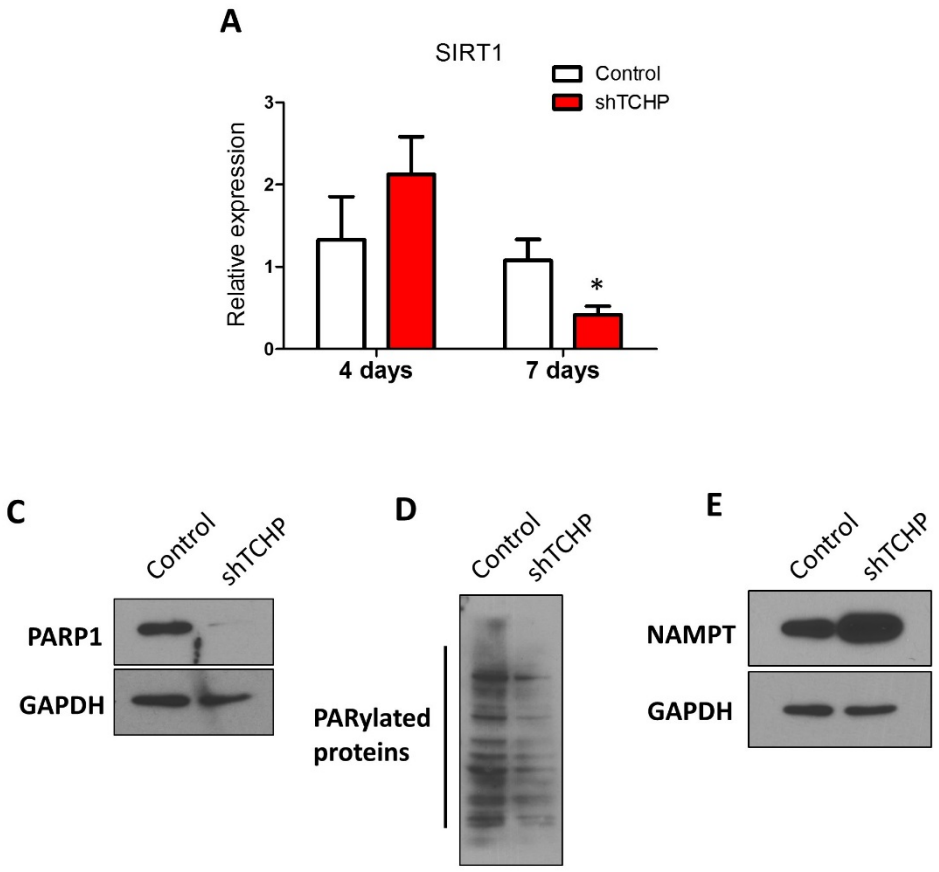

Figure 5.7: TCHP KD regulates SIRT1 and PARP1 abundance.
A Relative SIRT1 mRNA expression in Control and TCHP KD cells; **C,** PARP1 abundance and **D,** parylated protein products assessed by WB in Control and TCHP KD cells; **E** levels of NAMPT protein revealed by Western blot analysis in Control and KD cells. Data are means ± SEM, n=2; *p < 0.05 (Student's t test).

5.4 **Discussion**

Since TCHP was shown to be associated with the outer mitochondrial membrane (Cerqua, Anesti et al. 2010), the main hypothesis of this Chapter was to assess what impact, if any, does TCHP KD have on the functionality of endothelial mitochondria. I was therefore interested in understanding whether lack of TCHP would have any detrimental effects on mitochondrial function and localization.

5.4.1 **Mitochondria localization and size**

Analysis of mitochondria localization in TCHP KD showed a no significant difference compared with control cells, even though the outline trend of moving mitochondria towards the nuclei took shape. To confirm the trend the number of cells to analyse need to be increased and more accurate quantification up to the plasma membrane might be required. Moreover, before further molecular testing of the mitochondria could be performed with confidence, quantification of total mitochondrial mass under both control and TCHP KD conditions were assessed. The results obtained show no change in mitochondrial mass in TCHP KD HUVECs at 7 days.

5.4.2 **Effect of TCHP KD on ROS production**

Elevated levels mitochondrial ROS are often positively correlated to increased cellular stress. Previous work has shown the importance ROS can play as secondary messengers influencing gene expression under particular stress conditions (Al-Mehdi, Pastukh et al. 2012). Due to the role, ROS has been shown to play in cellular stress response and endothelial dysfunction (Madamanchi and Runge 2007), I aimed to quantify the mitochondrial ROS levels in control vs TCHP KD cells. A significant change in mitochondrial ROS was evident under TCHP KD conditions at 7 days after infection. This results might be in agreement with the previous chapter results, in fact there are evidence that increase ROS are require to induce and expand the autophagy response(Scherz-Shouval, Shvets et al. 2007). In this perspective

increased ROs in KD cells might be the cellular response to the decline of autophagic flux. In addition ROS elevation may contribute, through NF-KB activation, to the pro-inflammatory phenotype seen aster TCHP loss.

5.4.3 **Mitochondria bioenergetics**

To assess TCHP KD effect on the ability of mitochondria to respond to stress Seahorse mitochondrial respiration analysis was performed. The Seahorse XF Mito Stress Test generated profiles that describe the mitochondria's ability to respond to several stresses. The stresses are induced by the sequential additional of compounds that inhibit specific regions of the ETC machinery. Inhibiting these complexes over a time course while measuring OCR allows numerous aspects of mitochondrial function to be assessed. I have demonstrated that TCHP deficiency strongly reduced the mitochondrial reserve capacity, a characteristic feature of mitochondrial dysfunction. Reserve mitochondrial capacity could be a measure of how much mitochondria are able to adapt their energy production in stress situation requiring increased energy demand. Noteworthy, reduced reserve capacity is often associated with mitochondrial dysfunction in a series of different pathological condition (Brand and Nicholls 2011). Moreover the reserve capacity may be considered an indirect measurement of the efficiency by which mitochondrial complexes work so a reduction in mitochondrial reserve capacity might underlie a functional and or structural defect of ETC complexes.

Isolation and separation of the ETC/OXPHOS complexes using Native-PAGE was performed to further investigate potential deficit in their abundance or structural defect. Quantification of the Western blots showed an increase in all mitochondrial complexes under TCHP KD conditions, therefore, a general increase in oxidative phosphorylation machinery is present in mitochondria seven days in TCHP KD. The complex that was shown to increase most under TCHP KD conditions was complex III/CoQH2-cytochrome c reductase. This observation was interesting as it has been suggested that increased electron leakage from complex III and complex I both contributed to greater ROS levels and subsequent elevated H2O2 levels (Jastroch, Divakaruni et

al. 2010). Increased levels of both these complexes particularly complex III may suggest the reason for higher mitochondrial ROS production in KD cells.

5.4.4. **Effect of TCHP KD on EC energy balance**

Reduced mitochondrial reserve capacity may alternatively been caused by insufficient bioavailability of substrate supplying the TCA cycle or deficiency in essential ETC complex enzyme cofactors NADH and FADH. To this regard were measured the concentration of ATP and NAD/NADH. Interestingly both ATP levels and total NAD (NADt) dropped in TCHP KD cells. Reduced glycolysis may have been the cause for less ATP produced, moreover since NAD is a cofactor for GAPDH, an essential glycolytic enzyme, the observed decline in ATP may be secondary to the fall in NADt bioavailability. The reduction in NADt concentration might be caused by an increased consumption rate or a delay in the recycle of the intermediate following the utilisation by cellular enzymes. Given that PARP1 and SIRT1, two major NAD consumers, are indeed down-regulated in our model, It was sensitive to hypothesize a possible defect in the NAD recycling chain. To further address this point was checked the abundance of NAMPT, the rate liming step enzyme for the NAD salvage pathway. Surprisingly were observed increased levels of NAMPT possibly suggesting a compensatory reinforcement of the NAD salvage pathway, to better cope with decreasing NAD levels. Data of this part are very preliminary and need further investigation, for example only the main NAMPT over a total of three isoforms was assessed and this may lead to incomplete picture of the total NAD salvage capacity of the cell. Secondly it would be desirable and more relevant testing the enzymatic activity of NAMPT from TCHP KD.

5.4.5 **Conclusion**

In summary, the effect of TCHP KD on mitochondrial functionality was first assessed by quantifying total mitochondrial ROS. This experiment showed no statistically significant change in mitochondrial ROS levels. Secondly mitochondrial mass was quantified using two methods. Using flow cytometry and imaging analysis, I have demonstrated no persuasive change in mitochondrial mass. Investigation into the ETC complexes revealed an overall trend of increasing levels of mitochondrial ETC machinery present seven days after TCHP KD. Finally, Seahorse analysis revealed a change in the ability of mitochondria to respond to stress in TCHP KD cells. This interesting observation could be an area for further investigation.

CHAPTER 6:
Discussion and Conclusions

The vascular endothelium, the functional lining of blood vessels, plays a critical role in vascular homeostasis. Whereas normal endothelial function is thought to be atheroprotective, endothelial dysfunction is increased in atherosclerotic conditions such as coronary heart and peripheral artery disease (PAD) and is an independent predictor of future cardiovascular events. The most severe form of PAD, critical limb ischaemia (CLI), occurs when arterial blood flow is restricted, causing inadequate perfusion of capillary beds to sustain tissue viability. About 20% of the UK population aged 55-75 years suffer PAD, equating to a prevalence of 850,000 people, of whom 5% have symptomatic critical limb ischaemia (CLI) (Aboyans, Ricco et al. 2017). Although endovascular interventions and open surgical techniques are the main therapeutic options for limb salvage, a significant proportion of patients with CLI are not eligible and foot amputation remains the ultimate alternative, with an associated yearly mortality rate >25%. There is an increasing interest in identifying novel targets and developing therapy to improve endothelial function in the hope to reduce disease progression and future cardiovascular risk. There is evidence that endothelial dysfunction in patients with PAD can be improved; however, development of additional medical therapies for endothelial dysfunction is an area of unmet medical need with a currently limited research pipeline.

The work contained in this thesis was designed to clarify the role of TCHP in EC function and its mechanisms. The work utilised a number of experimental approaches to provide a complete picture of the role of TCHP in ECs through the regulation of autophagy and, hence, reveal whether it is a promising target for further investigation.

6.1 **TCHP in endothelial cell function**

The TCHP gene is located on chromosome 12q24 that is frequently deleted in a variety of malignant neoplasms (Shiseki, Kohno et al. 1996, Schmutte, Baffa et al. 1997, Sattler, Rohde et al. 1999, Aubele, Cummings et al. 2000). Human TCHP is a protein of about 62 kDa that is ubiquitously expressed and

it is deleted or mutated in about 11% of various cancer-derived cell lines and solid tumors. Reduced TCHP expression was found in 22% of advanced bladder cancers and in 23% of breast carcinomas analysed (Vecchione, Fassan et al. 2009, Kim, Kim et al. 2010, Fassan, D'Arca et al. 2011). A specific link between TCHP overexpression and the decreased level of the heat-shock protein Hsp27 and its cellular phosphorylation status has been previously determined (Vecchione, Fassan et al. 2009). Hsp27 shows cytoprotective effects, it interferes directly with caspase activation, modulates oxidative stress and regulates cytoskeleton scaffolding (Parcellier, Schmitt et al. 2003).

Using a commercial antibody, THCP localization was predominantly in the cytoplasm and showed a strong overlap with the MitoTracker-stained mitochondria. As TCHP lacks a canonical mitochondrial targeting sequence or a clear transmembrane domain for insertion into the mitochondrial membrane (Nishizawa, Izawa et al. 2005, Vecchione, Fassan et al. 2009), I can assume that TCHP doesn't bind directly mitochondria but it can shift from a mitochondrial localization to the cytoplasm, thus suggesting dynamic regulation in the cell. The function of TCHP in ECs has not been investigated before, although its cellular localization, expression and regulation of Hsp27, suggests it has a role in regulation of migration, proliferation and angiogenesis.

Microtubules and the actin cytoskeleton function in cooperation in normal endothelium and under conditions of barrier loss and impairment of migration. Their coordination is accomplished at several levels by cross-linker proteins which join microtubules and actin filaments (Bershadsky, Kozlov et al. 2006), as well as by small GTPases of the Rho family which mediate dynamics and organization in both the actin network and microtubules (Palazzo, Joseph et al. 2001). The cytoskeleton reorganization can change the cell shape to provoke intercellular gap formation and provides structural basis for a hyperpermeability, the main cause of vascular endothelial dysfunction. This phenomenon is common for a number of pathological states and diseases (inflammation, asthma, sepsis, acute lung injury,

ischemia, diabetes) and can lead to severe, and even fatal, organ dysfunction (Bogatcheva and Verin 2008, Kasa, Csortos et al. 2015).

Chapter 3 reported evidence that reduced TCHP in endothelial cells impaired their capacity to form tubule-like structures *in vitro*, to migrate and proliferate, and caused the appearance of abnormal microtubule structure. In controls, cytoplasmic tubulin filaments showed normal appearance, radiating from a central point to the cell periphery. Silencing of TCHP in HUVECs, however, produced marked changes in the tubulin cytoskeleton organization showing a complete loss of microtubules, thus regulating EC migration and barrier function of ECs.

One of the most dramatic changes of microtubule organization is found at the transition from interphase to mitosis during cell cycle. During mitosis, microtubules are much more dynamic and are organized into a dense bipolar structure, the spindle, whereas microtubules in interphase are less dynamic and are arranged in a radial array (Meunier and Vernos 2012). In agreement with the role of microtubules during cell cycle, I observed a reduction in S phase and an accumulation in G2/M phase of cell cycle in TCHP KD cells compared with control.

Consistent with defective cell cycle progression, cells with decreased levels of TCHP showed a senescent-like phenotype characterized by elevated levels of p16 and p12, and transcription and secretion of senescence-associated pro-inflammatory cytokines, such as IL-6 and IL-8. The senescent phenotype was further confirmed by staining for β-Galactosidase activity and western blot for p16 and mTOR phosphorylation.

Centrosomes are the tiny organelles found in most eukaryotic systems. By their ability to anchor, organize and nucleate microtubules, they play a crucial role in establishing spindle bipolarity and in ensuring the fidelity of cell division. Defects in centrosome structure and function often result in mitotic catastrophe, cell cycle arrest, cell death, genomic instability and/or aneuploidy, leading to human disorders such as primary microcephaly, cancer and ciliopathies (Chavali, Putz et al. 2014). Interestingly, genomic

instability and aneuploidy are also hallmarks of aging and cellular senescence (Hernandez-Segura, Nehme et al. 2018).

Our understanding of the connection between TCHP downregulation and senescence remains undeveloped. In this Thesis, I have focused on existing evidence suggesting that these two phenomena are indeed related, along with the emerging view that TCHP downregulation represents a form of cellular stress that is necessary and sufficient to trigger a permanent cell cycle arrest and senescence.

Finally, of interest for this Thesis, a series of recent publications has revealed that the biogenesis and trafficking of autophagosomes depend on the activities of several cytoskeletal components, including actin assembly factors, membrane–cytoskeleton scaffolds, signalling proteins, and microtubule- and actin-based motors (Kast and Dominguez 2017). The analysis of the phenotype of TCHP KD cells and the strong impact on microtubule organization prompted analysis of the involvement of the autophagic pathway in TCHP KD cells.

6.2 **TCHP as novel regulator of autophagy**

Autophagy is an essential quality control function of the cell. It selectively degrades harmful protein aggregates and/or damaged organelles, enabling maintenance of cellular homeostasis. Basal autophagy also mediates proper cardiovascular function. A variety of cardiovascular risk factors cause defective autophagy due to accumulation of unfolded proteins within the cells. This induces high levels of metabolic stress and impairs functionality of ECs, reducing level of NO (Nussenzweig, Verma et al. 2015). Recent studies suggest that autophagy plays a protective role for other aspects of endothelial function. For example, autophagy has been shown to regulate both the release of von Willibrand factor from ECs, and angiogenic activity (as reflected by endothelial sprouting, proliferation, and tube formation; (Torisu, Torisu et al. 2013).

In this Thesis, I have shown that TCHP downregulation impairs basal autophagy leading to the accumulation of unresolved autophagosomes, SQSTM1 and protein aggregates. Although the exact molecular mechanism remains not completely known, I have disclosed a widespread alteration of autophagic flux; but showing a strong activation of the endolysosomal pathway.

The experiment reported in Chapter 4 provided a clear interpretation of the blockage of the autophagic flux. Accumulation of LC3 and SQSTM1 and the use of the LC3 double reporter vector demonstrated that autophagic flux is reduced in TCHP KD cells. Experiments are on-going in the lab to understand whether the reduction of autophagic flux is due to an impairment of the autophagosome formation or closure. Moreover, I have also assessed that the autophagic flux in these conditions is not completely blocked but it is reversed by starvation, opening the possibility that TCHP-dependent reduction of autophagy could be pharmacologically re-activated.

Interestingly, I have observed an activation of the endolysosomal pathway in TCHP KD cells. The collection and transport of cellular waste to lysosomes requires complex logistics. The cell has developed different routes for transporting extracellular and intracellular waste to the lysosome. Extracellular material reaches the lysosome mainly through endocytosis. The capture of extracellular material and integral membrane proteins occurs through specific endocytosis mechanisms according to the nature of the cargo. After internalization, the receptors are routed to early endosomes (Sorkin and von Zastrow 2009). From the endosomes, the receptors can either be recycled back to the plasma membrane to allow for repeated receptor activation, or be sorted and targeted for lysosomal degradation, resulting in the termination of receptor signalling (Raiborg and Stenmark 2009).

Intracellular materials reach the lysosome through the process of autophagy, a “self-eating” catabolic pathway that is used by cells to capture their own cytoplasmic components destined for degradation and recycling. Three types of autophagy have been identified: microautophagy, chaperone-mediated

autophagy and macroautophagy. During microautophagy, cytosolic proteins are engulfed into the lysosome through the direct invagination of lysosomal or endosomal membranes (Sahu, Kaushik et al. 2011). In chaperone-mediated autophagy, cytosolic proteins are transported into the lysosomal lumen through chaperone- and receptor-mediated internalization, which requires the unfolding of proteins and their translocation through the LAMP2a protein (Cuervo and Dice 1996). Macroautophagy, herein referred to as autophagy, relies on the biogenesis of autophagosomes, double membrane-bound vesicles that sequester cytoplasmic material and then fuse with lysosomes (Ravikumar, Sarkar et al. 2010). Thus, the role of all three types of autophagy in degradation and recycling processes is strictly dependent on lysosomal function.

6.3 **Role of TCHP in mitochondrial function and bioenergetics**

TCHP plays an important role in the physiology of mitochondria (Vecchione, Fassan et al. 2009, Cerqua, Anesti et al. 2010). TCHP reside on outer OMM where they make contact with Mfn2 promoting a fission-like phenotype and a redistribution of mitochondria near the nuclear membranes (Vecchione, Fassan et al. 2009, Cerqua, Anesti et al. 2010). Moreover, TCHP regulates ER–mitochondria tethering via Mfn2 acting as a negative modulator of ER–mitochondria juxtaposition and conferring resistance to H_2O_2-induced cell death (Cerqua, Anesti et al. 2010). Recently, it has been reported that keratins, likely through TCHP-mtf2 interactions, regulate both structural and dynamic functions of β-cell mitochondria, which could have implications for downstream insulin secretion (Silvander, Kvarnstrom et al. 2017). In line with these studies, I have investigated the role of TCHP in EC mitochondria and the contribution of TCHP in ROS production and mitochondrial bioenergetics. Although our results are still preliminary, TCHP KD cells showed an interesting profile.

First, the lack of TCHP in ECs did not affect the position of mitochondria, their size and I didn’t observe any sign of mitochondria elongation, as

reported (Cerqua, Anesti et al. 2010). The main difference between my results and the previous studies is on the use of a cell line instead of primary cells, such as HUVECs. Indeed, HUVECS already have very long mitochondria and knock-down of TCHP neither affected their position nor promoted a fission-like phenotype. Interestingly, TCHP KD cells showed an increase in mitochondrial ROS, showing a possible activation of stress signalling within the cells. These results need further investigation because it is not clear whether the level of mitochondrial ROS produced by the cells is critical to determine the phenotype observed in the ECs. However, these results prompted analysis of mitochondrial respiration and function using Seahorse technology.

The ETC is the major site of non-enzymatic superoxide formation within mitochondria (Turrens 2003). The ETC is made up of four multi-protein complexes (I-IV) embedded in the inner membrane. Complex I and II oxidize NADH and FADH2 respectively, transferring the resulting electrons to ubiquinol, which carries electrons to Complex III. Complex III shunts the electrons across the intermembrane space to cytochrome c, which brings electrons to complex IV. Complex IV then uses the electrons to reduce oxygen to water. Mitochondrial complexes I, II, and III generate superoxide (Murphy, Bers et al. 2009). Complex I and II generate ROS within the mitochondrial matrix while complex III generates ROS into either the matrix or the intermembrane space (Treberg, Quinlan et al. 2010) . Superoxide generated in the intermembrane space can escape into the cytoplasm through voltage-dependent anion channels (Han, Antunes et al. 2003).

Using several small molecules which inhibit the mitochondrial complexes during the Seahorse experiment, I have demonstrated that TCHP deficiency strongly reduced the mitochondrial reserve capacity, a characteristic feature of mitochondrial dysfunction (Brand and Nicholls 2011).

With this in mind, I have then quantified the amount of mitochondrial complexes using Native-Page gel. The analysis showed an increase of complex III/CoQH2-cytochrome c reductase in TCHP KD cells. The results are in contradiction with the level of ROS produced in TCHP KD cells,

therefore cell with increased level of complex III should show a reduced level of ROS.

Moreover, mitochondrial complex III is responsible for the production of ATP in the cells. Analysis of energy production in the cells showed that ATP levels dropped and total NAD amount is reduced at 7 days after TCHP KD.

The discrepancy of results between the level of mitochondria bioenergetics and the total content of ATP and NAD in the TCHP KD cells showed the possible involvement of pathway that exclude a direct involvement of mitochondria in the control of energy balance of the cells. Indeed, glycolysis is essential as ECs primarily rely on this pathway for ATP production. A future line of research will be analysis of the metabolic pathway and glucose metabolism in TCHP KD cells.

6.4 **Future work**

6.4.1 **Identification of TCHP partner proteins and their functions**

In proliferating cells, TCHP serves as a hub not only for appendage-associated NIN involved in microtubules anchoring at the mother centriole (Ibi, Zou et al. 2011) but also for centriole-associated AuroraA implicated in the destabilization of cilia (Inaba, Goto et al. 2016). On the other hand, in differentiated, non-dividing epithelial cells, TCHP is translocated from centrioles to keratin filaments and desmosomes (Nishizawa, Izawa et al. 2005). Thus, the function and localization of TCHP depend on its partner proteins. This observation immediately raises the question of which proteins directly interact with TCHP in the ECs. This part of the study will be performed in collaboration with University of Edinburgh Proteomic Facility. To identify proteins that interact with TCHP, Iwill express an epitope-tagged TCHP (FLAG-TCHP) in the cells using a plasmid. After a FLAG-immunoprecipitation, partner proteins are separated by gel-electrophoresis, then subsequently digested in-gel with a protease (typically trypsin) and analysed using LTQ-Orbitrap Velos Mass Spectrometer (MS). As trypsin hydrolyses the protein amide backbone selectively the peptide fragments act as a fingerprint of a particular protein, which can be used to match to

sequence databases. Further peptides may be fragmented in the MS to yield sequence information to confirm or refute the identity of the isolated proteins. The combination of MS data leads to high confidence identification of proteins of interest. Such MS data can then be used to apply bioinformatics tools to confidently identify the proteins present in the sample. Iwill further confirm the protein partners by using the endogenous TCHP immunoprecipitation, followed by specific immunoblot. Using protein pull-down assays with tagged TCHP deletion mutants I will aim to discover regions of TCHP that are necessary to bind partner proteins. To study whether the identified TCHP-binding proteins have an impact on TCHP activity, the localization using confocal microscopy of TCHP-binding proteins will be explored in TCHP KD cells.

6.4.2 **Role of TCHP in post-ischaemic angiogenesis**

The role of the TCHP in post-ischaemic neovascularisation and blood flow recovery will be addressed using a murine model of critical limb ischaemia. For this proposal, Iwill generate mice with endothelial selective TCHP KO (Tchp-EC-KO) through breeding the conditional KO mice with mice carrying Cre recombinase under the Ve-cadherin promoter. Controls will consist of VE-cadherin Cre strain mice and mice homozygous for the loxP flanked allele.

The basal cardiovascular phenotype of the Tchp-EC-KO mice will be characterized in the reference of 2 control strains. An Ultrasonics Vevo 770 high resolution ultrasound scanner unit will be used to assess standard LV (left ventricle) images to assess systolic and diastolic function (Meloni, Marchetti et al. 2013).

Once the basal cardiovascular phenotype of KO mice has been characterized, limb ischaemia protocol will be initiated. Pre-clinical imaging of perfusion and neovascularization (angiogenesis and arteriogenesis). Subgroups of mice will be used for sequential assessments of blood flow

recovery in the mouse paws (at 3, 7, 14, and 21 days post-ischaemia) using the Moor FLPI-2 Doppler blood flow imager (Caporali, Meloni et al. 2011, Caporali, Meloni et al. 2015).

6.5 **Conclusion**

I have identified TCHP as a novel regulator of autophagy and EC function. Loss of TCHP function in ECs *in vitro* led to defective autophagy, resulting in accumulation of unfolded protein aggregates and SQSTM1; thus, impairing EC function. Moreover, the block of autophagic flux in ECs resulted in premature cellular senescence, appearance of SASP, including IL-6 and IL-8 cytokine, and increased expression of p16. This phenotype is caused by activation of the mTOR pathway and was rescued by re-activation of autophagy by the mTOR inhibitor Torin-1. Ialso observed loss of TCHP and an increase of protein aggregates and SQSTM1 in the local vessel wall derived-ECs, from patients with vascular dysfunction and premature coronary artery disease.

References

Aboyans, V., J. B. Ricco, M. L. Bartelink, M. Bjorck, M. Brodmann, T. Cohner, J. P. Collet, M. Czerny, M. De Carlo, S. Debus, C. Espinola-Klein, T. Kahan, S. Kownator, L. Mazzolai, R. Naylor, M. Roffi, J. Rother, M. Sprynger, M. Tendera, G. Tepe, M. Venermo, C. Vlachopoulos and I. Desormais (2017). "[2017 ESC Guidelines on the Diagnosis and Treatment of Peripheral Arterial Diseases, in collaboration with the European Society for Vascular Surgery (ESVS)]." Kardiol Pol **75**(11): 1065-1160.

Acosta, J. C., A. Banito, T. Wuestefeld, A. Georgilis, P. Janich, J. P. Morton, D. Athineos, T. W. Kang, F. Lasitschka, M. Andrulis, G. Pascual, K. J. Morris, S. Khan, H. Jin, G. Dharmalingam, A. P. Snijders, T. Carroll, D. Capper, C. Pritchard, G. J. Inman, T. Longerich, O. J. Sansom, S. A. Benitah, L. Zender and J. Gil (2013). "A complex secretory program orchestrated by the inflammasome controls paracrine senescence." Nat Cell Biol **15**(8): 978-990.

Adams, R. H. and K. Alitalo (2007). "Molecular regulation of angiogenesis and lymphangiogenesis." Nat Rev Mol Cell Biol **8**(6): 464-478.

Al Suwaidi, J., S. T. Higano, D. R. Holmes, Jr., R. Lennon and A. Lerman (2001). "Obesity is independently associated with coronary endothelial dysfunction in patients with normal or mildly diseased coronary arteries." J Am Coll Cardiol **37**(6): 1523-1528.

Al-Mehdi, A. B., V. M. Pastukh, B. M. Swiger, D. J. Reed, M. R. Patel, G. C. Bardwell, V. V. Pastukh, M. F. Alexeyev and M. N. Gillespie (2012). "Perinuclear mitochondrial clustering creates an oxidant-rich nuclear domain required for hypoxia-induced transcription." Sci Signal **5**(231): ra47.

Anderson, T. J., F. Charbonneau, L. M. Title, J. Buithieu, M. S. Rose, H. Conradson, K. Hildebrand, M. Fung, S. Verma and E. M. Lonn (2011). "Microvascular function predicts cardiovascular events in primary prevention: long-term results from the Firefighters and Their Endothelium (FATE) study." Circulation **123**(2): 163-169.

Ao, X., L. Zou and Y. Wu (2014). "Regulation of autophagy by the Rab GTPase network." Cell Death Differ **21**(3): 348-358.

Arcaro, G., A. Cretti, S. Balzano, A. Lechi, M. Muggeo, E. Bonora and R. C. Bonadonna (2002). "Insulin causes endothelial dysfunction in humans: sites and mechanisms." Circulation **105**(5): 576-582.

Arroyo, A. G. and M. L. Iruela-Arispe (2010). "Extracellular matrix, inflammation, and the angiogenic response." Cardiovasc Res **86**(2): 226-235.

Aubele, M. M., M. C. Cummings, A. E. Mattis, H. F. Zitzelsberger, A. K. Walch, M. Kremer, H. Hofler and M. Werner (2000). "Accumulation of chromosomal imbalances from intraductal proliferative lesions to adjacent in situ and invasive ductal breast cancer." Diagn Mol Pathol **9**(1): 14-19.

Augustin, H. G., G. Y. Koh, G. Thurston and K. Alitalo (2009). "Control of vascular morphogenesis and homeostasis through the angiopoietin-Tie system." Nat Rev Mol Cell Biol **10**(3): 165-177.

Bach, M., M. Larance, D. E. James and G. Ramm (2011). "The serine/threonine kinase ULK1 is a target of multiple phosphorylation events." Biochem J **440**(2): 283-291.

Bao, W., P. Qin, S. Needle, C. L. Erickson-Miller, K. J. Duffy, J. L. Ariazi, S. Zhao, A. R. Olzinski, D. J. Behm, G. C. Pipes, B. M. Jucker, E. Hu, J. J. Lepore and R. N. Willette (2010). "Chronic inhibition of hypoxia-inducible factor prolyl 4-hydroxylase improves ventricular performance, remodeling, and vascularity after myocardial infarction in the rat." J Cardiovasc Pharmacol **56**(2): 147-155.

Bautista-Nino, P. K., E. Portilla-Fernandez, D. E. Vaughan, A. H. Danser and A. J. Roks (2016). "DNA Damage: A Main Determinant of Vascular Aging." Int J Mol Sci **17**(5).

Beardsley, A., K. Fang, H. Mertz, V. Castranova, S. Friend and J. Liu (2005). "Loss of caveolin-1 polarity impedes endothelial cell polarization and directional movement." J Biol Chem **280**(5): 3541-3547.

Bentley, K., G. Mariggi, H. Gerhardt and P. A. Bates (2009). "Tipping the balance: robustness of tip cell selection, migration and fusion in angiogenesis." PLoS Comput Biol **5**(10): e1000549.

Bershadsky, A., M. Kozlov and B. Geiger (2006). "Adhesion-mediated mechanosensitivity: a time to experiment, and a time to theorize." Curr Opin Cell Biol **18**(5): 472-481.

Bharath, L. P., R. Mueller, Y. Li, T. Ruan, D. Kunz, R. Goodrich, T. Mills, L. Deeter, A. Sargsyan, P. V. Anandh Babu, T. E. Graham and J. D. Symons (2014). "Impairment of autophagy in endothelial cells prevents shear-stress-induced increases in nitric oxide bioavailability." Can J Physiol Pharmacol **92**(7): 605-612.

Bogatcheva, N. V. and A. D. Verin (2008). "The role of cytoskeleton in the regulation of vascular endothelial barrier function." Microvasc Res **76**(3): 202-207.

Boger, R. H., S. R. Lentz, S. M. Bode-Boger, H. R. Knapp and W. G. Haynes (2001). "Elevation of asymmetrical dimethylarginine may mediate endothelial dysfunction during experimental hyperhomocyst(e)inaemia in humans." Clin Sci (Lond) **100**(2): 161-167.

Bonora, M., M. R. Wieckowski, D. A. Sinclair, G. Kroemer, P. Pinton and L. Galluzzi (2018). "Targeting mitochondria for cardiovascular disorders: therapeutic potential and obstacles." Nat Rev Cardiol.

Brand, M. D. and D. G. Nicholls (2011). "Assessing mitochondrial dysfunction in cells." Biochem J **435**(2): 297-312.

Bravo-San Pedro, J. M., G. Kroemer and L. Galluzzi (2017). "Autophagy and Mitophagy in Cardiovascular Disease." Circ Res **120**(11): 1812-1824.

Brittan, M., A. Hunter, M. Boulberdaa, T. Fujisawa, E. M. Skinner, A. S. Shah, A. H. Baker and N. L. Mills (2015). "Impaired vascular function and repair in patients with premature coronary artery disease." Eur J Prev Cardiol **22**(12): 1557-1566.

Brownlee, M. (2001). "Biochemistry and molecular cell biology of diabetic complications." Nature **414**(6865): 813-820.

Caja, S. and J. A. Enriquez (2017). "Mitochondria in endothelial cells: Sensors and integrators of environmental cues." Redox Biol **12**: 821-827.

Canto, C., K. J. Menzies and J. Auwerx (2015). "NAD(+) Metabolism and the Control of Energy Homeostasis: A Balancing Act between Mitochondria and the Nucleus." Cell Metab **22**(1): 31-53.

Caporali, A., M. Meloni, A. Nailor, T. Mitic, S. Shantikumar, F. Riu, G. B. Sala-Newby, L. Rose, M. Besnier, R. Katare, C. Voellenkle, P. Verkade, F. Martelli, P. Madeddu and C. Emanueli (2015). "p75(NTR)-dependent activation of NF-kappaB regulates microRNA-503 transcription and pericyte-endothelial crosstalk in diabetes after limb ischaemia." Nat Commun **6**: 8024.

Caporali, A., M. Meloni, C. Vollenkle, D. Bonci, G. B. Sala-Newby, R. Addis, G. Spinetti, S. Losa, R. Masson, A. H. Baker, R. Agami, C. le Sage, G. Condorelli, P. Madeddu, F. Martelli and C. Emanueli (2011). "Deregulation of microRNA-503 contributes to diabetes mellitus-induced impairment of endothelial function and reparative angiogenesis after limb ischemia." Circulation **123**(3): 282-291.

Caporali, A., E. Pani, A. J. Horrevoets, N. Kraenkel, A. Oikawa, G. B. Sala-Newby, M. Meloni, B. Cristofaro, G. Graiani, A. S. Leroyer, C. M. Boulanger,

G. Spinetti, S. O. Yoon, P. Madeddu and C. Emanueli (2008). "Neurotrophin p75 receptor (p75NTR) promotes endothelial cell apoptosis and inhibits angiogenesis: implications for diabetes-induced impaired neovascularization in ischemic limb muscles." Circ Res **103**(2): e15-26.

Carmeliet, P. (2005). "Angiogenesis in life, disease and medicine." Nature **438**(7070): 932-936.

Carmeliet, P. and R. K. Jain (2011). "Molecular mechanisms and clinical applications of angiogenesis." Nature **473**(7347): 298-307.

Carmeliet, P. and R. K. Jain (2011). "Principles and mechanisms of vessel normalization for cancer and other angiogenic diseases." Nat Rev Drug Discov **10**(6): 417-427.

Cerqua, C., V. Anesti, A. Pyakurel, D. Liu, D. Naon, G. Wiche, R. Baffa, K. S. Dimmer and L. Scorrano (2010). "Trichoplein/mitostatin regulates endoplasmic reticulum-mitochondria juxtaposition." EMBO Rep **11**(11): 854-860.

Cesselli, D., A. Aleksova, E. Mazzega, A. Caragnano and A. P. Beltrami (2017). "Cardiac stem cell aging and heart failure." Pharmacol Res.

Chang, J., Y. Wang, L. Shao, R. M. Laberge, M. Demaria, J. Campisi, K. Janakiraman, N. E. Sharpless, S. Ding, W. Feng, Y. Luo, X. Wang, N. Aykin-Burns, K. Krager, U. Ponnappan, M. Hauer-Jensen, A. Meng and D. Zhou (2016). "Clearance of senescent cells by ABT263 rejuvenates aged hematopoietic stem cells in mice." Nat Med **22**(1): 78-83.

Chavali, P. L., M. Putz and F. Gergely (2014). "Small organelle, big responsibility: the role of centrosomes in development and disease." Philos Trans R Soc Lond B Biol Sci **369**(1650).

Chen, Z. H., J. F. Cao, J. S. Zhou, H. Liu, L. Q. Che, K. Mizumura, W. Li, A. M. Choi and H. H. Shen (2014). "Interaction of caveolin-1 with ATG12-ATG5 system suppresses autophagy in lung epithelial cells." Am J Physiol Lung Cell Mol Physiol **306**(11): L1016-1025.

Chien, Y., C. Scuoppo, X. Wang, X. Fang, B. Balgley, J. E. Bolden, P. Premsrirut, W. Luo, A. Chicas, C. S. Lee, S. C. Kogan and S. W. Lowe (2011). "Control of the senescence-associated secretory phenotype by NF-kappaB promotes senescence and enhances chemosensitivity." Genes Dev **25**(20): 2125-2136.

Childs, B. G., M. Durik, D. J. Baker and J. M. van Deursen (2015). "Cellular senescence in aging and age-related disease: from mechanisms to therapy." Nat Med **21**(12): 1424-1435.

Childs, B. G., M. Gluscevic, D. J. Baker, R. M. Laberge, D. Marquess, J. Dananberg and J. M. van Deursen (2017). "Senescent cells: an emerging target for diseases of ageing." Nat Rev Drug Discov **16**(10): 718-735.

Chouinard-Pelletier, G., E. D. Jahnsen and E. A. Jones (2013). "Increased shear stress inhibits angiogenesis in veins and not arteries during vascular development." Angiogenesis **16**(1): 71-83.

Claesson-Welsh, L. (2015). "Vascular permeability--the essentials." Ups J Med Sci **120**(3): 135-143.

Corum, D. G., P. N. Tsichlis and R. C. Muise-Helmericks (2014). "AKT3 controls mitochondrial biogenesis and autophagy via regulation of the major nuclear export protein CRM-1." FASEB J **28**(1): 395-407.

Costa, C., J. Incio and R. Soares (2007). "Angiogenesis and chronic inflammation: cause or consequence?" Angiogenesis **10**(3): 149-166.

Cuervo, A. M. and J. F. Dice (1996). "A receptor for the selective uptake and degradation of proteins by lysosomes." Science **273**(5274): 501-503.

Cuervo, A. M. and E. Wong (2014). "Chaperone-mediated autophagy: roles in disease and aging." Cell Res **24**(1): 92-104.

Dai, D. F., P. S. Rabinovitch and Z. Ungvari (2012). "Mitochondria and cardiovascular aging." Circ Res **110**(8): 1109-1124.

Dai, X. Y., M. M. Zhao, Y. Cai, Q. C. Guan, Y. Zhao, Y. Guan, W. Kong, W. G. Zhu, M. J. Xu and X. Wang (2013). "Phosphate-induced autophagy counteracts vascular calcification by reducing matrix vesicle release." Kidney Int **83**(6): 1042-1051.

Davalos, A. R., J. P. Coppe, J. Campisi and P. Y. Desprez (2010). "Senescent cells as a source of inflammatory factors for tumor progression." Cancer Metastasis Rev **29**(2): 273-283.

Davidson, S. M. and M. R. Duchen (2007). "Endothelial mitochondria: contributing to vascular function and disease." Circ Res **100**(8): 1128-1141.

de Almeida, A., T. P. Ribeiro and I. A. de Medeiros (2017). "Aging: Molecular Pathways and Implications on the Cardiovascular System." Oxid Med Cell Longev **2017**: 7941563.

Dejana, E. (2004). "Endothelial cell-cell junctions: happy together." Nat Rev Mol Cell Biol **5**(4): 261-270.

Dimri, G. P., X. Lee, G. Basile, M. Acosta, G. Scott, C. Roskelley, E. E. Medrano, M. Linskens, I. Rubelj, O. Pereira-Smith and et al. (1995). "A biomarker that identifies senescent human cells in culture and in aging skin in vivo." Proc Natl Acad Sci U S A **92**(20): 9363-9367.

Dranka, B. P., B. G. Hill and V. M. Darley-Usmar (2010). "Mitochondrial reserve capacity in endothelial cells: The impact of nitric oxide and reactive oxygen species." Free Radic Biol Med **48**(7): 905-914.

Dromparis, P. and E. D. Michelakis (2013). "Mitochondria in vascular health and disease." Annu Rev Physiol **75**: 95-126.

Duchen, M. R. (2004). "Roles of mitochondria in health and disease." Diabetes **53 Suppl 1**: S96-102.

Egami, K., T. Murohara, M. Aoki and T. Matsuishi (2006). "Ischemia-induced angiogenesis: role of inflammatory response mediated by P-selectin." Journal of Leukocyte Biology **79**(5): 971-976.

Egashira, K., T. Inou, Y. Hirooka, H. Kai, M. Sugimachi, S. Suzuki, T. Kuga, Y. Urabe and A. Takeshita (1993). "Effects of age on endothelium-dependent vasodilation of resistance coronary artery by acetylcholine in humans." Circulation **88**(1): 77-81.

Eilken, H. M. and R. H. Adams (2010). "Dynamics of endothelial cell behavior in sprouting angiogenesis." Curr Opin Cell Biol **22**(5): 617-625.

Eisenberg-Lerner, A. and A. Kimchi (2012). "PKD at the crossroads of necrosis and autophagy." Autophagy **8**(3): 433-434.

Elanchezhian, R., P. Palsamy, C. J. Madson, D. W. Lynch and T. Shinohara (2012). "Age-related cataracts: homocysteine coupled endoplasmic reticulum stress and suppression of Nrf2-dependent antioxidant protection." Chem Biol Interact **200**(1): 1-10.

Eltzschig , H. K. and P. Carmeliet (2011). "Hypoxia and Inflammation." New England Journal of Medicine **364**(7): 656-665.

Emanueli, C., M. B. Salis, A. Pinna, T. Stacca, A. F. Milia, A. Spano, J. Chao, L. Chao, L. Sciola and P. Madeddu (2002). "Prevention of diabetes-induced microangiopathy by human tissue kallikrein gene transfer." Circulation **106**(8): 993-999.

Fassan, M., D. D'Arca, J. Letko, A. Vecchione, M. P. Gardiman, P. McCue, B. Wildemore, M. Rugge, D. Shupp-Byrne, L. G. Gomella, A. Morrione, R. V. Iozzo and R. Baffa (2011). "Mitostatin is down-regulated in human prostate cancer and suppresses the invasive phenotype of prostate cancer cells." PLoS One **6**(5): e19771.

Feng, Y., D. He, Z. Yao and D. J. Klionsky (2014). "The machinery of macroautophagy." Cell Res **24**(1): 24-41.

Ferrand, M., O. Kirsh, A. Griveau, D. Vindrieux, N. Martin, P. A. Defossez and D. Bernard (2015). "Screening of a kinase library reveals novel pro-senescence kinases and their common NF-kappaB-dependent transcriptional program." Aging (Albany NY) **7**(11): 986-1003.

Fischer, R. S., M. Gardel, X. Ma, R. S. Adelstein and C. M. Waterman (2009). "Local cortical tension by myosin II guides 3D endothelial cell branching." Curr Biol **19**(3): 260-265.

Fleming, A., T. Noda, T. Yoshimori and D. C. Rubinsztein (2011). "Chemical modulators of autophagy as biological probes and potential therapeutics." Nat Chem Biol **7**(1): 9-17.

Fontana, L., M. Vinciguerra and V. D. Longo (2012). "Growth factors, nutrient signaling, and cardiovascular aging." Circ Res **110**(8): 1139-1150.

Ford, M. A., J. P. McConnell, S. Lavi, C. S. Rihal, A. Prasad, G. S. Sandhu, S. J. Hartman, L. O. Lerman and A. Lerman (2009). "Coronary artery endothelial dysfunction is positively correlated with low density lipoprotein and inversely correlated with high density lipoprotein subclass particles measured by nuclear magnetic resonance spectroscopy." Atherosclerosis **207**(1): 111-115.

Foreman, K. E. and J. Tang (2003). "Molecular mechanisms of replicative senescence in endothelial cells." Exp Gerontol **38**(11-12): 1251-1257.

Freund, A., C. K. Patil and J. Campisi (2011). "p38MAPK is a novel DNA damage response-independent regulator of the senescence-associated secretory phenotype." EMBO J **30**(8): 1536-1548.

Fukuhara, S. and N. Mochizuki (2010). "[Signaling mechanism involved in regulation of endothelial cell-cell junctions]." Yakugaku Zasshi **130**(11): 1413-1420.

Galie, P. A., D. H. Nguyen, C. K. Choi, D. M. Cohen, P. A. Janmey and C. S. Chen (2014). "Fluid shear stress threshold regulates angiogenic sprouting." Proc Natl Acad Sci U S A **111**(22): 7968-7973.

Galluzzi, L., J. M. Bravo-San Pedro, B. Levine, D. R. Green and G. Kroemer (2017). "Pharmacological modulation of autophagy: therapeutic potential and persisting obstacles." Nat Rev Drug Discov **16**(7): 487-511.

Garcia-Mata, R., Z. Bebok, E. J. Sorscher and E. S. Sztul (1999). "Characterization and dynamics of aggresome formation by a cytosolic GFP-chimera." J Cell Biol **146**(6): 1239-1254.

Garg, S., C. Bourantas and P. W. Serruys (2013). "New concepts in the design of drug-eluting coronary stents." Nat Rev Cardiol **10**(5): 248-260.

Gerhardt, H. (2008). "VEGF and endothelial guidance in angiogenic sprouting." Organogenesis **4**(4): 241-246.

Gerhardt, H., M. Golding, M. Fruttiger, C. Ruhrberg, A. Lundkvist, A. Abramsson, M. Jeltsch, C. Mitchell, K. Alitalo, D. Shima and C. Betsholtz (2003). "VEGF guides angiogenic sprouting utilizing endothelial tip cell filopodia." J Cell Biol **161**(6): 1163-1177.

Gewirtz, D. A. (2013). "Autophagy and senescence: a partnership in search of definition." Autophagy **9**(5): 808-812.

Ghaffari, S., R. L. Leask and E. A. Jones (2015). "Flow dynamics control the location of sprouting and direct elongation during developmental angiogenesis." Development **142**(23): 4151-4157.

Giedt, R. J., D. R. Pfeiffer, A. Matzavinos, C. Y. Kao and B. R. Alevriadou (2012). "Mitochondrial dynamics and motility inside living vascular endothelial cells: role of bioenergetics." Ann Biomed Eng **40**(9): 1903-1916.

Goukassian, D. A., G. Qin, C. Dolan, T. Murayama, M. Silver, C. Curry, E. Eaton, C. Luedemann, H. Ma, T. Asahara, V. Zak, S. Mehta, A. Burg, T. Thorne, R. Kishore and D. W. Losordo (2007). "Tumor Necrosis Factor-α Receptor p75 Is Required in Ischemia-Induced Neovascularization." Circulation **115**(6): 752-762.

Grivennikov, S. I., F. R. Greten and M. Karin (2010). "Immunity, Inflammation, and Cancer." Cell **140**(6): 883-899.

Grote, K., H. Schuett, G. Salguero, C. Grothusen, J. Jagielska, H. Drexler, P. F. Mühlradt and B. Schieffer (2010). "Toll-like receptor 2/6 stimulation promotes angiogenesis via GM-CSF as a potential strategy for immune defense and tissue regeneration." Blood **115**(12): 2543-2552.

Grote, K., H. Schütt and B. Schieffer (2011). "Toll-Like Receptors in Angiogenesis." The Scientific World JOURNAL **11**: 981-991.

Guo, F., X. Li, J. Peng, Y. Tang, Q. Yang, L. Liu, Z. Wang, Z. Jiang, M. Xiao, C. Ni, R. Chen, D. Wei and G. X. Wang (2014). "Autophagy regulates vascular endothelial cell eNOS and ET-1 expression induced by laminar shear stress in an ex vivo perfused system." Ann Biomed Eng **42**(9): 1978-1988.

Gutierrez, J., S. W. Ballinger, V. M. Darley-Usmar and A. Landar (2006). "Free radicals, mitochondria, and oxidized lipids: the emerging role in signal transduction in vascular cells." Circ Res **99**(9): 924-932.

Guzik, T., R. Korbut and T. Adamek-Guzik (2003). "Nitric oxide and superoxide in inflammation and immune regulation." J Physiol Pharmacol **54**: 469-487.

Hamuro, M., J. Polan, M. Natarajan and S. Mohan (2002). "High glucose induced nuclear factor kappa B mediated inhibition of endothelial cell migration." Atherosclerosis **162**(2): 277-287.

Han, D., F. Antunes, R. Canali, D. Rettori and E. Cadenas (2003). "Voltage-dependent anion channels control the release of the superoxide anion from mitochondria to cytosol." J Biol Chem **278**(8): 5557-5563.

Hellstrom, M., L. K. Phng and H. Gerhardt (2007). "VEGF and Notch signaling: the yin and yang of angiogenic sprouting." Cell Adh Migr **1**(3): 133-136.

Hellwig-Burgel, T., K. Rutkowski, E. Metzen, J. Fandrey and W. Jelkmann (1999). "Interleukin-1beta and tumor necrosis factor-alpha stimulate DNA binding of hypoxia-inducible factor-1." Blood **94**(5): 1561-1567.

Hernandez-Segura, A., J. Nehme and M. Demaria (2018). "Hallmarks of Cellular Senescence." Trends Cell Biol.

Herranz, N., S. Gallage, M. Mellone, T. Wuestefeld, S. Klotz, C. J. Hanley, S. Raguz, J. C. Acosta, A. J. Innes, A. Banito, A. Georgilis, A. Montoya, K. Wolter, G. Dharmalingam, P. Faull, T. Carroll, J. P. Martinez-Barbera, P. Cutillas, F. Reisinger, M. Heikenwalder, R. A. Miller, D. Withers, L. Zender, G. J. Thomas and J. Gil (2015). "mTOR regulates MAPKAPK2 translation to control the senescence-associated secretory phenotype." Nat Cell Biol **17**(9): 1205-1217.

Hingorani, A. D., J. Cross, R. K. Kharbanda, M. J. Mullen, K. Bhagat, M. Taylor, A. E. Donald, M. Palacios, G. E. Griffin, J. E. Deanfield, R. J. MacAllister and P. Vallance (2000). "Acute systemic inflammation impairs endothelium-dependent dilatation in humans." Circulation **102**(9): 994-999.

Hoefer, I. E., N. van Royen, J. E. Rectenwald, E. Deindl, J. Hua, M. Jost, S. Grundmann, M. Voskuil, C. K. Ozaki, J. J. Piek and I. R. Buschmann (2004). "Arteriogenesis Proceeds via ICAM-1/Mac-1- Mediated Mechanisms." Circulation Research **94**(9): 1179-1185.

Ibi, M., P. Zou, A. Inoko, T. Shiromizu, M. Matsuyama, Y. Hayashi, M. Enomoto, D. Mori, S. Hirotsune, T. Kiyono, S. Tsukita, H. Goto and M. Inagaki (2011). "Trichoplein controls microtubule anchoring at the centrosome by binding to Odf2 and ninein." J Cell Sci **124**(Pt 6): 857-864.

Inaba, H., H. Goto, K. Kasahara, K. Kumamoto, S. Yonemura, A. Inoko, S. Yamano, H. Wanibuchi, D. He, N. Goshima, T. Kiyono, S. Hirotsune and M. Inagaki (2016). "Ndel1 suppresses ciliogenesis in proliferating cells by regulating the trichoplein-Aurora A pathway." J Cell Biol **212**(4): 409-423.

Inoko, A., M. Matsuyama, H. Goto, Y. Ohmuro-Matsuyama, Y. Hayashi, M. Enomoto, M. Ibi, T. Urano, S. Yonemura, T. Kiyono, I. Izawa and M. Inagaki (2012). "Trichoplein and Aurora A block aberrant primary cilia assembly in proliferating cells." J Cell Biol **197**(3): 391-405.

Ito, W. D., M. Arras, B. Winkler, D. Scholz, J. Schaper and W. Schaper (1997). "Monocyte Chemotactic Protein-1 Increases Collateral and Peripheral Conductance After Femoral Artery Occlusion." Circulation Research **80**(6): 829-837.

Jastroch, M., A. S. Divakaruni, S. Mookerjee, J. R. Treberg and M. D. Brand (2010). "Mitochondrial proton and electron leaks." Essays Biochem **47**: 53-67.

Jendrach, M., S. Pohl, M. Voth, A. Kowald, P. Hammerstein and J. Bereiter-Hahn (2005). "Morpho-dynamic changes of mitochondria during ageing of human endothelial cells." Mech Ageing Dev **126**(6-7): 813-821.

Johnson, S. C., P. S. Rabinovitch and M. Kaeberlein (2013). "mTOR is a key modulator of ageing and age-related disease." Nature **493**(7432): 338-345.

Johnston, J. A., C. L. Ward and R. R. Kopito (1998). "Aggresomes: a cellular response to misfolded proteins." J Cell Biol **143**(7): 1883-1898.

Jurk, D., C. Wilson, J. F. Passos, F. Oakley, C. Correia-Melo, L. Greaves, G. Saretzki, C. Fox, C. Lawless, R. Anderson, G. Hewitt, S. L. Pender, N. Fullard, G. Nelson, J. Mann, B. van de Sluis, D. A. Mann and T. von Zglinicki (2014). "Chronic inflammation induces telomere dysfunction and accelerates ageing in mice." Nat Commun **2**: 4172.

Kasa, A., C. Csortos and A. D. Verin (2015). "Cytoskeletal mechanisms regulating vascular endothelial barrier function in response to acute lung injury." Tissue Barriers **3**(1-2): e974448.

Kasahara, K., Y. Kawakami, T. Kiyono, S. Yonemura, Y. Kawamura, S. Era, F. Matsuzaki, N. Goshima and M. Inagaki (2014). "Ubiquitin-proteasome system controls ciliogenesis at the initial step of axoneme extension." Nat Commun **5**: 5081.

Kast, D. J. and R. Dominguez (2017). "The Cytoskeleton-Autophagy Connection." Curr Biol **27**(8): R318-R326.

Kawai, T. and S. Akira (2006). "TLR signaling." Cell Death Differ **13**(5): 816-825.

Kido, M., L. Du, C. C. Sullivan, X. Li, R. Deutsch, S. W. Jamieson and P. A. Thistlethwaite (2005). "Hypoxia-inducible factor 1-alpha reduces infarction and attenuates progression of cardiac dysfunction after myocardial infarction in the mouse." J Am Coll Cardiol **46**(11): 2116-2124.

Kim, Y. C. and K. L. Guan (2015). "mTOR: a pharmacologic target for autophagy regulation." J Clin Invest **125**(1): 25-32.

Kim, Y. R., S. S. Kim, N. J. Yoo and S. H. Lee (2010). "Mutational Analysis of MITOSTATIN, a Candidate Tumor-Suppressor Gene, at a Mononucleotide Repeat in Gastric and Colorectal Carcinoma." Gut Liver **4**(1): 149-150.

Klionsky, D. J., F. C. Abdalla, H. Abeliovich, R. T. Abraham, A. Acevedo-Arozena, K. Adeli, L. Agholme, M. Agnello, P. Agostinis, J. A. Aguirre-Ghiso, et al (2012). "Guidelines for the use and interpretation of assays for monitoring autophagy." Autophagy **8**(4): 445-544.

Klionsky, D. J., K. Abdelmohsen, A. Abe, M. J. Abedin, H. Abeliovich, A. Acevedo Arozena, H. Adachi, C. M. Adams, P. D. Adams, K. Adeli, P. J. Aet al (2016). "Guidelines for the use and interpretation of assays for monitoring autophagy (3rd edition)." Autophagy **12**(1): 1-222.

Klionsky, D. J., P. Codogno, A. M. Cuervo, V. Deretic, Z. Elazar, J. Fueyo-Margareto, D. A. Gewirtz, G. Kroemer, B. Levine, N. Mizushima, D. C. Rubinsztein, M. Thumm and S. A. Tooze (2010). "A comprehensive glossary of autophagy-related molecules and processes." Autophagy **6**(4): 438-448.

Kluge, A., R. Zimmermann, B. Münkel, M. Mohri, S. Sack, J. Schaper and W. Schaper (1995). "Insulin-like growth factor I is involved in inflammation linked angiogenic processes after microembolisation in porcine heart." Cardiovascular Research **29**(3): 407-415.

Konisti, S., S. Kiriakidis and E. M. Paleolog (2012). "Hypoxia[mdash]a key regulator of angiogenesis and inflammation in rheumatoid arthritis." Nat Rev Rheumatol **8**(3): 153-162.

Kopito, R. R. (2000). "Aggresomes, inclusion bodies and protein aggregation." Trends Cell Biol **10**(12): 524-530.

Kundu, J. K. and Y.-J. Surh (2008). "Inflammation: Gearing the journey to cancer." Mutation Research/Reviews in Mutation Research **659**(1–2): 15-30.

Kundu, J. K. and Y.-J. Surh (2012). "Emerging avenues linking inflammation and cancer." Free Radical Biology and Medicine **52**(9): 2013-2037.

Kwon, Y. W., S. C. Heo, G. O. Jeong, J. W. Yoon, W. M. Mo, M. J. Lee, I.-H. Jang, S. M. Kwon, J. S. Lee and J. H. Kim (2013). "Tumor necrosis factor-α-activated mesenchymal stem cells promote endothelial progenitor cell homing and angiogenesis." Biochimica et Biophysica Acta (BBA) - Molecular Basis of Disease **1832**(12): 2136-2144.

Laberge, R. M., Y. Sun, A. V. Orjalo, C. K. Patil, A. Freund, L. Zhou, S. C. Curran, A. R. Davalos, K. A. Wilson-Edell, S. Liu, C. Limbad, M. Demaria, P. Li, G. B. Hubbard, Y. Ikeno, M. Javors, P. Y. Desprez, C. C. Benz, P. Kapahi, P. S. Nelson and J. Campisi (2015). "MTOR regulates the pro-tumorigenic senescence-associated secretory phenotype by promoting IL1A translation." Nat Cell Biol **17**(8): 1049-1061.

Lakatta, E. G. (2003). "Arterial and cardiac aging: major shareholders in cardiovascular disease enterprises: Part III: cellular and molecular clues to heart and arterial aging." Circulation **107**(3): 490-497.

Lakatta, E. G. and D. Levy (2003). "Arterial and cardiac aging: major shareholders in cardiovascular disease enterprises: Part I: aging arteries: a "set up" for vascular disease." Circulation **107**(1): 139-146.

Lakatta, E. G. and D. Levy (2003). "Arterial and cardiac aging: major shareholders in cardiovascular disease enterprises: Part II: the aging heart in health: links to heart disease." Circulation **107**(2): 346-354.

Lamalice, L., F. Le Boeuf and J. Huot (2007). "Endothelial cell migration during angiogenesis." Circ Res **100**(6): 782-794.

Lamb, C. A., A. Longatti and S. A. Tooze (2016). "Rabs and GAPs in starvation-induced autophagy." Small GTPases: 0.

Lamers, M. L., M. E. Almeida, M. Vicente-Manzanares, A. F. Horwitz and M. F. Santos (2011). "High glucose-mediated oxidative stress impairs cell migration." PLoS One **6**(8): e22865.

Landmesser, U., S. Spiekermann, S. Dikalov, H. Tatge, R. Wilke, C. Kohler, D. G. Harrison, B. Hornig and H. Drexler (2002). "Vascular oxidative stress and endothelial dysfunction in patients with chronic heart failure: role of xanthine-oxidase and extracellular superoxide dismutase." Circulation **106**(24): 3073-3078.

LaRocca, T. J., R. A. Gioscia-Ryan, C. M. Hearon, Jr. and D. R. Seals (2013). "The autophagy enhancer spermidine reverses arterial aging." Mech Ageing Dev **134**(7-8): 314-320.

LaRocca, T. J., G. D. Henson, A. Thorburn, A. L. Sindler, G. L. Pierce and D. R. Seals (2012). "Translational evidence that impaired autophagy contributes to arterial ageing." J Physiol **590**(14): 3305-3316.

Larsson, E., P. Fredlund Fuchs, J. Heldin, I. Barkefors, C. Bondjers, G. Genove, C. Arrondel, P. Gerwins, C. Kurschat, B. Schermer, T. Benzing, S. J. Harvey, J. Kreuger and P. Lindahl (2009). "Discovery of microvascular miRNAs using public gene expression data: miR-145 is expressed in pericytes and is a regulator of Fli1." Genome Med **1**(11): 108.

Lavi, S., A. Prasad, E. H. Yang, V. Mathew, R. D. Simari, C. S. Rihal, L. O. Lerman and A. Lerman (2007). "Smoking is associated with epicardial coronary endothelial dysfunction and elevated white blood cell count in patients with chest pain and early coronary artery disease." Circulation **115**(20): 2621-2627.

Leibovich, S. J., J.-F. Chen, G. Pinhal-Enfield, P. C. Belem, G. Elson, A. Rosania, M. Ramanathan, C. Montesinos, M. Jacobson, M. A. Schwarzschild, J. S. Fink and B. Cronstein (2002). "Synergistic Up-Regulation of Vascular Endothelial Growth Factor Expression in Murine Macrophages by Adenosine A(2A) Receptor Agonists and Endotoxin." The American Journal of Pathology **160**(6): 2231-2244.

Levine, B., M. Packer and P. Codogno (2015). "Development of autophagy inducers in clinical medicine." J Clin Invest **125**(1): 14-24.

Li, L., W. Chen, A. Rezvan, H. Jo and D. G. Harrison (2011). "Tetrahydrobiopterin deficiency and nitric oxide synthase uncoupling contribute to atherosclerosis induced by disturbed flow." Arterioscler Thromb Vasc Biol **31**(7): 1547-1554.

Li, P. F., R. Dietz and R. von Harsdorf (1997). "Differential effect of hydrogen peroxide and superoxide anion on apoptosis and proliferation of vascular smooth muscle cells." Circulation **96**(10): 3602-3609.

Li, R. and G. G. Gundersen (2008). "Beyond polymer polarity: how the cytoskeleton builds a polarized cell." Nat Rev Mol Cell Biol **9**(11): 860-873.

Liu, Y., H. Li, A. H. Bubolz, D. X. Zhang and D. D. Gutterman (2008). "Endothelial cytoskeletal elements are critical for flow-mediated dilation in human coronary arterioles." Med Biol Eng Comput **46**(5): 469-478.

Loinard, C., A. Ginouves, J. Vilar, C. Cochain, Y. Zouggari, A. Recalde, M. Duriez, B. I. Levy, J. Pouyssegur, E. Berra and J. S. Silvestre (2009). "Inhibition of prolyl hydroxylase domain proteins promotes therapeutic revascularization." Circulation **120**(1): 50-59.

Long, X., S. Ortiz-Vega, Y. Lin and J. Avruch (2005). "Rheb binding to mammalian target of rapamycin (mTOR) is regulated by amino acid sufficiency." J Biol Chem **280**(25): 23433-23436.

Longatti, A. and S. A. Tooze (2012). "Recycling endosomes contribute to autophagosome formation." Autophagy **8**(11): 1682-1683.

Lundman, P., M. J. Eriksson, M. Stuhlinger, J. P. Cooke, A. Hamsten and P. Tornvall (2001). "Mild-to-moderate hypertriglyceridemia in young men is associated with endothelial dysfunction and increased plasma concentrations of asymmetric dimethylarginine." J Am Coll Cardiol **38**(1): 111-116.

Madamanchi, N. R. and M. S. Runge (2007). "Mitochondrial dysfunction in atherosclerosis." Circ Res **100**(4): 460-473.

Mahmoud, M. M., H. R. Kim, R. Xing, S. Hsiao, A. Mammoto, J. Chen, J. Serbanovic-Canic, S. Feng, N. P. Bowden, R. Maguire, M. Ariaans, S. E. Francis, P. D. Weinberg, K. van der Heiden, E. A. Jones, T. J. Chico, V. Ridger and P. C. Evans (2016). "TWIST1 Integrates Endothelial Responses to Flow in Vascular Dysfunction and Atherosclerosis." Circ Res **119**(3): 450-462.

Mai, S., M. Klinkenberg, G. Auburger, J. Bereiter-Hahn and M. Jendrach (2010). "Decreased expression of Drp1 and Fis1 mediates mitochondrial elongation in senescent cells and enhances resistance to oxidative stress through PINK1." J Cell Sci **123**(Pt 6): 917-926.

Markossian, K. A. and B. I. Kurganov (2004). "Protein folding, misfolding, and aggregation. Formation of inclusion bodies and aggresomes." Biochemistry (Mosc) **69**(9): 971-984.

Martin, A., M. R. Komada and D. C. Sane (2003). "Abnormal angiogenesis in diabetes mellitus." Med Res Rev **23**(2): 117-145.

Martinet, W., D. M. Schrijvers, A. G. Herman and G. R. De Meyer (2006). "z-VAD-fmk-induced non-apoptotic cell death of macrophages: possibilities and limitations for atherosclerotic plaque stabilization." Autophagy **2**(4): 312-314.

Masotti, A., M. R. Miller, A. Celluzzi, L. Rose, F. Micciulla, P. W. Hadoke, S. Bellucci and A. Caporali (2016). "Regulation of angiogenesis through the efficient delivery of microRNAs into endothelial cells using polyamine-coated carbon nanotubes." Nanomedicine **12**(6): 1511-1522.

Matsumoto, T., P. Schiller, L. C. Dieterich, F. Bahram, Y. Iribe, U. Hellman, C. Wikner, G. Chan, L. Claesson-Welsh and A. Dimberg (2008). "Ninein is expressed in the cytoplasm of angiogenic tip-cells and regulates tubular morphogenesis of endothelial cells." Arterioscler Thromb Vasc Biol **28**(12): 2123-2130.

Matsunaga, T., K. Iguchi, T. Nakajima, I. Koyama, T. Miyazaki, I. Inoue, S. Kawai, S. Katayama, K. Hirano, S. Hokari and T. Komoda (2001). "Glycated high-density lipoprotein induces apoptosis of endothelial cells via a mitochondrial dysfunction." Biochem Biophys Res Commun **287**(3): 714-720.

McHugh, D. and J. Gil (2018). "Senescence and aging: Causes, consequences, and therapeutic avenues." J Cell Biol **217**(1): 65-77.

McMahon, S., M. Charbonneau, S. Grandmont, D. E. Richard and C. M. Dubois (2006). "Transforming growth factor beta1 induces hypoxia-inducible

factor-1 stabilization through selective inhibition of PHD2 expression." J Biol Chem **281**(34): 24171-24181.

Meijer, A. J., S. Lorin, E. F. Blommaart and P. Codogno (2015). "Regulation of autophagy by amino acids and MTOR-dependent signal transduction." Amino Acids **47**(10): 2037-2063.

Meloni, M., M. Marchetti, K. Garner, B. Littlejohns, G. Sala-Newby, N. Xenophontos, I. Floris, M. S. Suleiman, P. Madeddu, A. Caporali and C. Emanueli (2013). "Local inhibition of microRNA-24 improves reparative angiogenesis and left ventricle remodeling and function in mice with myocardial infarction." Mol Ther **21**(7): 1390-1402.

Mercer, T. J., A. Gubas and S. A. Tooze (2018). "A molecular perspective of mammalian autophagosome biogenesis." J Biol Chem **293**(15): 5386-5395.

Meunier, S. and I. Vernos (2012). "Microtubule assembly during mitosis - from distinct origins to distinct functions?" J Cell Sci **125**(Pt 12): 2805-2814.

Michaelis, U. R. (2014). "Mechanisms of endothelial cell migration." Cell Mol Life Sci **71**(21): 4131-4148.

Minamino, T. and I. Komuro (2008). "Vascular aging: insights from studies on cellular senescence, stem cell aging, and progeroid syndromes." Nat Clin Pract Cardiovasc Med **5**(10): 637-648.

Mizuno-Yamasaki, E., F. Rivera-Molina and P. Novick (2012). "GTPase networks in membrane traffic." Annu Rev Biochem **81**: 637-659.

Mizushima, N. and M. Komatsu (2011). "Autophagy: renovation of cells and tissues." Cell **147**(4): 728-741.

Murphy, E., D. Bers and R. Rizzuto (2009). "Mitochondria: from basic biology to cardiovascular disease." J Mol Cell Cardiol **46**(6): 765-766.

Murphy, M. P. (2012). "Modulating mitochondrial intracellular location as a redox signal." Sci Signal **5**(242): pe39.

Neill, T., A. Torres, S. Buraschi, R. T. Owens, J. B. Hoek, R. Baffa and R. V. Iozzo (2014). "Decorin induces mitophagy in breast carcinoma cells via peroxisome proliferator-activated receptor gamma coactivator-1alpha (PGC-1alpha) and mitostatin." J Biol Chem **289**(8): 4952-4968.

Ney, P. A. (2015). "Mitochondrial autophagy: Origins, significance, and role of BNIP3 and NIX." Biochim Biophys Acta **1853**(10 Pt B): 2775-2783.

Niccoli, T. and L. Partridge (2012). "Ageing as a risk factor for disease." Curr Biol **22**(17): R741-752.

Nishikawa, T., D. Edelstein, X. L. Du, S. Yamagishi, T. Matsumura, Y. Kaneda, M. A. Yorek, D. Beebe, P. J. Oates, H. P. Hammes, I. Giardino and M. Brownlee (2000). "Normalizing mitochondrial superoxide production blocks three pathways of hyperglycaemic damage." Nature **404**(6779): 787-790.

Nishizawa, M., I. Izawa, A. Inoko, Y. Hayashi, K. Nagata, T. Yokoyama, J. Usukura and M. Inagaki (2005). "Identification of trichoplein, a novel keratin filament-binding protein." J Cell Sci **118**(Pt 5): 1081-1090.

Noonan, D. M., A. De Lerma Barbaro, N. Vannini, L. Mortara and A. Albini (2008). "Inflammation, inflammatory cells and angiogenesis: decisions and indecisions." Cancer and Metastasis Reviews **27**(1): 31-40.

Norman, J. M., G. M. Cohen and E. T. Bampton (2010). "The in vitro cleavage of the hAtg proteins by cell death proteases." Autophagy **6**(8): 1042-1056.

North, B. J. and D. A. Sinclair (2012). "The intersection between aging and cardiovascular disease." Circ Res **110**(8): 1097-1108.

Nussenzweig, S. C., S. Verma and T. Finkel (2015). "The role of autophagy in vascular biology." Circ Res **116**(3): 480-488.

Oakes, S. A. and F. R. Papa (2015). "The role of endoplasmic reticulum stress in human pathology." Annu Rev Pathol **10**: 173-194.

Palazzo, A. F., H. L. Joseph, Y. J. Chen, D. L. Dujardin, A. S. Alberts, K. K. Pfister, R. B. Vallee and G. G. Gundersen (2001). "Cdc42, dynein, and dynactin regulate MTOC reorientation independent of Rho-regulated microtubule stabilization." Curr Biol **11**(19): 1536-1541.

Palmer, A. K., T. Tchkonia, N. K. LeBrasseur, E. N. Chini, M. Xu and J. L. Kirkland (2015). "Cellular Senescence in Type 2 Diabetes: A Therapeutic Opportunity." Diabetes **64**(7): 2289-2298.

Paone, A., R. Galli, C. Gabellini, D. Lukashev, D. Starace, A. Gorlach, P. De Cesaris, E. Ziparo, D. Del Bufalo, M. V. Sitkovsky, A. Filippini and A. Riccioli (2010). "Toll-like Receptor 3 Regulates Angiogenesis and Apoptosis in Prostate Cancer Cell Lines through Hypoxia-Inducible Factor 1α." Neoplasia (New York, N.Y.) **12**(7): 539-549.

Parcellier, A., E. Schmitt, S. Gurbuxani, D. Seigneurin-Berny, A. Pance, A. Chantome, S. Plenchette, S. Khochbin, E. Solary and C. Garrido (2003). "HSP27 is a ubiquitin-binding protein involved in I-kappaBalpha proteasomal degradation." Mol Cell Biol **23**(16): 5790-5802.

Park, H. J., F. Yang and S. W. Cho (2012). "Nonviral delivery of genetic medicine for therapeutic angiogenesis." Adv Drug Deliv Rev **64**(1): 40-52.

Passos, J. F., G. Saretzki, S. Ahmed, G. Nelson, T. Richter, H. Peters, I. Wappler, M. J. Birket, G. Harold, K. Schaeuble, M. A. Birch-Machin, T. B. Kirkwood and T. von Zglinicki (2007). "Mitochondrial dysfunction accounts for the stochastic heterogeneity in telomere-dependent senescence." PLoS Biol **5**(5): e110.

Peterson, T. R., S. S. Sengupta, T. E. Harris, A. E. Carmack, S. A. Kang, E. Balderas, D. A. Guertin, K. L. Madden, A. E. Carpenter, B. N. Finck and D. M. Sabatini (2011). "mTOR complex 1 regulates lipin 1 localization to control the SREBP pathway." Cell **146**(3): 408-420.

Phng, L. K. and H. Gerhardt (2009). "Angiogenesis: a team effort coordinated by notch." Dev Cell **16**(2): 196-208.

Pinilla-Macua, I. and A. Sorkin (2015). "Methods to study endocytic trafficking of the EGF receptor." Methods Cell Biol **130**: 347-367.

Pollet, I., C. J. Opina, C. Zimmerman, K. G. Leong, F. Wong and A. Karsan (2003). "Bacterial lipopolysaccharide directly induces angiogenesis through TRAF6-mediated activation of NF-κB and c-Jun N-terminal kinase." Blood **102**(5): 1740-1742.

Potente, M., H. Gerhardt and P. Carmeliet (2011). "Basic and therapeutic aspects of angiogenesis." Cell **146**(6): 873-887.

Psaltis, P. J. and R. D. Simari (2015). "Vascular wall progenitor cells in health and disease." Circ Res **116**(8): 1392-1412.

Pyo, J. O., S. M. Yoo, H. H. Ahn, J. Nah, S. H. Hong, T. I. Kam, S. Jung and Y. K. Jung (2013). "Overexpression of Atg5 in mice activates autophagy and extends lifespan." Nat Commun **4**: 2300.

Qin, L., Z. Wang, L. Tao and Y. Wang (2010). "ER stress negatively regulates AKT/TSC/mTOR pathway to enhance autophagy." Autophagy **6**(2): 239-247.

Quintero, M., S. L. Colombo, A. Godfrey and S. Moncada (2006). "Mitochondria as signaling organelles in the vascular endothelium." Proc Natl Acad Sci U S A **103**(14): 5379-5384.

Raiborg, C. and H. Stenmark (2009). "The ESCRT machinery in endosomal sorting of ubiquitylated membrane proteins." Nature **458**(7237): 445-452.

Ravikumar, B., S. Sarkar, J. E. Davies, M. Futter, M. Garcia-Arencibia, Z. W. Green-Thompson, M. Jimenez-Sanchez, V. I. Korolchuk, M. Lichtenberg, S. Luo, D. C. Massey, F. M. Menzies, K. Moreau, U. Narayanan, M. Renna, F. H. Siddiqi, B. R. Underwood, A. R. Winslow and D. C. Rubinsztein (2010). "Regulation of mammalian autophagy in physiology and pathophysiology." Physiol Rev **90**(4): 1383-1435.

Reuter, S., S. C. Gupta, M. M. Chaturvedi and B. B. Aggarwal (2010). "Oxidative stress, inflammation, and cancer: How are they linked?" Free Radical Biology and Medicine **49**(11): 1603-1616.

Rho, S. S., K. Ando and S. Fukuhara (2017). "Dynamic Regulation of Vascular Permeability by Vascular Endothelial Cadherin-Mediated Endothelial Cell-Cell Junctions." J Nippon Med Sch **84**(4): 148-159.

Risau, W. (1997). "Mechanisms of angiogenesis." Nature **386**(6626): 671-674.

Rubinsztein, D. C., P. Codogno and B. Levine (2012). "Autophagy modulation as a potential therapeutic target for diverse diseases." Nat Rev Drug Discov **11**(9): 709-730.

Rüegg, C. (2006). "Leukocytes, inflammation, and angiogenesis in cancer: fatal attractions." Journal of Leukocyte Biology **80**(4): 682-684.

Sahu, R., S. Kaushik, C. C. Clement, E. S. Cannizzo, B. Scharf, A. Follenzi, I. Potolicchio, E. Nieves, A. M. Cuervo and L. Santambrogio (2011). "Microautophagy of cytosolic proteins by late endosomes." Dev Cell **20**(1): 131-139.

Sakabe, M., J. Fan, Y. Odaka, N. Liu, A. Hassan, X. Duan, P. Stump, L. Byerly, M. Donaldson, J. Hao, M. Fruttiger, Q. R. Lu, Y. Zheng, R. A. Lang and M. Xin (2017). "YAP/TAZ-CDC42 signaling regulates vascular tip cell migration." Proc Natl Acad Sci U S A **114**(41): 10918-10923.

Sancak, Y., L. Bar-Peled, R. Zoncu, A. L. Markhard, S. Nada and D. M. Sabatini (2010). "Ragulator-Rag complex targets mTORC1 to the lysosomal

surface and is necessary for its activation by amino acids." Cell **141**(2): 290-303.

Sarkar, S. (2013). "Regulation of autophagy by mTOR-dependent and mTOR-independent pathways: autophagy dysfunction in neurodegenerative diseases and therapeutic application of autophagy enhancers." Biochem Soc Trans **41**(5): 1103-1130.

Sarkar, S., J. E. Davies, Z. Huang, A. Tunnacliffe and D. C. Rubinsztein (2007). "Trehalose, a novel mTOR-independent autophagy enhancer, accelerates the clearance of mutant huntingtin and alpha-synuclein." J Biol Chem **282**(8): 5641-5652.

Sarkar, S., V. I. Korolchuk, M. Renna, S. Imarisio, A. Fleming, A. Williams, M. Garcia-Arencibia, C. Rose, S. Luo, B. R. Underwood, G. Kroemer, C. J. O'Kane and D. C. Rubinsztein (2011). "Complex inhibitory effects of nitric oxide on autophagy." Mol Cell **43**(1): 19-32.

Sattler, H. P., V. Rohde, H. Bonkhoff, T. Zwergel and B. Wullich (1999). "Comparative genomic hybridization reveals DNA copy number gains to frequently occur in human prostate cancer." Prostate **39**(2): 79-86.

Scherz-Shouval, R., E. Shvets, E. Fass, H. Shorer, L. Gil and Z. Elazar (2007). "Reactive oxygen species are essential for autophagy and specifically regulate the activity of Atg4." EMBO J **26**(7): 1749-1760.

Schmittgen, T. D. and K. J. Livak (2008). "Analyzing real-time PCR data by the comparative C(T) method." Nat Protoc **3**(6): 1101-1108.

Schmutte, C., R. Baffa, L. M. Veronese, Y. Murakumo and R. Fishel (1997). "Human thymine-DNA glycosylase maps at chromosome 12q22-q24.1: a region of high loss of heterozygosity in gastric cancer." Cancer Res **57**(14): 3010-3015.

Semenza, G. L. (2012). "Hypoxia-inducible factors in physiology and medicine." Cell **148**(3): 399-408.

Settembre, C., C. Di Malta, V. A. Polito, M. Garcia Arencibia, F. Vetrini, S. Erdin, S. U. Erdin, T. Huynh, D. Medina, P. Colella, M. Sardiello, D. C. Rubinsztein and A. Ballabio (2011). "TFEB links autophagy to lysosomal biogenesis." Science **332**(6036): 1429-1433.

Settembre, E. C., P. R. Dormitzer and R. Rappuoli (2011). "Learning from the 2009 H1N1 pandemic: prospects for more broadly effective influenza vaccines." J Mol Cell Biol **3**(3): 144-146.

Sharaf, B. L., C. J. Pepine, R. A. Kerensky, S. E. Reis, N. Reichek, W. J. Rogers, G. Sopko, S. F. Kelsey, R. Holubkov, M. Olson, N. J. Miele, D. O. Williams, C. N. Merz and W. S. Group (2001). "Detailed angiographic analysis of women with suspected ischemic chest pain (pilot phase data from the NHLBI-sponsored Women's Ischemia Syndrome Evaluation [WISE] Study Angiographic Core Laboratory)." Am J Cardiol **87**(8): 937-941; A933.

Sheetz, M. J. and G. L. King (2002). "Molecular understanding of hyperglycemia's adverse effects for diabetic complications." JAMA **288**(20): 2579-2588.

Shen, H. M. and N. Mizushima (2014). "At the end of the autophagic road: an emerging understanding of lysosomal functions in autophagy." Trends Biochem Sci **39**(2): 61-71.

Shi, Y., S. H. Tan, S. Ng, J. Zhou, N. D. Yang, G. B. Koo, K. A. McMahon, R. G. Parton, M. M. Hill, M. A. Del Pozo, Y. S. Kim and H. M. Shen (2015). "Critical role of CAV1/caveolin-1 in cell stress responses in human breast cancer cells via modulation of lysosomal function and autophagy." Autophagy **11**(5): 769-784.

Shiseki, M., T. Kohno, J. Adachi, T. Okazaki, T. Otsuka, H. Mizoguchi, M. Noguchi, S. Hirohashi and J. Yokota (1996). "Comparative allelotype of early and advanced stage non-small cell lung carcinomas." Genes Chromosomes Cancer **17**(2): 71-77.

Silvander, J. S. G., S. M. Kvarnstrom, A. Kumari-Ilieva, A. Shrestha, C. M. Alam and D. M. Toivola (2017). "Keratins regulate beta-cell mitochondrial morphology, motility, and homeostasis." FASEB J **31**(10): 4578-4587.

Son, S. M. (2012). "Reactive oxygen and nitrogen species in pathogenesis of vascular complications of diabetes." Diabetes Metab J **36**(3): 190-198.

Song, J. W. and L. L. Munn (2011). "Fluid forces control endothelial sprouting." Proc Natl Acad Sci U S A **108**(37): 15342-15347.

Sorkin, A. and M. von Zastrow (2009). "Endocytosis and signalling: intertwining molecular networks." Nat Rev Mol Cell Biol **10**(9): 609-622.

Suchting, S., C. Freitas, F. le Noble, R. Benedito, C. Breant, A. Duarte and A. Eichmann (2007). "The Notch ligand Delta-like 4 negatively regulates endothelial tip cell formation and vessel branching." Proc Natl Acad Sci U S A **104**(9): 3225-3230.

Sutendra, G., P. Dromparis, P. Wright, S. Bonnet, A. Haromy, Z. Hao, M. S. McMurtry, M. Michalak, J. E. Vance, W. C. Sessa and E. D. Michelakis (2011). "The role of Nogo and the mitochondria-endoplasmic reticulum unit in pulmonary hypertension." Sci Transl Med **3**(88): 88ra55.

Szulcek, R., H. J. Bogaard and G. P. van Nieuw Amerongen (2014). "Electric cell-substrate impedance sensing for the quantification of endothelial proliferation, barrier function, and motility." J Vis Exp(85).

Tait, S. W. and D. R. Green (2013). "Mitochondrial regulation of cell death." Cold Spring Harb Perspect Biol **5**(9).

Takeda, K. and S. Akira (2004). "TLR signaling pathways." Seminars in Immunology **16**(1): 3-9.

Tang, X., Y. X. Luo, H. Z. Chen and D. P. Liu (2014). "Mitochondria, endothelial cell function, and vascular diseases." Front Physiol **5**: 175.

Tanida, I. (2011). "Autophagosome formation and molecular mechanism of autophagy." Antioxid Redox Signal **14**(11): 2201-2214.

Thoreen, C. C., S. A. Kang, J. W. Chang, Q. Liu, J. Zhang, Y. Gao, L. J. Reichling, T. Sim, D. M. Sabatini and N. S. Gray (2009). "An ATP-competitive mammalian target of rapamycin inhibitor reveals rapamycin-resistant functions of mTORC1." J Biol Chem **284**(12): 8023-8032.

Topal, G., A. Brunet, E. Millanvoye, J. L. Boucher, F. Rendu, M. A. Devynck and M. David-Dufilho (2004). "Homocysteine induces oxidative stress by uncoupling of NO synthase activity through reduction of tetrahydrobiopterin." Free Radic Biol Med **36**(12): 1532-1541.

Torisu, T., K. Torisu, I. H. Lee, J. Liu, D. Malide, C. A. Combs, X. S. Wu, Rovira, II, M. M. Fergusson, R. Weigert, P. S. Connelly, M. P. Daniels, M. Komatsu, L. Cao and T. Finkel (2013). "Autophagy regulates endothelial cell processing, maturation and secretion of von Willebrand factor." Nat Med **19**(10): 1281-1287.

Toso, A., A. Revandkar, D. Di Mitri, I. Guccini, M. Proietti, M. Sarti, S. Pinton, J. Zhang, M. Kalathur, G. Civenni, D. Jarrossay, E. Montani, C. Marini, R. Garcia-Escudero, E. Scanziani, F. Grassi, P. P. Pandolfi, C. V. Catapano and A. Alimonti (2014). "Enhancing chemotherapy efficacy in Pten-deficient prostate tumors by activating the senescence-associated antitumor immunity." Cell Rep **9**(1): 75-89.

Towers, C. G. and A. Thorburn (2016). "Therapeutic Targeting of Autophagy." EBioMedicine **14**: 15-23.

Treberg, J. R., C. L. Quinlan and M. D. Brand (2010). "Hydrogen peroxide efflux from muscle mitochondria underestimates matrix superoxide production--a correction using glutathione depletion." FEBS J **277**(13): 2766-2778.

Tressel, S. L., R. P. Huang, N. Tomsen and H. Jo (2007). "Laminar shear inhibits tubule formation and migration of endothelial cells by an angiopoietin-2 dependent mechanism." Arterioscler Thromb Vasc Biol **27**(10): 2150-2156.

Turrens, J. F. (2003). "Mitochondrial formation of reactive oxygen species." J Physiol **552**(Pt 2): 335-344.

Unterluggauer, H., E. Hutter, R. Voglauer, J. Grillari, M. Voth, J. Bereiter-Hahn, P. Jansen-Durr and M. Jendrach (2007). "Identification of cultivation-independent markers of human endothelial cell senescence in vitro." Biogerontology **8**(4): 383-397.

Vacek, T. P., J. C. Vacek, N. Tyagi and S. C. Tyagi (2012). "Autophagy and heart failure: a possible role for homocysteine." Cell Biochem Biophys **62**(1): 1-11.

Valdes, A. M., D. Glass and T. D. Spector (2013). "Omics technologies and the study of human ageing." Nat Rev Genet **14**(9): 601-607.

Vanhoutte, P. M., H. Shimokawa, M. Feletou and E. H. Tang (2017). "Endothelial dysfunction and vascular disease - a 30th anniversary update." Acta Physiol (Oxf) **219**(1): 22-96.

Vecchione, A., M. Fassan, V. Anesti, A. Morrione, S. Goldoni, G. Baldassarre, D. Byrne, D. D'Arca, J. P. Palazzo, J. Lloyd, L. Scorrano, L. G. Gomella, R. V. Iozzo and R. Baffa (2009). "MITOSTATIN, a putative tumor suppressor on chromosome 12q24.1, is downregulated in human bladder and breast cancer." Oncogene **28**(2): 257-269.

Vergnani, L., S. Hatrik, F. Ricci, A. Passaro, N. Manzoli, G. Zuliani, V. Brovkovych, R. Fellin and T. Malinski (2000). "Effect of native and oxidized low-density lipoprotein on endothelial nitric oxide and superoxide production : key role of L-arginine availability." Circulation **101**(11): 1261-1266.

Vicencio, J. M., C. Ortiz, A. Criollo, A. W. Jones, O. Kepp, L. Galluzzi, N. Joza, I. Vitale, E. Morselli, M. Tailler, M. Castedo, M. C. Maiuri, J. Molgo, G. Szabadkai, S. Lavandero and G. Kroemer (2009). "The inositol 1,4,5-

trisphosphate receptor regulates autophagy through its interaction with Beclin 1." Cell Death Differ **16**(7): 1006-1017.

Wang, L., M. Cano and J. T. Handa (2014). "p62 provides dual cytoprotection against oxidative stress in the retinal pigment epithelium." Biochim Biophys Acta **1843**(7): 1248-1258.

Wei, Y., S. Pattingre, S. Sinha, M. Bassik and B. Levine (2008). "JNK1-mediated phosphorylation of Bcl-2 regulates starvation-induced autophagy." Mol Cell **30**(6): 678-688.

Weis, S. M. and D. A. Cheresh (2005). "Pathophysiological consequences of VEGF-induced vascular permeability." Nature **437**(7058): 497-504.

West, X. Z., N. L. Malinin, A. A. Merkulova, M. Tischenko, B. A. Kerr, E. C. Borden, E. A. Podrez, R. G. Salomon and T. V. Byzova (2010). "Oxidative stress induces angiogenesis by activating TLR2 with novel endogenous ligands." Nature **467**(7318): 972-976.

Wigley, W. C., R. P. Fabunmi, M. G. Lee, C. R. Marino, S. Muallem, G. N. DeMartino and P. J. Thomas (1999). "Dynamic association of proteasomal machinery with the centrosome." J Cell Biol **145**(3): 481-490.

Willems, P. H., R. Rossignol, C. E. Dieteren, M. P. Murphy and W. J. Koopman (2015). "Redox Homeostasis and Mitochondrial Dynamics." Cell Metab **22**(2): 207-218.

Williams, R. S., L. Cheng, A. W. Mudge and A. J. Harwood (2002). "A common mechanism of action for three mood-stabilizing drugs." Nature **417**(6886): 292-295.

Xu, M., T. Tchkonia, H. Ding, M. Ogrodnik, E. R. Lubbers, T. Pirtskhalava, T. A. White, K. O. Johnson, M. B. Stout, V. Mezera, N. Giorgadze, M. D. Jensen, N. K. LeBrasseur and J. L. Kirkland (2015). "JAK inhibition alleviates the cellular senescence-associated secretory phenotype and frailty in old age." Proc Natl Acad Sci U S A **112**(46): E6301-6310.

Xu, W. and S. C. Erzurum (2011). "Endothelial cell energy metabolism, proliferation, and apoptosis in pulmonary hypertension." Compr Physiol **1**(1): 357-372.

Yeboah, J., A. R. Folsom, G. L. Burke, C. Johnson, J. F. Polak, W. Post, J. A. Lima, J. R. Crouse and D. M. Herrington (2009). "Predictive value of brachial flow-mediated dilation for incident cardiovascular events in a population-

based study: the multi-ethnic study of atherosclerosis." Circulation **120**(6): 502-509.

Yorimitsu, T., U. Nair, Z. Yang and D. J. Klionsky (2006). "Endoplasmic reticulum stress triggers autophagy." J Biol Chem **281**(40): 30299-30304.

Youm, Y. H., R. W. Grant, L. R. McCabe, D. C. Albarado, K. Y. Nguyen, A. Ravussin, P. Pistell, S. Newman, R. Carter, A. Laque, H. Munzberg, C. J. Rosen, D. K. Ingram, J. M. Salbaum and V. D. Dixit (2013). "Canonical Nlrp3 inflammasome links systemic low-grade inflammation to functional decline in aging." Cell Metab **18**(4): 519-532.

Zhang, G., J. Li, S. Purkayastha, Y. Tang, H. Zhang, Y. Yin, B. Li, G. Liu and D. Cai (2013). "Hypothalamic programming of systemic ageing involving IKK-beta, NF-kappaB and GnRH." Nature **497**(7448): 211-216.

Zhang, Y., X. Gao, L. J. Saucedo, B. Ru, B. A. Edgar and D. Pan (2003). "Rheb is a direct target of the tuberous sclerosis tumour suppressor proteins." Nat Cell Biol **5**(6): 578-581.

Zhuo, Y., S. H. Li, M. S. Chen, J. Wu, H. Y. Kinkaid, S. Fazel, R. D. Weisel and R. K. Li (2010). "Aging impairs the angiogenic response to ischemic injury and the activity of implanted cells: combined consequences for cell therapy in older recipients." J Thorac Cardiovasc Surg **139**(5): 1286-1294, 1294 e1281-1282.

Ziegler, D. V., C. D. Wiley and M. C. Velarde (2015). "Mitochondrial effectors of cellular senescence: beyond the free radical theory of aging." Aging Cell **14**(1): 1-7.